OPTIMIZING PLASMA-ASSISTED EXTRACTION OF SPIRULINA-DERIVED BIOACTIVE COMPOUNDS FOR WOUND HEALING APPLICATIONS

By

Elsbeth Joan R. Evangelista,RPh

2328769

A thesis submitted to Flinders University

For the degree of

Master of Biotechnology

College of Medicine & Public Health

03 November 2025

Principal Supervisor: Dr. Andrew Hayles

Co-Supervisor: Prof. Krasimir Vasilev

Mentors: Ms. Thi Giang Tuyet Pham & Quan Trong Luu

Table of Contents

LIST OF FIGURES

LIST OF TABLES

LIST OF ABBREVIATIONS

Abbreviation	Full Form
AMR	Antimicrobial Resistance
BCA	Bicinchoninic acid
BSA	Bovine Serum Albumin
CCD	Central Composite Design
CFU	Colony Forming Unit
CPC	C-phycocyanin
DBD	Dielectric barrier discharge
DPPH	2,2-diphenyl-1-picrylhydrazyl
EPS	Extracellular Polymeric Substances
EFM	Epifluorescence Microscopy
LC-MS	Liquid chromatography mass spectrometry
MIC	Minimum Inhibitory Concentration
MRSA	Methicillin-Resistant *Staphylococcus aureus*
PBS	Phosphate Buffered Saline
PCB	Phycocyanobilin
PI	Propidium Iodide
ROS	Reactive Oxygen Species
RSM	Response Surface Methodology
SEM	Scanning Electron Microscopy
TSB	Tryptic Soy Broth
TPU	Thermoplastic Polyurethane
UV-VIS	Ultraviolet-Visible Spectroscopy
VLU	Venous Leg Ulcer

ABSTRACT

Chronic wound infections remain an increasingly burdensome threat to public health, globally demanding innovative and novel therapeutic approaches. *Spirulina maxima*, a blue-green microalga rich in bioactive compounds including c-phycocyanin, antioxidant, and bioactive compounds including essential proteins, has exemplified wound healing potential. However, conventional extraction methods often limit recovery efficiency of these promising bioactive compounds due to their energy-intensive nature, which compromise the quality and reduces extraction yield leading to several scientific limitations. In this study, plasma-assisted extraction using dielectric barrier discharge (DBD) atmospheric plasma technology were utilized to optimize the yield and bioactive efficacy of *S. maxima.* The purpose of this study is to comprehensively determine the optimal processing parameters including voltage level (kV), treatment time (min), and NaCl concentration (g/L) for plasma-assisted extraction of *S. maxima*-derived bioactive compounds. Additionally, the study aims to evaluate the spectrum of antibacterial activity of the optimized plasma-treated *S. maxima* against a variety of clinically relevant Gram-positive and Gram-negative pathogens related to wound healing. To fine-tune the key parameters of plasma-assisted extraction, a Central Composite Design (CCD) was employed using Design Expert software. An optimized plasma condition setting of 3kV voltage, 7.42 minutes, 0.75 g/L NaCl concentration was identified to provide sufficient control causing to generate reactive oxygen and nitrogen species for effective cell wall disruption without any further degradation significantly enhanced c-phycocyanin (CPC) concentration compared to conventional freeze-thaw method and untreated *S.maxima* supernatant. The antioxidant capacity is evaluated using the DPPH radical scavenging assay, reveals a preserved capacity post-plasma treatment. Morphological analyses in SEM and epifluorescence analysis reveals that extensive plasma-induced cell way disruption after plasma exposure can directly correlate with improved bioactive compound release. Among all tested conditions, the optimized 3kV plasma treatment condition stands out enhancing the antibacterial capacity of plasma-treated *S. maxima* supernatant with a greater effect observed in Gram-positive bacteria, specifically *Staphylococcus epidermidis*, and a significant effectiveness against *Staphylococcus aureus* as confirmed by CFU enumeration, and flow cytometry assays. While a notable antibacterial capacity was observed in Gram-negative *Pseudomonas aeruginosa,* and a lower sensitivity was shown by *Escherichia coli* to the plasma-treated extract. Despite these current results, some limitation must be recognized and be addressed for future visions. By integrating innovative plasma-assisted technology, it contributes to microalgal technology by discovering a new innovative extraction technique that provides a promising strategy that may offer innovative solution for chronic wound applications.

SIGNED DECLARATION

I certify that this thesis:

1. does not incorporate without acknowledgment any material previously submitted for a degree or diploma in any university

2. and the research within will not be submitted for any other future degree or diploma without the permission of Flinders University; and

3. to the best of my knowledge and belief, does not contain any material previously published or written by another person except where due reference is made in the text.

Signed by: **Elsbeth Joan R. Evangelista**
Date: 03 November 2025

ACKNOWLEDGEMENT

With humble gratitude, I dedicated this work to all those who believed in me and stood by my side throughout this journey. I would like to express my sincere appreciation to Him for blessing me with all the patience, and determination despite every setback to keep moving forward.

First and foremost, I am sincerely grateful to my principal supervisor Dr. Andrew Hayles for being my constant source of encouragement, support and guidance throughout this nine-month research project. Your patience and kindness have given me the confidence to keep trying and remind me that I am capable of so much more than I realize across many aspects of this journey. This work wouldn't be possible without you.

To Ms. Thi Giang Tuyet Pham and Quan Trong Luu, my mentors, who have consistently offered guidance and support, providing me essential laboratory techniques and hands-on guidance. Thank you for your willingness to help whenever I am in doubt. Your encouragement to "always try your best" has helped me come this far.

To Prof. Krasimir Vasilev and the whole Biomedical Nanoengineering Laboratory team, thank you for creating a supportive space for everyone. Your dedication during late night laboratory work inspires me to strive harder.

To my family, mum, dad, my sister Eana, my brother Juan, and most specially to my grandmother who is currently fighting cancer, we made it! Along the way, I learned to be brave, not because I knew what to do, but because I was made brave by the people, I love the most. This is all for you. And lastly, to Danny who has become my family, giving me strength while I'm far away from home. Thank you for being my constant source of strength.

Balancing academic commitments and personal life at the same time is a huge achievement. It wouldn't be possible without perseverance, support and faith. Every kindness shown to me is a gift I have strived to pay forward in every way possible. When God pushes you to the edge of difficulty, trust Him fully. With Him, all things are possible (Matthew 19:26).

CHAPTER ONE: LITERATURE REVIEW

INTRODUCTION

Chronic wound infections are a significant burden that prolongs recovery and increasing the risk of severe complications (Percival et al., 2005). This problem is further compounded by growing threat of antimicrobial resistance (AMR), an increasingly burdensome threat to public health, that demands innovative and novel therapeutic approaches (*Wound Australia* 2022). AMR has emerged as a high-impact public health concern, and is considered a silent epidemic, leading to an estimated 10 million deaths per year worldwide by 2050 (Leaper et al., 2015). These infections are frequently the cause of delayed healing in acute open wounds, leading to a chronic wound (Hurlow & Bowler, 2022). The term 'chronic wound' is usually defined as a wound that fails to progress by 20-40% improvement after 4 to 8 weeks of optimal therapy (Hoang et al., 2022).

This health challenge is commonly associated with prolonged suffering, increased treatment cost burden, and a serious health risk, highlighting the urgent need for accessible and efficient wound treatment (Carter et al., 2023). For this reason, experts worldwide are focused on exploring novel treatment that can prevent the growing social and economic consequences.

Bacterial and viral pathogens may often penetrate the host through an open wound (Siddiqui & Bernstein, 2010). To minimize this burden, the ideal intervention is to eliminate potential pathogens before they can establish an infection (Siddiqui & Bernstein, 2010). However, due to the common use of antibiotics and silver-based treatments in wound care, pathogens such as *P. aeruginosa* and *S. aureus* are increasingly becoming resistant to conventional antimicrobial compounds (Pham et al., 2024).

As conventional treatment loses its effectiveness, *Spirulina maxima*, a blue-green microalgae, has gained interest (Marjanović et al., 2024). Rich in beneficial bioactive compounds, it shows strong antibacterial, anti-inflammatory, and antioxidant properties making it a promising option for wound care (Pham et al., 2024). However, inefficient conventional extraction methods may limit the effectiveness of these compounds, preventing these bioactives to be utilized at their full potential (Jaeschke et al., 2021). Therefore, alternative approaches are necessary.

Plasma-assisted technology has emerged as an attractive approach to enhance the wound healing potential of *S. maxima* (Pham, 2023). This approach functions by selectively disrupting cell membrane, facilitating cell wall permeability, making it easier to penetrate resulting to an increasing extraction efficacy by 15-40%, yielding better antibacterial, anti-inflammatory and antioxidant properties (Pham et al., 2024). Despite its potential, limited research has been conducted and demonstrating the need for further exploration.

1.1 Chronic Wound Infection

1.1.1 Chronic Wound

A wound is defined as any injury or damage to the skin's surface, if poorly managed, can result in infections leading to death (Siddiqui & Bernstein, 2010). Chronic wound is classified into two categories depending on its period of healing (Siddiqui & Bernstein, 2010). First is the acute wound which usually heals after 10 days without any complications, while chronic wounds are characterized as wounds that remains in the inflammatory stage and fail to progress through the usual stages of healing within the anticipated time frame, usually after 4-8 weeks (Hoang et al., 2022).

1.1.2 Bacterial Colonization

All wounds have the potential to become contaminated by bacteria from the surrounding skin, the local environment, and patient sources (Hoang et al., 2022). Bacterial colonization is where the proliferating bacteria are present in an open wound; these colonizing bacteria can begin to form biofilm matrix, leading to further difficulties in treatment and immune response (Grossart et al., 2003).

1.1.3 The Biofilm Matrix

The presence of biofilm matrix in existing wound may delay wound healing, creates persistent inflammatory response, and granulation of tissue formation (Thomson, 2011). Biofilm has been present in 70-80% of chronic wounds (Thomson, 2011). This complex structure consists of aggregated microorganisms embedded in a self-produced protective matrix, called extracellular polymeric substances (EPS) matrix made up of polysaccharides, protein, and extracellular DNA, which increases tolerance to antimicrobials, limiting drug penetration and host defenses that impede tissue regeneration contributing to chronic wound persistence (Thomson, 2011).

Figure removed due to copyright restriction.

Figure 1. Biofilm formation stages. A.) Biofilm formation in microorganism **B.)** Adhesin and fimbriae in cell attachment **C.)** EPS components in mature biofilm **D.)** Dispersion in biofilm (Kumar et al., 2023).

1.1.4 The Growing Challenge of Chronic Wound Infections and Antimicrobial Resistance (AMR) in Modern Healthcare

Chronic wounds and chronic wound infection demonstrate a mutual relationship which is further intensified by the growing complications with antimicrobial resistance (AMR) (Percival et al., 2005). It is considered AMR when microorganism decrease in sensitivity and no longer responds to antimicrobial treatment as quantified by an increase in the minimum inhibitory concentration beyond a defined threshold (Percival et al., 2005). The misuse and overuse of antibacterial agents, self-medication, and incomplete administration of antibiotic dosage are considered the major reason for the emergence of antimicrobial isolates (Leaper et al., 2015).

In the context of chronic wounds, the minimum inhibitory concentration (MIC), which is known as the lowest concentration needed to inhibit the visible growth, increases by a considerable amount, resulting to a declining effectiveness of antibiotics (Kowalska-Krochmal & Dudek-Wicher, 2021). For effective anti-bacterial therapy, the pathogens at the site of infection must be exposed to a drug concentration sufficiently high to inhibit bacterial growth or even eliminate the pathogen from the site (Hurlow & Bowler, 2022). Notably, 70% of chronic wound bacteria exhibit resistance to at least one commonly used antibiotic (Hoang et al., 2022). The continued downfall of antibiotics necessitated alternative options for therapeutic control of microbial threats.

AMR has emerged as a high-impact public health concern, with approximately 2.8 million cases of clinical infection such as foot and leg ulcers and an estimated 10 million deaths per year worldwide by 2050 (Leaper et al., 2015). Globally, antibiotic-resistant wound infections account for an estimated 25% to 40% of hospital bed occupancy among patients suffering from chronic wounds (Siddiqui & Bernstein, 2010). In Australia, approximately 420,000 individuals are currently affected by chronic wound infection caused by multidrug-resistant pathogens, such as foot and leg ulcers, and more than 350,000 of those affected are aged 65 years or older mostly prevalent in hospitals and aged care facilities resulting to a treatment expense exceeding $4,000 per individual (*Wound Australia* 2022).These figures highlight the urgent need for accessible and innovative strategies to overcome Antimicrobial Resistance (AMR) both in Australia and worldwide.

1.2 Microbiology of Chronic Wound Infection

Chronic wound infection are difficult to manage due to their capacity to form biofilms which significantly contributes to delaying the healing process (Leaper et al., 2015). Several pathogens associated with chronic wounds typically capable of forming biofilms such as Methicillin-Resistant *Staphylococcus aureus* strains (MRSA), the leading cause of wound infection and *Pseudomonas spp*.

Based on reports, leg ulcers, show a prevalence of *S. aureus* ranging from 43% of infected cases to 88% of non-infected ones, whereas *P. aeruginosa* has been found in 7% to 33% of such ulcers (Leaper et al., 2015). These two major pathogens are particularly known to be the most prevalent and clinically significant pathogens to cause infections in chronic skin wounds, making them a relevant choice for this research. *S. epidermidis* has also been frequently associated with 50% venous leg ulcer (VLU), known for its capacity to form biofilms which has been associated with the ability to impair re-epithelialization (Dinić et al., 2024). Additionally, *Escherichia coli*, are capable of penetrating impaired skin barriers, can invade open wounds, and generate toxins that slow down the healing process and exacerbate inflammation (Landén et al., 2016). This set of pathogens will be assessed with Plasma-treated *S. maxima* extract to determine their optimized effect on chronic wound healing.

1.2.1 Treatment Burdens and Drawbacks for Chronic Wound Infection

Treatment burden is associated with the workload of healthcare and how it impacts patients' everyday functionality and well-being, including healthcare expenses, hospital stay, and recovery challenges (Sen, 2021). Today, the global advanced wound care market size is worth $ 11.57 billion and anticipated to grow worth $ 20.21 billion by 2035 (*Advanced Wound Care Market*, 2024).

For Medicare beneficiaries in Australia, the burden of chronic wound is notable, with 16.1% of beneficiaries estimatedly, 10.8 million patients diagnosed with at least one type of wound in 2021 (Carter et al., 2023). Medicare wound care expenditure of 26.3 billion AUD particularly affecting among the elderly population, with over 350,000 cases reported annually among aged 65 years old and above (Carter et al., 2023). Finally, an outpatient expense ranging from 9.9 to 35.8 billion AUD in 2021 exceeding inpatient costs given the fact that most of the chronic wound patients do not need hospitalization, but need consistent long-term medical attention (Carter et al., 2023).These figures underline the urgency of finding efficient and affordable solutions to improve treatment efficiency and reduce healthcare expenses for better recovery.

On the other hand, silver-based treatment utilized for antimicrobial wound treatment to reduce risk for nosocomial infections has been made possible by advancements in biotechnology (Kalantari et al., 2020). However, these treatments are not without limitations. Long exposure to silver can lead to damaging healthy tissues, which can slow down the healing process (Percival et al., 2005).

Given these limitations, the exploration of natural products, nanomaterials, and plasma-assisted extraction methods created new avenues towards the search for novel therapeutic substitutes for existing treatments.

1.3 *Spirulina maxima*

1.3.1 *Spirulina maxima* as a Source of Bioactive Compounds

Efforts are being made around the world today to isolate new and safe medicinal wound healing solutions (Grosshagauer et al., 2020). Despite the abundance of naturally occurring substances that have significant role in wound healing, microalgae and cyanobacteria have drawn the attention of researchers, turning their interest towards spirulina species such as *Spirulina maxima* which has been utilized in biomedical, food, cosmetics, pharmaceuticals and nutraceuticals (Ragusa et al., 2021).

Spirulina maxima, also known as *Limnospira maxima* a blue-green filamentous, multicellular organism belongs to *Arthrospira* genus a species under the phylum cyanobacteria (Pham et al., 2024). It has a distinct helical form characteristic with 3 to 12 µm thickness and 500 µm length known for its bioactive compounds including c-phycocyanin, anthocyanin and active oligosaccharides, well known for its anti-microbial, anti-inflammatory and antioxidant properties making it an ideal treatment for chronic wound (Figure 2) (Pham et al., 2024).

Figure removed due to copyright restriction.

Figure 2. Cyanobacteria *S. maxima* at 40x magnification. Helical form with 3 to 12 µm thickness, a diameter 10 to 70 µm and 500 µm in length (Jacuinde-Ruíz & González-Hernández,2024)

Even though *Spirulina maxima* has been explored in numerous fields, there are still limited research on how its rich source of bioactive compounds can be utilized for wound healing applications (Marjanović et al., 2024). In addition, *S. maxima* can be used in a variety of alga-based topical preparations, including gels, creams, and dressings, making it able to be used with a wide range of wounds and treatment strategies, which gives an avenue of novel possibilities for future research in wound management (Ragusa et al., 2021).

Figure removed due to copyright restriction.

Figure 3. *Spirulina maxima* in raw and processed forms. **A.)** Filamentous microalgae biomass **B.)** *Spirulina maxima* in powder form (AgriFarming, 2025).

1.3.2 Biochemical Composition of *Spirulina maxima*

Spirulina spp. incudes the well-known *Spirulina maxima* and *Spirulina plantensis*, which possess distinct morphological and ultrastructural characteristics (Grosshagauer et al., 2020). However, *S. maxima* has been chosen for this research as a potential extract for wound-healing for several important reasons.

Like other *Spirulina spp, S. maxima* contains essential compounds that have been reported to have potent bioactive properties, such as rich protein contents (Figure 4) higher than other *Spirulina spp*. (Marjanović et al., 2024). It contains a rich cell growth-promoting properties due to its protein content (55-70%) including all essential amino acids important for wound matrix synthesis such as glycine which is necessary for the synthesis of collagen, proline which promotes tissue regeneration and arginine which enhances the circulation of the blood, polysaccharide (10-20%) that triggers on

immune modulation, lipids (5-10%), essential fatty acids (18%), vitamins, and minerals including vitamin B12, pro-vitamin A (β – Carotene), vitamin E (Tocopherol), iron, and magnesium for tissue strengthening making it highly promising natural treatment for chronic wound infection (Anvara & Nowruzib, 2021).

Figure removed due to copyright restriction.

Figure 4. Biochemical Composition of *Spirulina maxima* (Anvara & Nowruzib, 2021).

One study claims that under ideal growth conditions, *S. maxima* which is among the few dietary sources of gamma-linolenic acid (GLA), exhibits a significantly greater concentration of GLA, a fatty acid that shown an anti-inflammatory action and enhances skin regeneration, ranging from 11-16% in *S. maxima* and 12-14% in *S. plantensis* (Oliveira et al., 1999). However, this may still vary depending on the cultivation processes (Oliveira et al., 1999).

1.3.3 Wound Healing Potential of Spirulina-Derived Bioactive Compound

Wounds can be extremely unpleasant for patients and can also be a significant burden on society (Singh et al., 2017). Following an injury or trauma, the body's natural process of repair and regeneration of damaged tissue is widely referred to as wound healing (Liang et al., 2021). It is characterized by a sequence of complex biological processes such as inflammation, new tissue formation, and remodeling of preexisting tissue (Leaper et al., 2015). To restore skin barrier function, rapid wound closure and prompt regeneration are essential (Singh et al., 2017).

Wound regeneration usually depends on the coordination of four continuous processes including hemostasis (0- 1hr), inflammation (1-3 days), cellular proliferation (4-21 days), and remodeling and maturation phase (21 days-1 year) (Figure 5) (Liang et al., 2021). Dysfunction of any stages results to an impaired wound healing (Landén et al., 2016).

Figure removed due to copyright restriction.

Figure 5. Four Stages of Wound Regeneration. A.) Hemostasis (0-1hr)**, B.)** Inflammation (1-3 days)**, C.)** Cellular proliferation (4-21 days)**,** and **D.)** Remodeling (21 days-1 year) (Liang et al., 2021).

In the inflammatory phase, bioactive compounds like c-phycocyanin have been shown to regulate inflammation-related cytokines, which include TNF-α, IL-1β, and IL-6, and have been proven to lower oxidative stress, which controls excessive inflammation and enhanced immune-mediated modulations (Landén et al., 2016). In the proliferation phase, essential amino acids such as glycine, proline, and arginine stimulate the proliferation of fibroblasts and keratinocytes (Landén et al., 2016). They further enhance stimulating angiogenesis, providing oxygen and nutrients to the recovering tissue and the extracellular matrix, which accelerates tissue regeneration (Landén et al., 2016). In the remodeling stage, tissue alignment and reduction of free radical damage is sustained by polysaccharides and its natural antioxidant (Liang et al., 2021). In the maturation phase, the valuable

vitamins and minerals support more consistent collagen trend while improving tissue strength minimizing fibrosis and chronic wound formation (Landén et al., 2016).

Multiple research studies including Syarina et al. (2015) have revealed that methanol-based Spirulina extract on Human Dermal Fibroblast cells (HDF) can accelerate wound healing. They also performed an in vivo scratch assay, which exhibited an outstanding wound gap closure of 90.3% after 48 hours, compared to 55.2% in untreated controls.

1.3.4 Antimicrobial Potential of Spirulina-Derived Compounds on Wound-Associated Pathogens

Given its abundant, rich composition, *Spirulina spp.* has gained attention due to its interesting pharmacological features, as they can substitute for a synthetic antibiotic which could be promising with less side effects (Breijyeh & Karaman, 2024). *Spirulina spp.* have been proven to possess antibacterial properties against both Gram-positive and Gram–negative pathogens commonly associated with wound infections, which include *S. aureus, P. aeruginosa,* and *Escherichia coli,* among others.

A study by Kaushik and Chauhan (2008) demonstrates methanol-based Spirulina extract exhibited a broad spectrum of activity of 15.21 ± 0.1 mm against *S. aureus*, followed by 12.42 ± 0.47 mm against *E. coli* and 11.55 ± 0.38mm for *P. aeruginosa* and the result of minimum inhibitory concentration was recorded at 128 µg/ml, 256 µg/ml and >512 µg/ml against *S. aureus, E. coli and P. aeruginosa*.

To supplement these results, this demonstrates how effectively bacterial growth is suppressed by Spirulina extract, based on the zone of inhibition where clear diameter around the extract on an agar plate shows no bacterial growth (Hudzicki, 2009). In this case, it has shown a moderately to strong antibacterial potency where 15 mm often indicates a strong antimicrobial activity (Hudzicki, 2009). The MIC value provides a direct comparison of the activity of the extract and compounds and how capable it can inhibit the growth of certain bacteria (Kowalska-Krochmal & Dudek-Wicher, 2021).The lower MIC indicates that extract is more efficient in inhibiting the wound pathogens (Kowalska-Krochmal & Dudek-Wicher, 2021).

1.4 Extraction Techniques

1.4.1 Limitation of Conventional Extraction Methods for Microalgae

Learning about the potential use of *S. maxima* requires understanding the benefits and limitations associated with various conventional extraction methods resulting in low yield, potential degradation, and in some cases, may lead to toxicity (Jaeschke et al., 2021).

Recent advances in the extraction methods include mechanical cell disruptions (e.g. bed milling), Ultrasound-Assisted Extraction (UAE), and Pulse-Electric-Field-Assisted Extraction (PEF) (Jaeschke et al., 2021). These methods have its own advantages and drawbacks, in obtaining the bioactive compounds from the *S. maxima* extract which must be carefully considered.

The mechanical cell disruption methods, such as bead milling, break tough cell walls of microalgae by using a high-speed bead to create shear forces through turbulence, friction and collisions resulting to a high disruption rate efficacy of 80-85% and a biomass disruption capacity of 60-150g/L (Jaeschke et al., 2021). However, it's energy-intensive process can possibly degrade the bioactive compounds in *S. maxima*. In Ultrasound-Assisted Extraction (UAE), involves ultrasonic waves with a frequency of 20 kHz and 2000 kHz (Azwanida, 2015). These waves promote acoustic cavitation, a process in which bubbles form and collapse in a solvent medium, thereby increasing extraction yield (Azwanida, 2015). The advantage of this methods is its shorter processing time and its improved selectivity (Azwanida, 2015). On the other hand, Pulse Electric Field (PEF) uses short pulse of high-voltage, usually 1-60kV/cm, to initiate electroporation, facilitates compounds release. However, UAE and PEF have the possibility of extensive membrane disruption that may compromise the quality of *S. maxima* extracts leading to a reduced extraction yield (Jaeschke et al., 2021).

1.4.2 Enhancing Extraction Efficiency through Plasma-Assisted Mechanism

To maximize *Spirulina's* wound healing potential, it is essential to adopt a novel approach that does not limit its full potential (Jaeschke et al., 2021). To maximize the benefit of the bioactive compounds, present in *S. maxima,* which addresses its inherent limitations, the plasma-assisted mechanism represents a promising avenue for exploration.

Plasma involves the integration of energy into a gas such as nitrogen, argon and oxygen cause atoms to lose their outer electrons and become ionized, resulting in the separation of electrons from atoms

forming a charged ions and free electrons (Figure 6) (Nehra et al., 2008). This process is further enhanced by the production of reactive oxygen species (ROS) and reactive nitrogen species (RNS) during the process, which contributes to the cell wall disruption (D'Angola et al., 2022).Plasma-assisted extraction mechanism combines reactive ions, such as NO, NO_2, O_3, H_2O_2, OH etc., electrons, and radicals to precisely control disruption, by breaking important peptidoglycan bonds, such as C-O, C-N, or C-C bonds, enhancing extraction yield by 15-40% over the conventional method (Heydari et al., 2023).

There are two main classifications of plasma processes, where the temperature of various forms differs. First is the thermal plasma, which works in the highest energy densities (thermal equilibrium) (D'Angola et al., 2022). The atmospheric pressure plasma, also known as the non-thermal plasma, is mainly associated with its pressure condition (Nehra et al., 2008). The major drawbacks of thermal plasma are its extremely high gas temperatures, which result in severe quenching requirements and electrode issues that restrict the energy efficiency (D'Angola et al., 2022).

For these reasons, non-thermal plasma, such as dielectric barrier discharges (DBD) and atmospheric pressure plasma jet (APPJ), which have their unique characteristics and applications, has been utilized because of their excellent selectivity in plasma processes, ability to function at low temperatures, and lack of quenching and most specially making it ideal for delicate processes where heat sensitivity is a concern (Nehra et al., 2008).By utilizing ionized gas at a lower temperature, the atmospheric plasma approach is suitable for sensitive applications such as the extraction of *S. maxima* bioactive compounds.

Figure removed due to copyright restriction.

Figure 6. Plasma: The Four State of Matter. An Ionized gas from solid, liquid and gas state (Nehra et al., 2008).

1.4.3 Plasma-Assisted Extraction: Atmospheric Plasma Treatment Technology using Dielectric Barrier Discharge and its Application in Current Research

Plasma treatment technology has been highly beneficial because of its significant breakthroughs in diverse scientific areas. Recently, incorporation of plasma treatment to microalgae is gaining significant interest due to its promising potential (D'Angola et al., 2022). However, this approach needs further validation.

Among several approach of non-thermal plasma, recent research by Pham et al. (2024) a novel sustainable Argon Atmospheric Plasma Jet (Ar-APJ) technology was utilized to selectively disrupt the robust polysaccharide fragment in the cell wall of *S. maxima* directly in contact, close to the plasma jet nozzle (Figure 7). In this approach, a thin film made from *S. maxima* was used as an implant coating. Based on the results, plasma treatment induced 70-80% reduction of bacterial biofilm biovolume against *S. aureus* and *P. aeruginosa* while biofilm thickness reduction reached up to 75%. Furthermore, its antibacterial efficacy increases by 73% and 93% for *S. aureus* and *P. aeruginosa*. These findings suggest that the plasma-assisted thin-film layer promotes the release of C-phycocyanin overtime, which helps to kill bacteria and to prevent formation of biofilm.

Figure removed due to copyright restriction.

Figure 7. Schematic Illustration of Argon Atmospheric Plasma Jet System (Ar-APJ). A.) Optical emission spectroscopy characterization system **B.)** Outlet design of the plasma jet reactor (Pham et al., 2024).

Despite AR-APJ efficacy, a different non-thermal approach, using a dielectric barrier discharge (DBD) model, has been chosen for this research due to its broader and uniform plasma exposure over surfaces, reducing direct thermal damage (Monfaredi et al., 2024).

In this research, a customized atmospheric plasma treatment chamber system using a DBD technology setup will be developed to treat *S. maxima* biomass which a costly vacuum chamber and pumping station are not essential to atmospheric-plasma processes, providing a simpler configuration and straightforward design (Li et al., 2019). This provides an advantage of better control over treatment parameters while preserving the integrity of delicate bioactive compounds in *S. maxima* extract.

1.5 Optimizing Plasma-Assisted Extraction – Key Parameters

1.5.1 Key Parameters – Voltage Level, Treatment Time, Salt (NaCl) concentration

In this research, voltage level (kV), treatment time (min) and salt (NaCl) concentration (g/L) are essential factors to take into consideration. These key factors are essential to determine the bioactivity and extraction efficiency of the optimized *S. maxima* extract. However, understanding the concept how these parameters influence extraction outcomes is essential (Figure 7).

According to a recent study Monfaredi et al. (2024), dielectric barrier discharge (DBD) plasma treatment with argon as a gas was used to enhance the total phenolic content from arabica coffee subjecting to two different voltage (12 and 18 kV) in four treatment time periods (4,8,12, and 16 min). The result revealed a complex, non-linear connection between voltage level and treatment time. In a lower plasma strength (12 kV), An initial decrease by 15.59% after 4 minutes, and an increase by 14.82% at 8 minutes and a sudden decline over a longer duration was observed. In a higher plasma strength (18 kV), optimal extraction of TPC was achieved at 4 min, yielding about 29.34% improvement compared to the control. These results suggested that precision control over treatment processes is essential to achieve the best result for optimization. In the context of *Spirulina spp*., insufficient or excessive control of key parameters can result in alteration of plasma reactivity, leading to a possible risk of degradation of the compound if not properly optimized.

On the other hand, salt when dissolved in water (NaCl) is considered to be a good electric conductor due to the mobility of its ions (Zhang et al., 2022).This parameter promotes plasma-liquid interactions in the plasma-treated saline solution, which facilitates plasma energy transfer resulting to generation

of RONS enhancing an effective cell wall disruption leading to a strong antimicrobial potential (Zhang et al., 2022). Salt is also essential in regulating osmotic pressure since it creates stress on the cell membrane which results to release certain intracellular compounds depending on its salt concentration (Zhang et al., 2022). Therefore, precise fine-tuning of the key parameters is essential in achieving maximum yield efficacy of the *S. maxima* extract.

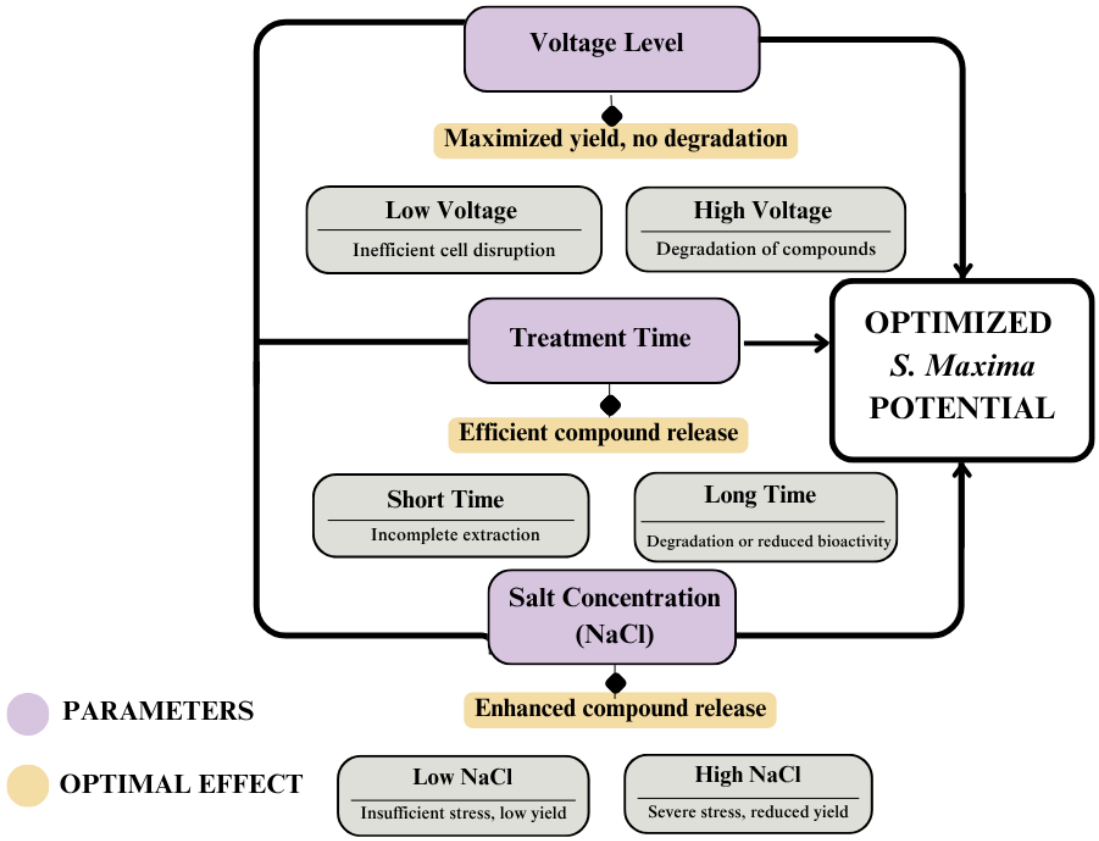

Figure 8. Influence of experimental parameters on optimized *S. maxima* potential.

1.6 Central Composite Design – Design Expert Software

1.6.1 Application of Central Composite Design in Optimization Extraction Efficiency

Optimization is significant when establishing an efficient extraction process, particularly when obtaining a bioactive compound from natural sources (Weremfo et al., 2023). Simple linear and interaction models are insufficient (Njoku & Otisi, 2023). Therefore, more advanced techniques such as Response Surface Methodology (RSM) are utilized to simulate such processes.

An experimental design called the Central Composite Design (CCD) concept, also known as Box-Wilson central composite design, is one of the most widely used experimental designs under RSM

(Njoku & Otisi, 2023). CCD has emerged and has been very handy as part of the optimization process due to its accuracy, not only to evaluate linear effects but also to capture quadratic and interaction effects among variables(Njoku & Otisi, 2023). The main objective of optimization is to minimize unfavorable or undesired outputs and maximize the desired outputs (Weremfo et al., 2023).

In RSM, the relationship between the response and independent variables is commonly represented by a General Second-Order Polynomial Equation (Equation 1) (Hadiyanto & Adetya, 2018).

Equation 1 General Second-Order Polynomial Equation in Response Surface Methodology (RSM) for process optimization.

$$Y = \beta_0 + \beta_1 X_1 + \beta_2 X_2 + \beta_3 X_3 + \beta_{11} X_1^2 + \beta_{22} X_2^2 + \beta_{33} X_3^2 + \beta_{12} X_1 X_2 + \beta_{13} X_1 X_3 + \beta_{23} X_2 X_3$$

In this model, Y represents the response variable, X1, X2, X3 correspond to the voltage level, treatment time, and salt (NaCl) concentration, b0 is the intercept constant, b1, b2, b3 are the linear coefficient, b11, b22, and b33 are quadratic coefficient, and b12 and b13, and b23 are interaction coefficient for each variable. These summarizes the influence of each factor and its interactions on the overall response (Hadiyanto & Adetya, 2018).

Based on a relevant study by Hadiyanto and Adetya (2018), CCD and RSM are beneficial in optimizing the extraction of lipids and proteins from *Spirulina platensis* employing an ultrasound-assisted osmotic shock technique. They used a Second-Order Polynomial Equation (Equation 1) for maximizing yield to model salt (NaCl) concentration, extraction time, and solvent to biomass ratio. This study established a solid foundation for using CCD in optimization processes involving *Spirulina spp.*

In this research, CCD is ideal to generate a mathematical model to predict and optimize parameters like voltage level, treatment time, and salt (NaCl) concentration during plasma-assisted extraction. The Design expert software is used for this research for its CCD functionality, to maximize the bioactivity of *S. maxima* while minimizing the experimental effort needed to evaluate the effects of multiple factors, ensuring correct statistical analysis, which can be generated in a surface/contour plot for visualizing how different factors influence the antibacterial yield to easily identify optimal conditions with reduced experimentation needed (Pinto et al., 2021).

1.7 Antibacterial Capacity of *Spirulina maxima*

1.7.1 Antibacterial Activity Assessment – Colony Forming Unit (CFU) Assay

CFU assay evaluates the number of viable bacterial cells (CFU/ mL) capable of forming colonies, a cluster of bacteria adhering to the treatment under particular growth conditions (Pochampally, 2008), making it an excellent option for evaluating the antibacterial potential of the optimized *S. maxima* extract.

To determine the number of the CFU, bacterial cultures are dispersed onto a semisolid medium by multiple dilutions form the initial sample (Bhuyan et al., 2023).Various studies have employed this assay for evaluating the antibacterial potential of *Spirulina spp*. In a recent study by Selim et al. (2025),the antibacterial potential of *S. maxima* extract was evaluated against *K. pneumoniae*, a predominant Gram -negative bacterium using CFU assay. The result shows a significant reduction of CFU counted which inhibited biofilm formation by 68.75%, suggesting an antibiofilm potential of optimized *S. maxima* against the tested carbapenem-resistant *K. pneumoniae*.

1.8 Antioxidant Activity of *Spirulina maxima*

1.8.1 Principles of Antioxidant Assay – 2,2-diphenyl-1-picrylhydrazyl DPPH Radical Scavenging Assay

S. maxima containing phenolic-rich compounds like tocopherols and β-carotene with antioxidant properties, can promote the function of the cells involved in tissue regeneration including fibroblasts and monocytes, reduction of inflammation, and protection from oxidative stress which is mostly associated with high levels of free radicals that may damage healthy tissues and slows down the healing process (Agustina et al., 2021).

According to a study by Miranda et al. (1998), *S. maxima* has exhibited a potent antioxidant activity yielding IC_{50} value of 0.18 mg/mL, indicating a notable free radical scavenging activity of 71% increase in plasma antioxidant capacity compared to a 54% increase from the control indication its strong antioxidant potential in wound healing.

In this research, the antioxidant activity of the optimized *S. maxima* extract is evaluated using the DPPH assay, a simple, rapid and precise assay where neutralization of naturally purple DPPH free radical produce a shift of pale yellow indicating the presence antioxidants from *S. maxima* extract

(Thaipong et al., 2006).Trolox which has a well-established antioxidant profile is used as a standard reference for the antioxidant activity (Thaipong et al., 2006).While not our main focus, this assay will serve as a supplementary method that supports broader investigation into wound healing.

1.9 Potential Application in Wound Healing

1.9.1 Potential Application of Optimized *S. maxima* Extract in a Hydrogel Matrix

After the optimization process, extracts will be potentially combine with a hydrogel matrix, a hydrophilic polymer network, not only due to their resilience in an aqueous environment, but also suited for moist wound conditions (Liang et al., 2021). It also has an appropriate three-dimensional (3D) porous surface microstructure like extracellular matrix (ECM), similarly found around cells in the body (Rosiak & Yoshii, 1999).

Hydrogel matrices are made from various natural hydrophilic polymers like chitosan, alginate, dextran, and proteins like collagen and gelatin, and synthetically made ones like ethylene glycol (PEG) and polyacrylamide (PAM) promotes cell adhesion, structural support for tissue, and regulate cell processes, making it a competitive candidate for wound applications (Yang et al., 2018). Incorporation of hydrogel matrices can be applied through synthetic wound care dressings, antibacterial bandages, implants, drug delivery systems such as transdermal system and polymeric systems, dental and ophthalmic applications (Yang et al., 2018).

1.10 Gap of knowledge, Aim, Hypothesis, and Novelty of the Research Project

1.10.1 Gap of knowledge

Previous research has shown that plasma-assisted treatment of *Spirulina maxima* can gently disrupt its cell wall into a thin-film coating that promotes the release of bioactive compounds without compromising its integrity (Pham et al., 2024). However, precise plasma parameter settings has been left undiscovered and further investigation are needed for its clinical requirement. Therefore, determining the precise variations in plasma-assisted extraction parameters, including voltage level (kV), treatment time (min), and NaCl concentration (g/L) is essential to identify the optimized parameter settings to maximize the bioactivity for improved therapeutic outcomes for further wound healing applications.

1.10.2 Research question

The research question is “how do variations in plasma-assisted extraction parameters including voltage level (kV), treatment time (min), and NaCl concentration (g/L) influence the yield and bioactivity of plasma-treated *Spirulina maxima* extract for potential wound healing applications?”.

1.10.3 Research aims

Aim 1: To comprehensively determine the optimal plasma processing parameters including voltage level (kV), treatment time (min), and NaCl concentration (g/L) for plasma-assisted extraction of *S. maxima*-derived bioactive compounds

Aim 2: To evaluate and measure the spectrum of antibacterial activity of the optimized plasma-treated *S. maxima* against a variety of clinically relevant Gram-positive and Gram-negative pathogens, including isolates of *S. aureus*, *S. epidermidis, P. aeruginosa*, and *E. coli.*

1.10.4 Research Hypothesis

By fine-tuning plasma-assisted parameters, the extraction of *Spirulina maxima* bioactive compounds can be enhanced, leading to more potent antibacterial and antioxidant properties for improved therapeutic outcomes for wound healing applications.

1.10.5 Significance of the Research to Biotechnology

While this research addresses gaps in optimal extraction and bioactivity evaluation of *Spirulina maxima* for wound care applications, future studies may build upon the optimized results to provide sustained release of the optimized bioactive compounds at the wound site, that may enhance healing reducing reliance on conventional antibiotics while minimizing the risk of chronic wound infection leading to more sustainable wound care applications. By integrating innovative plasma-assisted technology, it contributes to biotechnology by innovating a new method that may significantly answer clinical needs and future biomedical solutions.

CHAPTER TWO: METHODOLOGY

2.1 Experimental Protocol Overview and Materials

This research was conducted at the Biomedical Nanoengineering Laboratory (BNL) at Flinders Medical Centre (FMC).

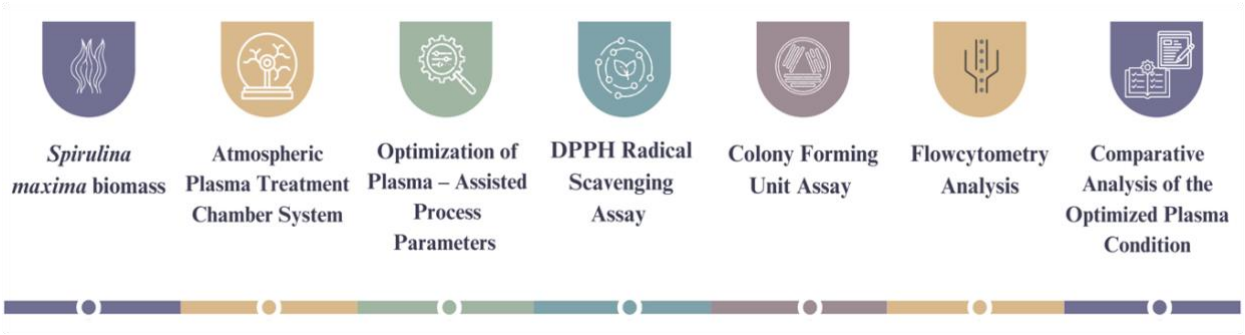

Figure 9. Summary of methodology from *Spirulina biomass* preparation, to incorporation and optimization of plasma-assisted process parameters for extraction of maximal CPC concentration into the atmospheric plasma treatment chamber system, to assess the wound healing capacity of plasma-assisted extraction of *Spirulina maxima*.

Analytical grade chemicals were used throughout this research. *Spirulina maxima* biomass was supplied by OXYMIN® SPIRULINA. Other reagents includes Trolox (Sigma-Aldrich); DPPH-2,2 diphenyl-1-picrylhydrazyl (Sigma-Aldrich); Sodium Chloride NaCl (Sigma-Aldrich); Methanol (Sigma-Aldrich). Bacterial strains used were *Staphylococcus aureus* (ATCC 25923); *Escherichia coli* (ATCC 25922); *Pseudomonas aeruginosa* (ATCC 15692); *Staphylococcus epidermidis* (ATCC 12228). Fluorescent dyes includes SYTO 9 (Thermo Scientific); Propidium Iodide-PI (Thermo Scientific). Culture media and buffers used includes Phosphate-Buffered Saline-PBS (Sigma-Aldrich); Tryptic Soy Broth-TSB (Sigma-Aldrich). Detailed information on the experimental reagents, culture media, fluorescents dyes, staining reagents and buffers along with manufacturer and its main application and purpose in the research were presented in the appendices under Table 10, 12, 13. Bacterial strains used in CFU enumeration and flow cytometry analysis were listed in appendices Table 11,while laboratory consumables, equipment, and software used were found in appendices Table 14,respectively.

2.2 *Spirulina maxima* biomass preparation

The microalgae with a concentration of 1 mg/ml was suspended in distilled water. Approximately 50 mg of *Spirulina maxima* biomass powder was weighed into each 50 mL centrifuge tube for the plasma treatment designed for each run.

2.3 Operation of Atmospheric Plasma Chamber System

A customized atmospheric plasma treatment chamber system using a DBD technology setup was used to treat *S. maxima* biomass. The cylindrical quartz glass plasma chamber setup featured an outside diameter of 40mm and an inside diameter of 36 mm, includes a plasma-generating region, an air input/output system, a thermoplastic polyurethane (TPU) seal block, and a branched airway that works together to regulate the flow and ensure efficient plasma generation during plasma treatment process (Figure 10). The chamber involves two electrodes separated by a dielectric barrier, applying an alternating electric distribution for the *S. maxima* sample with sufficient amplitude to a flow of air, sustaining DBD in a narrow gap between two parallel glass tubes positioned outside the discharge chamber not in contact with the plasma preventing arc formation (Kogelschatz, 2003). It functioned by subjecting a nitrogen gas with a flow rate of 1 L/min to a high-voltage of electric discharge, which enabled the nitrogen gas to ionize and generate plasma requiring more energy per unit volume of gas from plasma formation (Kogelschatz, 2003).

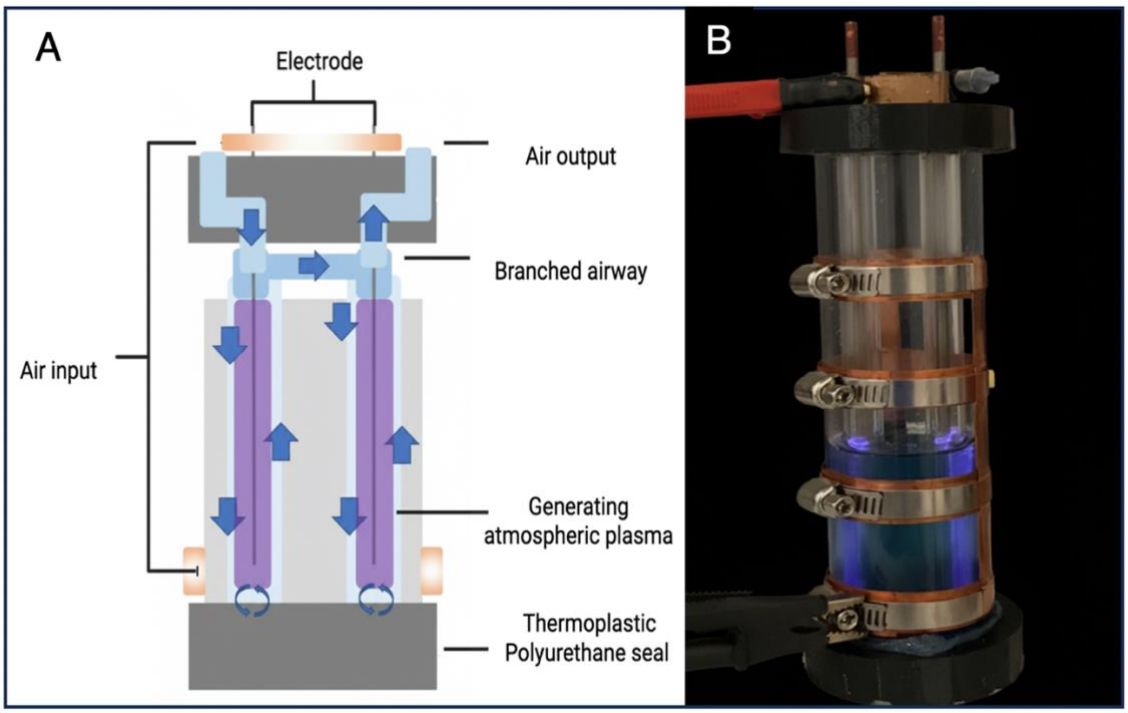

Figure 10. Atmospheric plasma treatment chamber system. A.) Schematic illustration of atmospheric plasma treatment chamber system using Dielectric Barrier Discharge DBD showing the two electrodes, plasma generating area, air input and output, branched airway, and seal. **B.)** Biomedical Nanoengineering Laboratory BNL in-house atmospheric plasma treatment chamber system using Dielectric Barrier Discharge DBD with actual optimized *Spirulina maxima* extract.

2.4 Central Composite Design – Design-Expert Software

Central Composite Design (CCD) was applied as an optimization strategy to explore and investigate the influence of multiple plasma treatment factors on the response variable, such as CPC

concentration. The Design-Expert software was utilized for this study to fine-tune the CCD model functionality, minimizing the number of experiments needed (Pinto et al., 2021).

To determine the optimum conditions, three process independent variable were considered: (A) voltage level , (B) treatment time, and (C) salt concentration. A total of 18 plasma runs, with varying process parameters, were designed and conducted using CCD to optimize the plasma treatment parameters and efficiently fit in a quadratic model, evaluating linearity and quadratic interaction between the individual and response variable.

Central Composite Design (CCD) is based on two level factorial design which consists of three types of experimental point, including the embedded four factorial design points with center points (0,0), and axial star points (0,+ α), (+α,0) (Montgomery et al., 2021). The four factorial design points (+1/-1) represents the combination where each factor is at its high (+1) and low (-1) levels, covering all possible extremes. The center points (0,0) correspond to the midpoint average level of all factors, including a group of axial star points (0,+ α), (+α,0) that allows estimation of curvature or the quadratic effects to capture non-linear influences (Montgomery et al., 2021). While the star points represents extreme low and high values for each factor, enhancing design predictive power (Montgomery et al., 2021). This combination of point in the experimental framework enables a robust model fitting and predictive optimum conditions for the atmospheric plasma treatment (Figure 10).

Figure removed due to copyright restriction.

Figure 11. A classic central composite design CCD graphic representation for two-factorial experimental design (Veza et al., 2023).

2.4.1 Minimum and Maximum Ranges of the Three Experimental Variables

A minimum and maximum value for each parameter: Voltage level (3kV-7kV), treatment time (1min-10 min) and salt concentration (0g/L-1g/L) were selected based on previous literature, and preliminary experimental trials. These ranges were fed into the Design Expert software to generate the table of experiments as the software output ensuring adequate coverage of the experimental space for reliable optimization of the response variable (Table 1) (Hadiyanto & Adetya, 2018).

Table 1. Minimum and maximum ranges of the three experimental variables; voltage level, treatment time and NaCl concentration for CCD optimization approach.

Experimental Parameter	Minimum	Maximum
Voltage level (kV)	3 kV	7Kv
Treatment Duration (min)	1 min	10 min
Salt (NaCl) Concentration	0 g/L	1g/L

2.4.2 Table of Experiment

The table of experiments or the design of experiments (Table 2) served as a design plan that dictated the combinations of plasma parameter variations that are required to establish a relationship between the individual parameters and determine its optimal combination for a randomized run order for unbiased execution for succeeding analysis and optimization.

Table 2. Table of Experiment from Data Expert Software version 13.

In this study, three main concentrations were used, 0.5g/L, 1g/L and 1.3409 g/L for the preparation of NaCl concentration based on the table of experiment. Run 1 and run 8 indicated negative values, these negative concentration values were not physically possible therefore, were excluded from the experimental setup (Ghelich et al., 2019).

2.4.3 Principles of Fit Statistics

The principle of fit summary was used to select the correct starting point for the final model; the suggested model should be considered a good starting point for the model fitting (Stat-Ease, 2025). The key fit statistics such as $R^{2,}$, adjusted R^2, predicted R^2, adequate precision, and standard deviation assessed how reliably each model fits the data within the design space (Stat-Ease, 2025). These fit statistic values were analyzed based on the experimental data generated by the Central Composite Design (CCD).

The key fit statistics commonly used in Central Composite Design (CCD) to ensure predictive quality data, reliable interpretation, and results within the design space were well defined and summarized below (Table 3):

Table 3. Interpretation of Key Model Fit Statistics (Stat-Ease, 2025)**.**

Fit Statistics	Interpretation	
R^2 (Coefficient of Determination)	How well your model explains the data	Value closer to 1 indicates a better fit; A low R^2 indicates an individual variation
Adjusted R^2	Provides more realistic measurement for the model performance	Value >0.8 are desirable
Predicted R^2	Measures how well the model predicts new data	Negative values indicate a poor prediction
Adequate Precision	Signal to noise ratio	Value > 4 indicates an adequate signal for prediction
Standard Deviation	Variation of residual error	Lower value indicates more precise and reliable model

2.4.4 Principles of Normal Plot Residuals Predicted vs. Actual from Design Expert Software

Design expert software was used in this research to validate and ensure the quality of the fitted regression model, assessing how well or how poor a model represents the experimental data (Njoku & Otisi, 2023). The regression model explains the relationship between dependent and independent variables within the design space. Residual explains the differences between the predicted values by the regression model and the actual response values from the experiment (Njoku & Otisi, 2023). The predicted vs actual was examined to assess the relationship how close the model's predicted values were to the actual experimental results (Stat-Ease, 2025). Data points near the diagonal line in the predicted vs actual plot indicates a strong agreement between predicted and actual experimental result which then supports the current model accuracy (Stat-Ease, 2025).

2.5 Integrated Atmospheric Plasma Chamber System for Enhanced CPC quantification of *Spirulina maxima*

For each plasma treatment run, approximately 50 mg of *Spirulina maxima* biomass powder was weighed into a 50 mL centrifuge tube. Afterward, 50 mL of NaCl solution, prepared by dissolving the required amount of NaCl in distilled water according to the design plan, was added to each centrifuge tube containing *S. maxima* powder. Based on table of experiments from the Data Expert software, the corresponding NaCl concentration was prepared and added to each sample. Each solution was placed into the atmospheric plasma chamber and set the appropriate voltage level to the specified treatment duration were set precisely as specified for each run and, the treatment process was repeated for all remaining runs, ensuring accurate plasma treatment conditions. The precise control of the plasma treatment parameters enhanced the reliability and accuracy of CPC quantification in *S. maxima* (Figure 12).

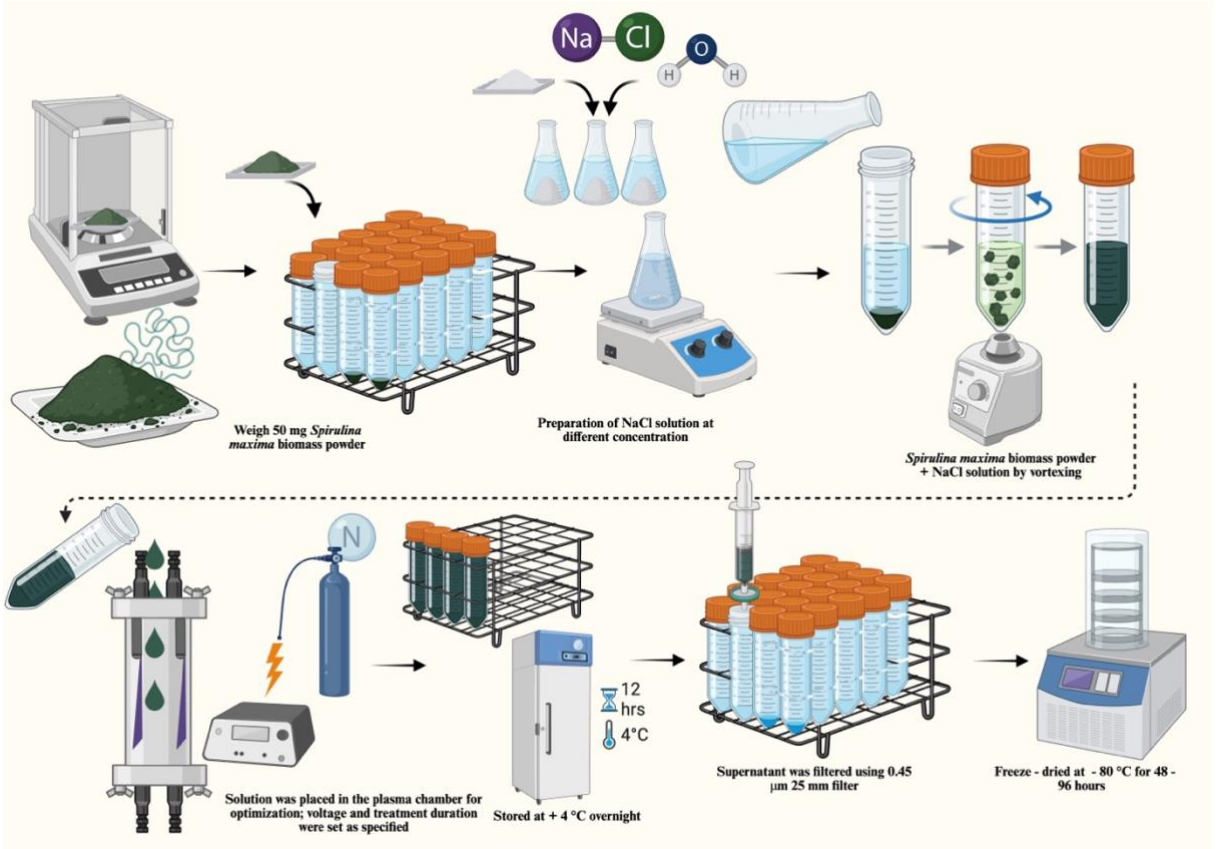

Figure 12. Schematic Illustration of the optimization process of *Spirulina maxima* for CPC concentration.

2.5.1 Post -Treatment Analysis

After plasma treatment, the plasma-treated samples were stored at + 4 °C overnight to preserve samples integrity. The supernatant was filtered using 0.45 µm filter (Agilent Technologies) and was freeze-dried at -80 °C for 48–96 hours to maintain and preserve the bioactivity of CPC and other bioactive compounds for further analysis (Figure 13). The content of c-phycocyanin concentration in each plasma run sample was measured and assessed using UV/VIS Lambda 365 (PerkinElmer) spectrophotometer at 620 nm (Figure 13).

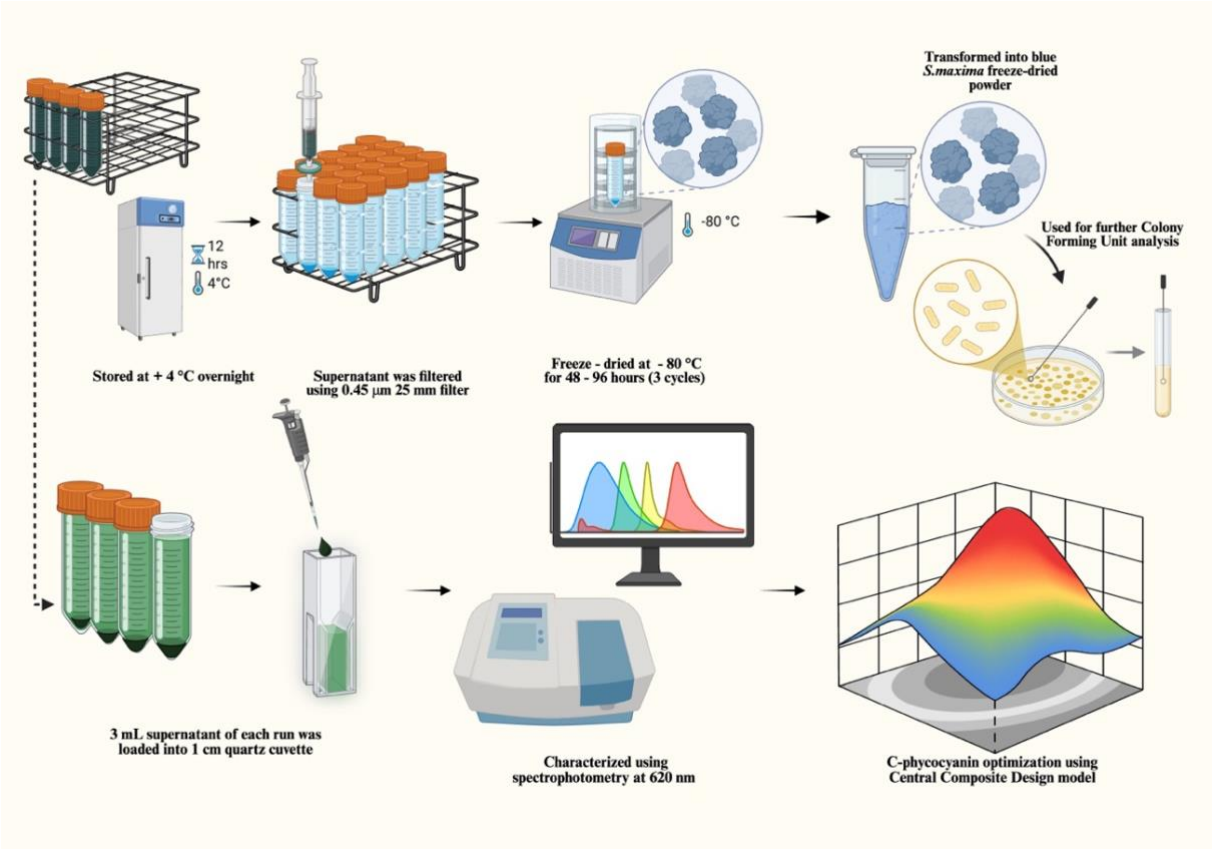

Figure 13. Schematic Illustration of the post treatment analysis process for *S. maxima.*

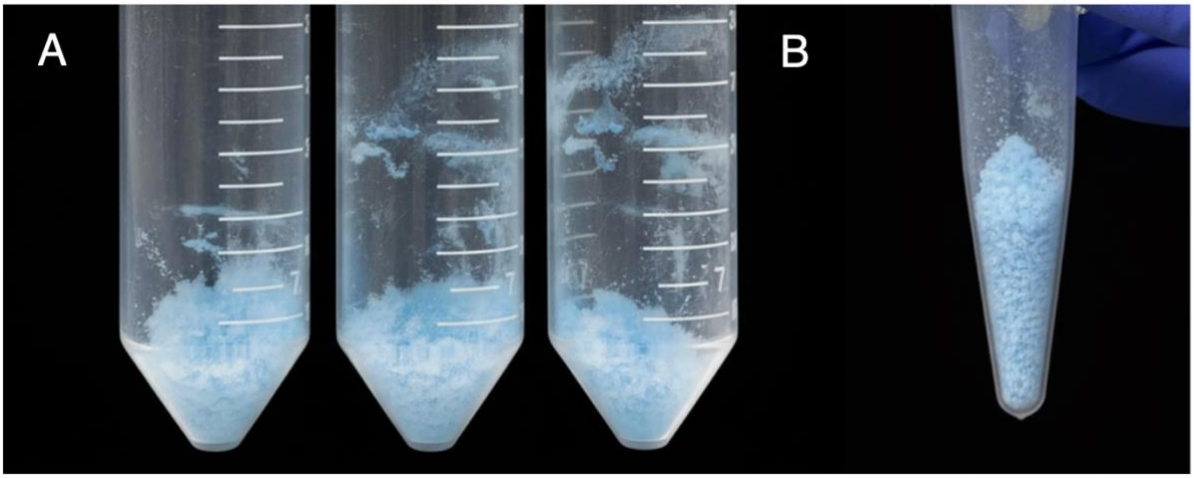

Figure 14. Actual plasma-treated freeze-dried *Spirulina maxima* sample in **A.)** 50 mL centrifuge tubes and **B.)** an Eppendorf tube.

2.6 Morphological Analysis of *Spirulina maxima* cell wall exposed to atmospheric plasma using Dielectric Barrier Discharge

2.6.1 Scanning Electron Microscopy (SEM)

2.6.1.1 Principle of SEM technique

Scanning Electron Microscopy (SEM) is a highly versatile technique that produces high precision image that specifically uses a highly-focused electron beam giving a high spatial resolution around 1nm for fine surface details allowing detailed visualization with a gray-scale images (Figure 15) (Nanoscience Instruments, 2025). The electron gun generates a beam of electrons of high energy in the range of 1,000 to 30,000 electron volts (eV) into a fine beam condenser lenses (Zhou et al., 2006). This electron beam is focused through the condenser lens and scanned over the sample surface by an electromagnetic scan coil to produce signals, mainly the secondary electrons to reveal sample in terms of morphology, topography, crystallography, grain orientation, composition and structural components with a nanoscale resolution (Akhtar et al., 2018).

Figure removed due to copyright restriction.

Figure 15. Scanning Electron Microscopy (SEM) A.) Schematic representation of the main parts of SEM **B.)** FEI Quanta F50 SEM machine (Thermo Fisher Scientific, Waltham, MA, USA).

2.6.1.2 Experimental details

In this study, the morphological structure of the optimized plasma-treated *S. maxima* was analyzed under FEI Quanta 450 SEM (Thermo Fisher Scientific, Waltham, MA, USA). Prior to the SEM examination, dried samples were mounted onto an aluminum specimen stubs and samples were coated with a thin layer of platinum using Ion Sputter Coater (TB SPUTTER, Quorum Technologies, UK) and carbon adhesive tape to enhance electrical conductivity during imaging. Morphological analysis of the optimized plasma-treated *S. maxima* was performed at a working distance of 11.2 mm working on an accelerating voltage of 10 kV. The imaging was conducted using a magnification of 6000 x with a specimen stage positioned at 0° horizontal plane, providing a sufficient resolution to efficiently characterize cell wall morphology and structural changes in the *S. maxima* filaments. Images were captured on a horizontal field width of 24.9 μm and 49.7 μm using the Everhart-Thornley detector (ETD) for secondary electron detection to have a highlight detailed surface topography.

2.6.2 Epifluorescence Microscopy

2.6.2.1 Principles of Epifluorescence technique

Epifluorescence Microscopy (EFM) is a kind of fluorescence imaging technique in which an intense multispectral light source used to stimulate a fluorescent molecule called fluorophore markers. These fluorophores absorb photons, causing electrons to move to a higher energy state. The excitation light was reflected from an angle of dichroic mirror and passed through the excitation and emission filter with appropriate band passes which blocked unwanted excitation wavelengths to illuminate within a sample. This produced a high-contrast images of target structure with high level of specificity achieving spatial resolution of 5-10 μm with a maximum of 100 μm thick and 0.1 mm depth (Figure 16) (Behbahaninia et al., 2013).

Figure removed due to copyright restriction.

Figure 16. Epifluorescence Microscopy EFM A.) Schematic representation of the main parts of Epifluorescence **B.)** Olympus IX83 EFM (Olympus Corporation, Tokyo, Japan).

2.6.2.2 Experimental Details

In this study, the morphological structure of the optimized plasma-treated *S. maxima* was analyzed using Olympus IX83 EFM (Olympus Corporation, Tokyo, Japan). Prior to EFM examination, a portion of dried sample was dissolved to a concentration of 0.1 mg/ml in distilled water, was placed into a glass slide and was air-dried to form a thin layer. The slides were stained with 0.01% calcofluor white (Sigma-Aldrich, Inc., Sanit Louis, USA) and 10% potassium hydroxide, which dissolved debris that could hinder fluorescence signal and increased visual sensitivity (Haldane & Robart, 1990). Morphological analysis of *S. maxima* was performed using a 60x objective lens (scale bar = 20 μm) and, 100x oil immersion lens (scale bar =10 μm) for higher magnification imaging. The dichroic mirror was positioned at a 45° angle, to efficiently reflect excitation light, provide sufficient resolution, and allow emitted fluorescence to reach the detector, enabling efficient characterization of cell wall morphology and structural changes in the *S. maxima* filaments.

2.7 DPPH Radical Scavenging Assay for Antioxidant activity

In this research, the antioxidant activity of the optimized *S. maxima* extract was evaluated using the DPPH radical assay (2,2-diphenyl-1-picrylhydrazyl), a simple, rapid and precise assay where neutralization of naturally purple DPPH free radical produced a shift of pale yellow indicating the presence antioxidants from *S. maxima* extract (Thaipong et al., 2006). This occurred when antioxidant compounds donates a hydrogen atom to the DPPH radical causing neutralization and resulting in the formation of hydrazine (DPPH-H) (Thaipong et al., 2006).

To prepare the DPPH stock solution, 2.4 mg of DPPH powder was dissolved into 10 ml methanol, and stock 1 was diluted into 45 ml of methanol to prepare the working solution. For the assay, 15 µl of the plasma sample extract and 285 µl of the DPPH working solution were added into a 96 - well microplate in triplicate. The plate was gently mixed, covered by an aluminum foil due to its light sensitivity, and incubated at 37 °C for 24 hours. Trolox, which has a well-established antioxidant profile, was used as the standard reference for the antioxidant activity (Thaipong et al., 2006). To prepare for the stock solution, 0.04 mg of Trolox was dissolved in 1 ml of methanol to achieve concentrations of 0.16 µm, 0.08 µm, 0.04 µm, 0.02 µm , 0.01 µm, 0.005 µm. 0.0025 µm, 0.00125 µm (Figure 38). The plate set-up included plasma samples (18 runs), blank sample (2 untreated), and a control that served as a baseline to measure the maximum absorbance of DPPH radical without any antioxidant present. Absorbance was measured using a Spectrophotometer Synergy-HTX multi plate reader (Biotek) at 515 nm wavelength (Figure 17). The results were expressed in µM Trolox Equivalent/g biomass (TE/g), and scavenging activity was determined by the formula presented below:

$$\textbf{\textit{Scavenging activity}} = \left(\frac{Absorbance\ of\ control - sample}{Absorbance\ of\ control}\right) * \mathbf{100}$$

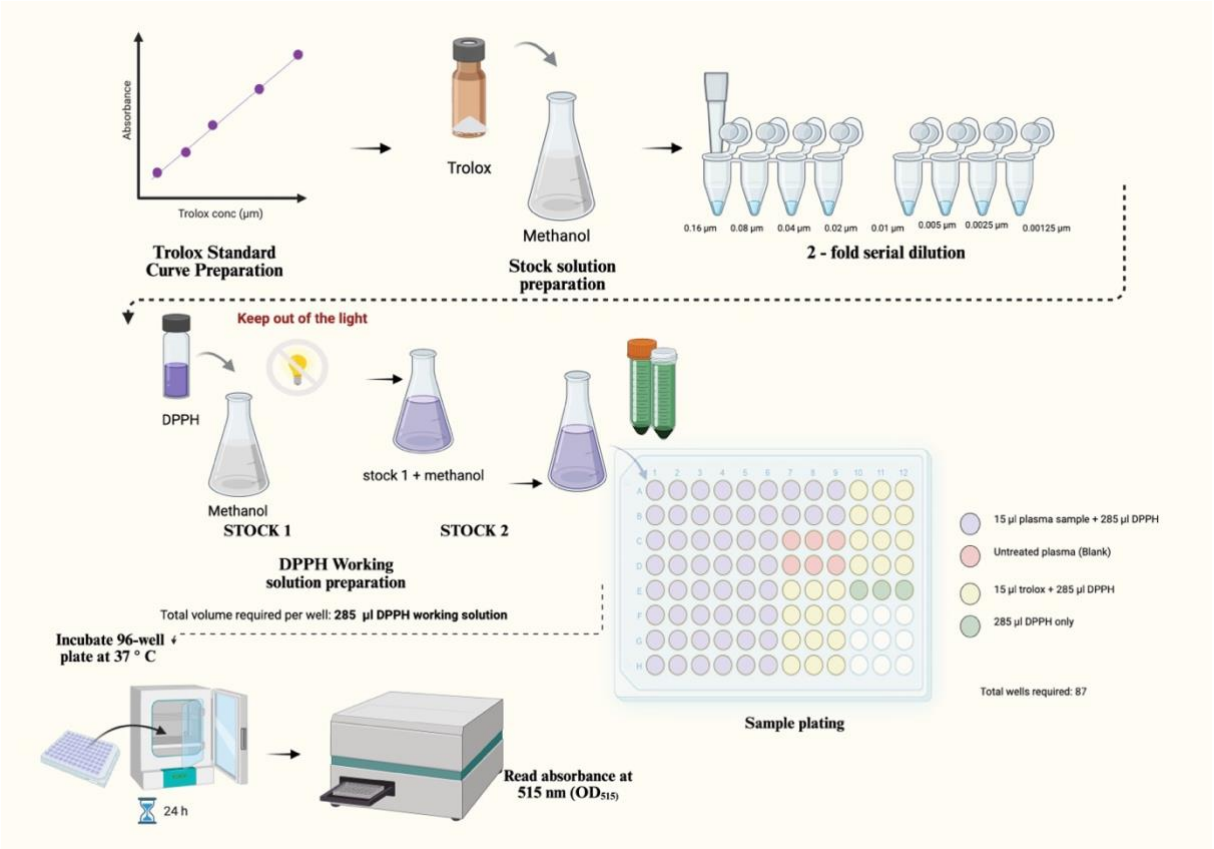

Figure 17. Schematic Illustration of the DPPH radical scavenging assay process.

2.8 UV-Vis Spectrophotometry to determine released C-phycocyanin concentration

2.8.1 Principles of UV-Vis

Ultraviolet (UV)-visible (VIS) spectroscopy was employed to quantitatively analyze CPC concentration. This analytical method used a light source to illuminate a sample with light across the ultraviolet to visible wavelengths, typically between 200-800 nm, and measured the absorbance spectra through the sample compared to the standard reference or a blank (Vogt et al., 2023). For C-phycocyanin (CPC), a visible range of 615-620 nm corresponds to the maximum absorbance peak, offering the greatest sensitivity wavelength for its detection (Na et al., 2025). A schematic layout of a UV - VIS spectrophotometry was illustrated in Figure 18, including the light source, double monochromator, sample cuvette, and detector.

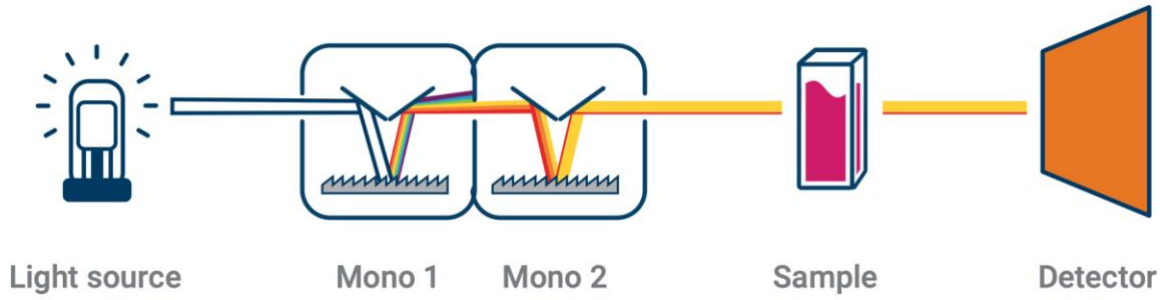

Figure 18. Schematic layout of a UV – VIS spectrophotometer including the light source, double monochromator, sample cuvette, and detector.

According to Beer-Lambert principles, absorbance **(A)** is directly proportional to the concentration **(c)** of the absorbing molecule, path length **(l)** or how far the light travels through sample, and the molar coefficient (**ε**) or how strong it absorbs the light. Therefore, the amount of light absorbed at CPC's maximum peak wavelength is directly proportional to CPC concentration in a specific sample.

$$A = \varepsilon cl$$

This method is chosen for this study due to its reliable and non-destructive nature which allows rapid quantification however, to have an accurate measurements, it requires consistent sample preparation, and appropriate solvent condition (Vogt et al., 2023).

2.8.2 Experimental details

To determine and measure the CPC concentration of each plasma run, each supernatant was collected and transferred into a quartz cuvette (1 cm path length), and a sample volume of 3 mL was loaded into the cuvette. The absorption spectra were measured using UV/VIS Lambda 365 (PerkinElmer) at 620 nm wavelength. This instrument used a deuterium lamp and tungsten lamp with a slit width of 1.0 nm to ensure spectral resolution (Vogt et al., 2023). The cuvette was thoroughly rinsed with distilled water before loading a new sample to ensure consistent absorption readings. Measurements were performed in triplicate to ensure precision, and average values were calculated. The CPC yield was determined by the formula presented below:

$$\textit{CPC yield (mg/mL)} = \left(\frac{A620 - 0.474 * A652}{5.34}\right)$$

where A620 corresponds to the maximum absorbance of CPC, A652 to account for overlapping absorbance that may be present in the extract to improve specificity (Na et al., 2025). 0.474 is the validated value coefficient for extent spectral overlap and 5.34 for accurate quantification (Pan-utai & Iamtham, 2019).

2.9 Biochemical analysis of *S. maxima*

2.9.1 C-phycocyanin purity

After extraction, C-phycocyanin purity was evaluated by the ratio absorbance of 620 nm divided by absorbance of 280 nm (A_{620}/A_{280}) , where A_{620} refers to the absorbance peak representing the maximum sensitivity and specificity for detecting CPC, and A_{280} refers to the absorbance of the total protein content, including unwanted protein contaminants which is a non-specific absorbance at 280 nm (Adjali et al., 2022).

$$\textit{CPC Purity ratio} = A_{620}/A_{280}$$

2.9.2 Total protein concentration of *S. maxima* extract

The protein content are reported as one of the biggest component of *S. maxima*'s bioactive composition and wound healing ability (Anvara & Nowruzib, 2021). To access any change in total protein content after plasma treatment, the bicinchoninic acid (BCA) protein assay was used for quantification. This assay was based on biuret reaction wherein protein reduce Cu^{2+} ions to Cu^{+} under alkaline environment (He, 2011). The sensitive and specific colorimetric detection of a purple-colored complex is produced when two molecules of bicinchoninic acid (BCA) formed by the chelation of one cuprous ion Cu^{+1} which is directly related to the amount of total protein present (Scientific, 2025). In this assay, freeze-dried plasma-treated samples were reconstituted in distilled water (50 µL per well) followed by the addition of 50 µL of Micro BCA as the working solution (A:B:C = 25:24:1) each well in triplicate, and then incubated at 37 °C for 2 hours. Bovine Serum Albumin (BSA) reagent, which has a well-established calibration profile, was used as a standard reference for the quantification of total protein (He, 2011) (Figure 39). Absorbance was measured using a Spectrophotometer Synergy-HTX multi plate reader (Biotek) at 562 nm wavelength.

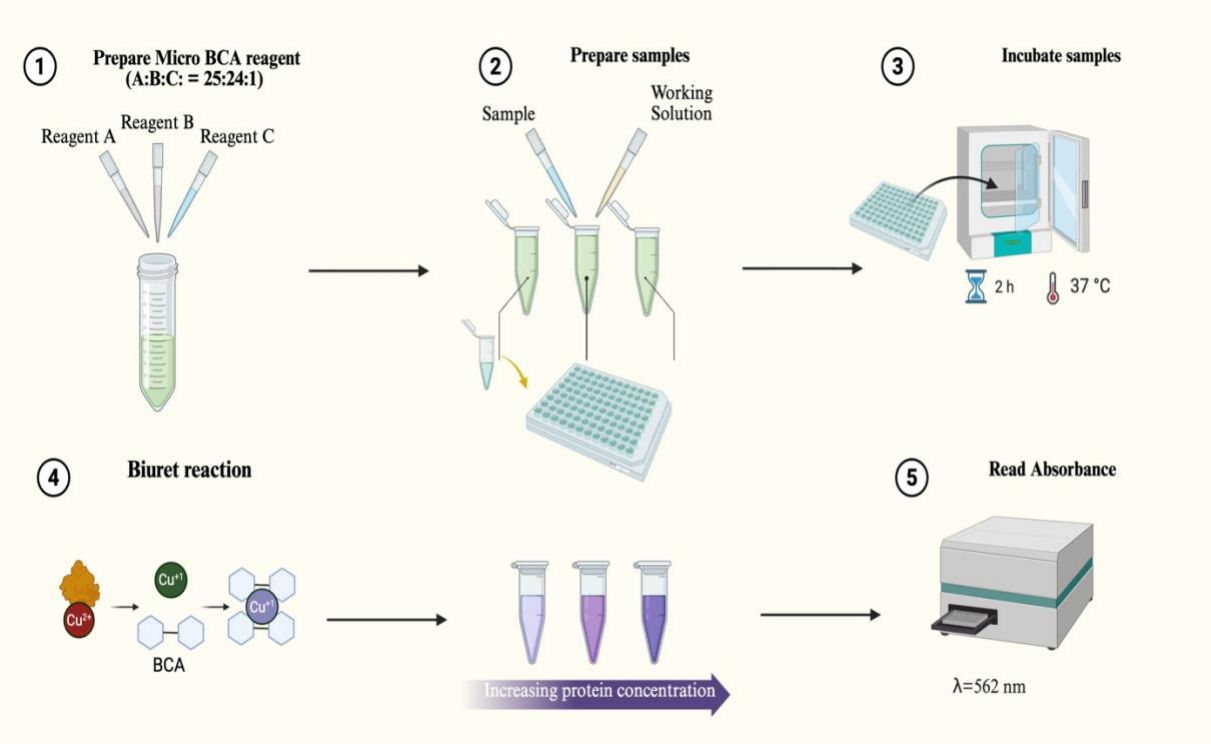

Figure 19. Schematic Illustration of the BCA assay for total protein concentration.

Figure removed due to copyright restriction.

Figure 20. Schematic Illustration of the principles BCA assay for total protein concentration showing reduction of Cu^{2+} ions to Cu^{+}followed by (Cu^{+} - 2 BCA) complex (Protein, 2025).

2.10 Colony Forming Unit (CFU) Assay for Antibacterial Activity

The overnight preculture bacterial suspension was prepared during the logarithmic growth phase, with its optical density initially measured at 600 nm (OD_{600}) using GeneQuant Pro RNA/DNA Calculator Spectrophotometer (Pharmacia Biotech, Cambridge, UK). Based on this measurement, bacterial suspension was diluted at 10^5 CFU/mL concentration to ensure wide and precise CFU counting. Using a 96-well plate (Nunc, Thermo Scientific, MA, USA), all freeze-dried plasma-treated samples (18 runs) were reconstituted in PBS to a final concentration of 30 mg/mL. Afterward, 50 µL of the diluted bacterial suspension was added to each well in triplicate, and plate was incubated at 37 °C for 18 hours. For additional sterility verification, each sample was filtered using a 0.20 µm filter (Agilent Technologies) to ensure a contaminated-free sample. Both pre-filter and post-filter aliquots were streaked out onto a separate petri dishes to confirm sterility.

Following an 18 hours incubation period, serial ten-fold dilutions of the bacterial suspension were performed until a 10^8 dilution factor was reached. After serial dilution, 10 µL of each dilution was uniformly plated onto the tryptic soy agar (TSA) plates, which provided a nutrient-rich solid surface for bacterial growth. The plates were incubated at 37 °C for 18-24 hour to allow bacterial colonies to grow. To evaluate the antibacterial activity for each run, the colonies grown on to the TSA plates were counted, ensuring accurate enumeration of viable bacteria. The bacterial reduction was determined by CFU/mL calculation formula and the log reduction formula presented below:

$$\boldsymbol{CFU/mL = \frac{Number\ of\ colonies}{Volume\ plated\ (mL)} * Dilution\ factor}$$

$$\boldsymbol{Percentage\ reduction} = \left(1 - \frac{CFU\ of\ treatment}{CFU\ of\ control}\right) * \mathbf{100}$$

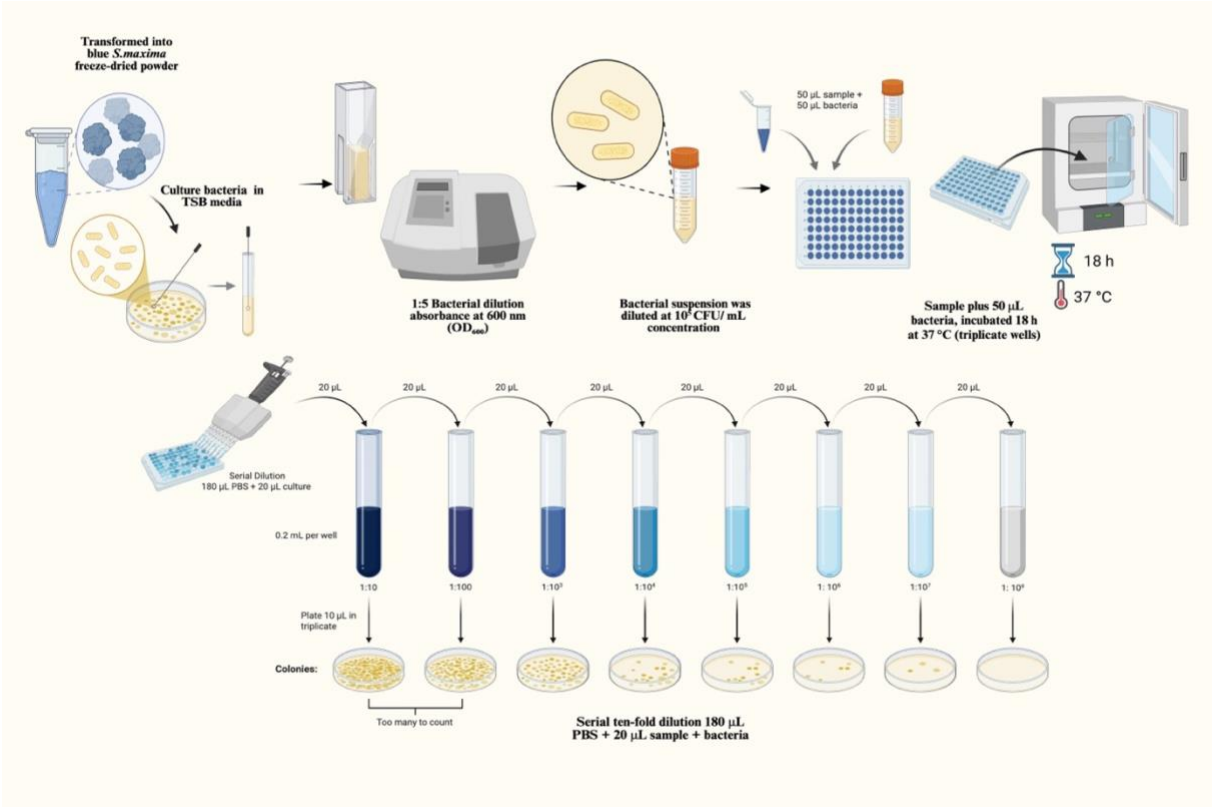

Figure 21. Schematic Illustration of the Colony Forming Unit (CFU) assay for antibacterial activity.

2.11 Flow cytometric analysis of *S. maxima*'s antibacterial activity on Gram-positive and Gram-negative pathogen

2.11.1 Principles of Flow cytometry

Flow cytometry is a well-established laser-based quantitative analysis used to measure and analyze the physical and chemical characteristics including cell size, granulation, viability and internal complexities as they flow through a laser beam in a fluid stream (Figure 22) (Adan et al., 2017). During the assay, it worked by fluorescent probe-labelled cell pass single file through a laser beam, which emit light of different wavelength and produce signals through a specific fluorescence dye (Manohar et al., 2021). In the bacterial viability assay, stained bacterial cell passed through the scatter light, allowing differentiation of live and dead populations based on fluorescence emission. Live cells, were stained with SYTO 9 (EX/EM = 480/500 nm), a green fluorescent dye that penetrates only live cells while, dead or damaged cells were stained with propidium iodide (PI) (EX/EM =535/617nm), which fluoresced red (Stiefel et al., 2015). When both dye used simultaneously, PI exhibits higher affinity for nucleic acid diminishing SYTO 9's green fluorescence (Stiefel et al., 2015).

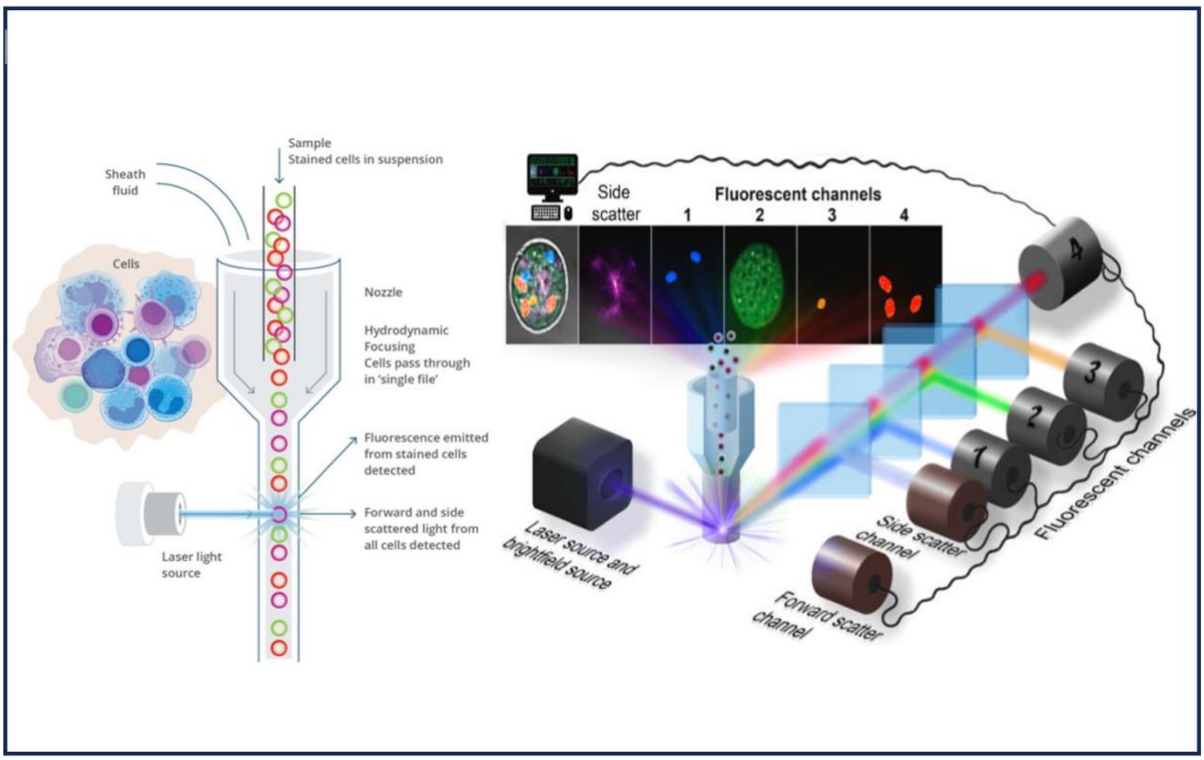

Figure 22. Schematic Illustration of optical system of Flow cytometry.

2.11.2 Experimental details

Cell viability of each sample was measured using CytoFLEX S flow cytometer (Beckman – Coulter, Brea, CA) with violet laser-side scatter (VSSC) with detector configuration channel of 610nm, 405, 405nm DAPI 450/45, KO525 BV510 525/40, violet 660 BV650 660/20 and 780/60 nm for small particle scatter, multicolor analysis, and proper spectral separation using bandpass filters to separate, individual dyes, simultaneously (Figure 22).

To validate SYTO 9 and Propidium Iodide (PI) for differentiation of live and dead bacteria, bacterial suspension with sample was incubated at 37 °C for 18 hours. After incubation, samples were centrifuged using a Thermo Scientific Heraeus Fresco 17 microcentrifuge (Thermo Fisher Scientific, Waltham, MA, USA) at 10,000 times gravity at 37 °C. The supernatant was removed, and cells were resuspended 200 µl of PBS containing 0.95% NaCl, centrifuge again, and washed again with 200 µl PBS (control only).

For dead bacteria control, unstained bacterial sample were incubated in a 100 ◦ C water bath for 30 min. Cytexpert 2.6 software was used for analysis. A concentration of 3 µl/mL of SYTO 9 and PI was added to each eppendorf tube. Samples were measured at a flow rate of 10 µl/min.

Figure removed due to copyright restriction.

Figure 23. A.) Optical detector filter configuration used for SYTO9 and PI fluorescence detection **B.)** CytoFLEX S flow cytometer (Beckman-Coulter, Brea, CA).

2.12 Statistical analysis

In this research, a one-way analysis of variance (ANOVA) was used to evaluate statistically significant differences among treatment groups. All statistical analyses were conducted using GraphPad Prism version 8, GraphPad Software, LLC (San Diego, California, USA) and Microsoft excel (Redmond, Washington, USA) with level of significance set at $p < 0.05$. This statistical tool was used to determine treatment effects on different bacterial growth and to assess cellular response under different treatment conditions.

Table 4. Statistical significance and P-value interpretation.

Symbol	P-value Range	Equivalent
ns	$p > 0.05$	Not significant
*	$p \leq 0.05$	Significant
**	$p \leq 0.01$	More significant
***	$p \leq 0.001$	Highly significant
****	$p \leq 0.0001$	Very highly significant

CHAPTER THREE: RESULT

3.1 Optimizing plasma process parameters for extraction of optimal CPC concentration

Optimizing plasma process parameters for extraction of the optimal CPC concentration is the most critical and essential part of the study since the success of the treatment depends on the optimal combination of each individual parameter including voltage level (kV) of plasma source, treatment time (min) or the duration of treatment, and salt (NaCl) concentration. These requires to establish a relationship between the individual parameters and determine its optimal combination for a randomized run order for unbiased execution for succeeding analysis and optimization. CPC was chosen as the optimized output due to its therapeutic potential protecting healthy cell from oxidative damage, helping to neutralize ROS during wound healing, reducing inflammation which minimizes tissue damage promoting regeneration of new healthy cells in chronic wounds. Therefore, optimizing higher CPC concentration is essential to enhances wound healing outcomes. The table of experiments from Design Expert Software and the result of each experimental run as outlined in Table 5 serves as a design plan dictates the combinations of plasma parameter variations. During the process of the optimization, 20 runs were conducted with CPC concentration quantified by UV-Vis spectrophotometry at 620nm using Beer-Lamber law excluding run 1 and 8 since negative values are not physically possible therefore, excluded from the experimental setup. This gives a varying voltage of 1.636 to 8.364 kV, treatment time from -2 to 13 min and NaCl concentration between – 0.34 to 1.34 g/L, resulting to an antioxidant capacity ranging from 0 to 0.023 mM TE/mg while CPC concentration of all runs varies from 0 to 26.01 μg/ml. The optimization were conducted using nitrogen gas as the main gas supply, delivered at a flowrate of 1L/min, ensuring consistent DBD gas distribution with the Atmospheric Plasma Chamber ensuring controlled gas environment.

3.1.1 Table of Experiment from Data Expert Software including CPC and Antioxidant Result

The table of experiment serves as a design plan dictates the combinations of plasma parameter variations necessary to establish a relationships between the individual variables, with results for CPC concentration and antioxidant capacity results shown below (Table 5):

Table 5. Table of Experiment from Design Expert Software.

Table of Experiment from Design Expert Software					
Run	**Factor 1**	**Factor 2**	**Factor 3**	**Antioxidant capacity**	**CPC concentration**
	A: Voltage Level	**B: Treatment Time**	**C: NaCl Concentration**		
	kV	**min**	**g/L**	**µM TE/mg**	**µg/ml**
18	8.36359	5.5	0.5	**0.0158156**	**22.5746**
2	7	1	1	**0.0134648**	**18.1092**
9	7	1	0	**0.0087703**	**18.3332**
15	7	10	0	**0.015605**	**8.22798**
17	7	10	1	**0.0224144**	**9.6309**
1	5	-2.06807	0.5	**0**	**0**
5	5	5.5	0.5	**0.0116573**	**19.5643**
7	5	5.5	1.3409	**0.0193892**	**17.0553**
8	5	5.5	-0.340896	**0**	**0**
10	5	13.0681	0.5	**0.0233683**	**9.74514**
13	5	5.5	0.5	**0.0142392**	**19.5413**
14	5	5.5	0.5	**0.0134238**	**20.4471**
16	5	5.5	0.5	**0.0121105**	**20.8358**
19	5	5.5	0.5	**0.0132982**	**20.922**
20	5	5.5	0.5	**0.0111588**	**20.0914**
3	3	1	0	**0.0074053**	**9.7433**
4	3	10	0	**0.0129731**	**20.0734**
6	3	10	1	**0.0214456**	**20.2268**
11	3	1	1	**0.0121364**	**18.7595**
12	1.63641	5.5	0.5	**0.0101001**	**26.01**

3.1.2 Fit Statistics

To assure the model's quality, reliability and predictive ability of the response surface model in plasma-treated *S. maxima,* the fit statistics are summarized in Table 6 and 7. The R^2 or the coefficient determination, shows how well the experimental data fits with the statistical analysis (Edwards et al., 2008). An R^2 close to 1.00 suggest an excellent fit confirming validity and reliability of the optimized treatment condition within the studied design space (Edwards et al., 2008). In this research, an R^2 value of 0.849 for CPC concentration and 0.8536 for antioxidant, along with adjusted R^2 of 0.8207 for CPC concentration and 0.7219 for antioxidant, indicate a good explanation of the high proportion of variability reflecting a strong model fit. A predicted R^2 of 0.73 for CPC indicates that model is capable of predicting new data points wherein, predictive R^2 close to adjusted R^2 ideally above 0.5 to 0.7 for more confidence in model prediction (Frost, 2020). However, a negative predicted R^2 - 0.1208

for antioxidant suggest that the current model lacks predictive capacity, model limitations and overfitting hence, further model refinement is required for improvement for more predictive antioxidant outcomes (Frost, 2020).

For CPC, a very low value of 0.0026 for the standard deviation and a coefficient variation of 20.25% indicates a precise experimental results closely clustered around the mean with consistent quality measurements agreed with each other showing minimal random error. In addition, the adequate precision of 17.8991 suggest that the design model have a strong predictive signal relative to the noise and can distinguish different response values therefore, a strong prediction capacity and can accurately predict outcomes on varying optimal combination.

Table 6. CPC Fit Statistics result.

CPC Fit Statistics			
Std. Dev	0.0026	**R2**	0.849
Mean	0.0129	**Adjusted R2**	0.8207
C.V.%	20.25	**Predicted R2**	0.73
		Adeq. Precision	17.8991

Table 7. Antioxidant Fit Statistics result.

Antioxidant Fit Statistics			
Std. Dev	3.82	**R2**	0.8536
Mean	15.99	**Adjusted R2**	0.7219
C.V.%	23.89	**Predicted R2**	-0.1208
		Adeq. Precision	8.5505

3.1.3 Normal Plot Residuals Predicted vs. Actual from Design Expert Software for CPC and Antioxidant

The actual data responses of CPC concentration and antioxidant plotted with the predicted responses are shown in Figure 24 as generated using design expert software. In both plots, scatter points distributed along with the diagonal line indicates a strong agreement that predicted values matches with the actual experimental results. This helps to evaluate the goodness of data fitting from the regression which refers to the relationship between dependent and independent variables (Ali & Younas, 2021). This visual alignment for both CPC and antioxidant reflecting good, though not

perfect model accuracy with most points clustering along the diagonal line but few dots showing minor deviation which indicates areas in residual fit may be further improved.

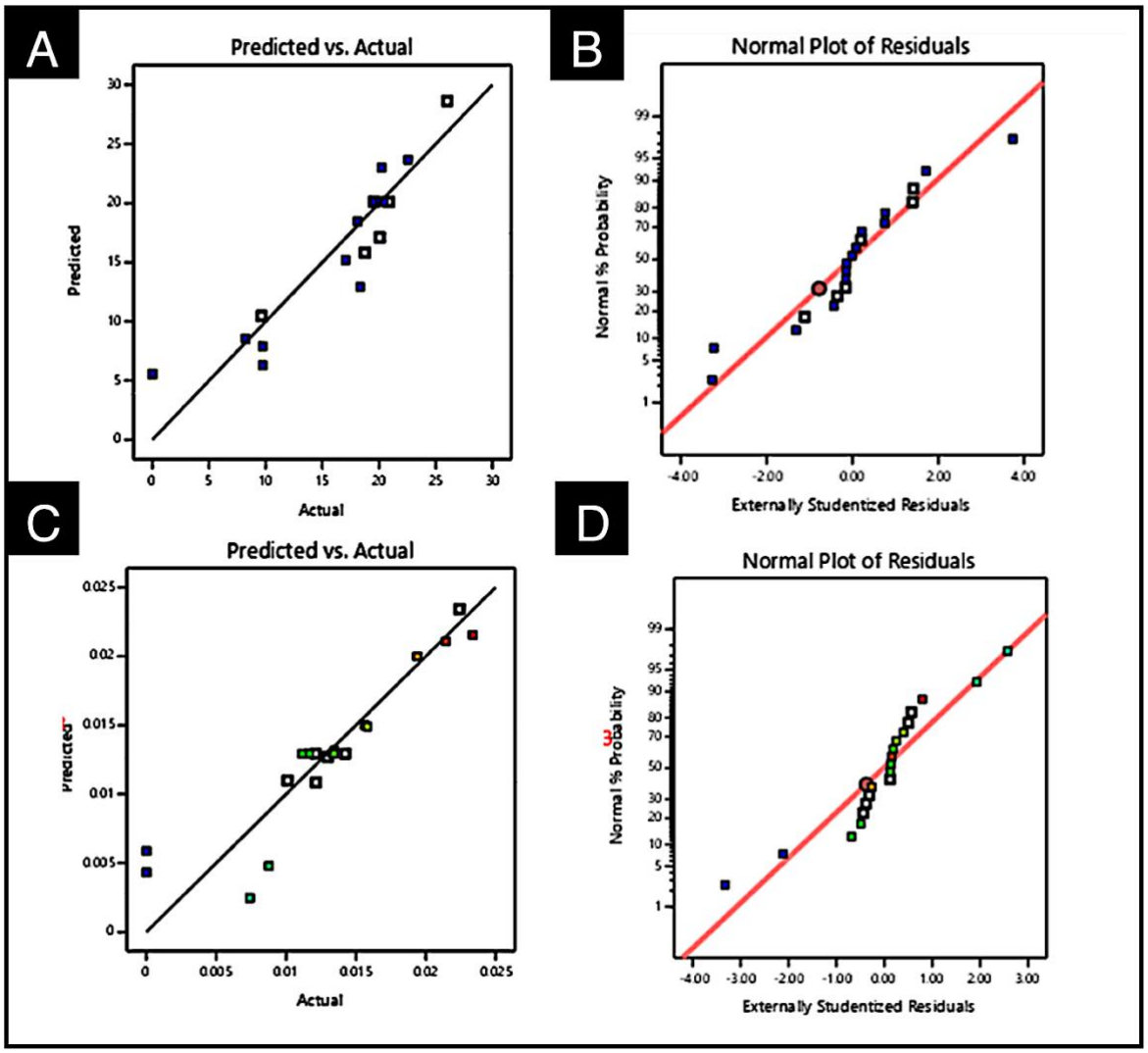

Figure 24.Normal Plot Residuals Predicted vs. Actual from Design Expert Software A.) Predicted vs. Actual for CPC concentration **B.)** Normal plot off residuals for CPC concentration **C.)** Predicted vs. Actual for antioxidant capacity **D.)** Normal plot off residuals for antioxidant capacity.

3.1.4 The highest C- phycocyanin and antioxidant capacity using Central Composite Design in Quadratic Plot Point

As described in Section 2.4 of Chapter 2, the Central Composite Design CCD framework provides foundational experimental design for this study by employing factorial points, center points, and axial star points to show linear and non-linear quadratic relationship between plasma treatment parameters (Montgomery et al., 2021). This model framework approach reflects in the results presented in Figure 25, which presents a 3D quadratic response surface plot displaying the yield of C-phycocyanin (CPC, µg/ml) and antioxidant capacity (µM) yielding across factors such as A) Power (kV), B) Treatment time (min), with C) NaCl concentration fixed at 0.5 (g/L) highlighting optimal zones. The color

gradient transition from green (lower CPC yield) through yellow to red (Higher CPC yield), indicates an increase in CPC yield. The x-axis represents the voltage use in the extraction process, while the y-axis represents the duration of the plasma treatment. In this figure, the peak CPC yield is observed at 26 μg/ml was achieved near 3kV presenting a red region on the surface color and a treatment time ranging approximately around 7.5 while antioxidant capacity was reached at 0.023 μM at 7kV and a treatment time of 10 mins at a concentration of 0.5 g/L NaCl. The contour lines at the bottom represents the level of C-phycocyanin (CPC) yield how factors like power and treatment time affect its extraction. The red dot indicates that the actual result has a higher CPC yield than the predicted result by the model indicating that a successful and optimal result is achieved, while space closer between contour lines represents how fast CPC yield changes, and contour line far apart represent a gradual changes means the yield is more steady across the design space (Montgomery et al., 2021).

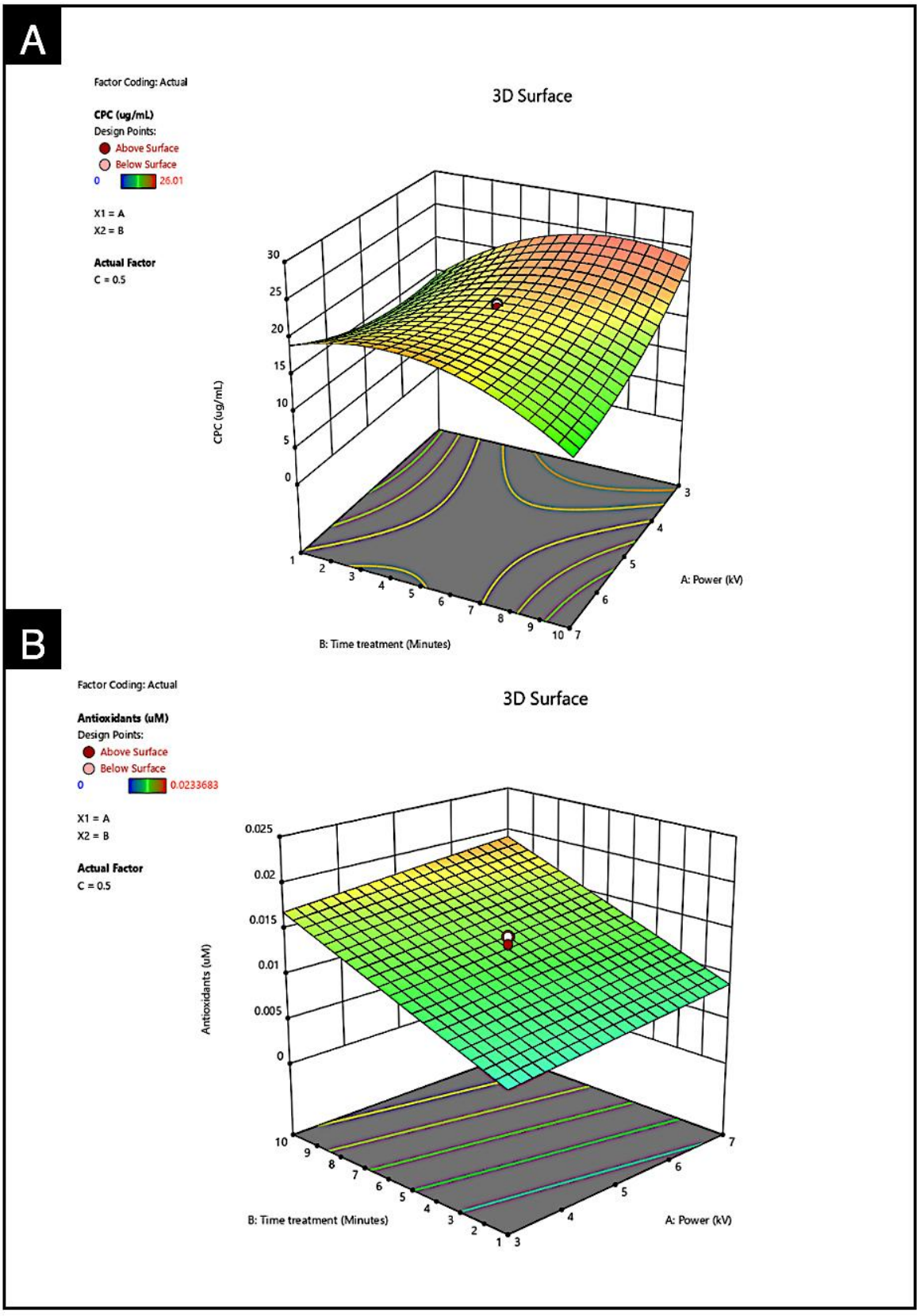

Figure 25. Quadratic Plot Points. A.) 3D Quadratic Response Surface Contour Plot Showing the Effect of Power (kV) and Time Treatment (min) on C-Phycocyanin (CPC) yield at 0.5 g/L NaCl Concentration **B.)** 3D Quadratic Response Surface Plot Showing the Effect of Power (kV) and Time Treatment (min) on antioxidant yield at 0.5 g/L NaCl Concentration.

3.2 Biochemical compounds

3.2.1 C-phycocyanin concentration and purity

CPC concentration of the extract were examined as μg/mL. After incorporation of the plasma-treatment, the result of the CPC concentration of the plasma-treated *S. maxima* are highly significantly different between 3kV, 7kV and untreated groups. The untreated group refers to supernatant collected from spirulina cell suspension without any cell-disrupting treatment. This serves as a control for any extracellular bioactive compounds that may be present in the spirulina dry powder. Based on the data, incorporation of 3kV plasma treatment yielded a higher CPC concentration, about 21μg/ml compared to 7kV at 12 μg/ml, and 15 μg/ml for the untreated group. The four asterisks comparing 3kV and 7 kV indicate a highly statistically significant difference ($p<0.0001$), and two asterisks comparing 3kV and untreated group showing a significant difference ($p<0.01$) between 3kV and untreated group. The 7kV plasma treatment from antioxidant resulted to a significantly lower CPC concentration, making 3kV from CPC the best condition. While in terms of CPC purity where higher value means a more purified pigment, 3kV plasma treatment significantly enhance the C-phycocyanin (CPC) purity achieving the highest value of 0.26 compared to 0.11 for 7kV ($p\leq 0.001$) but no significant difference in purity was observed in the untreated group (Figure 26).

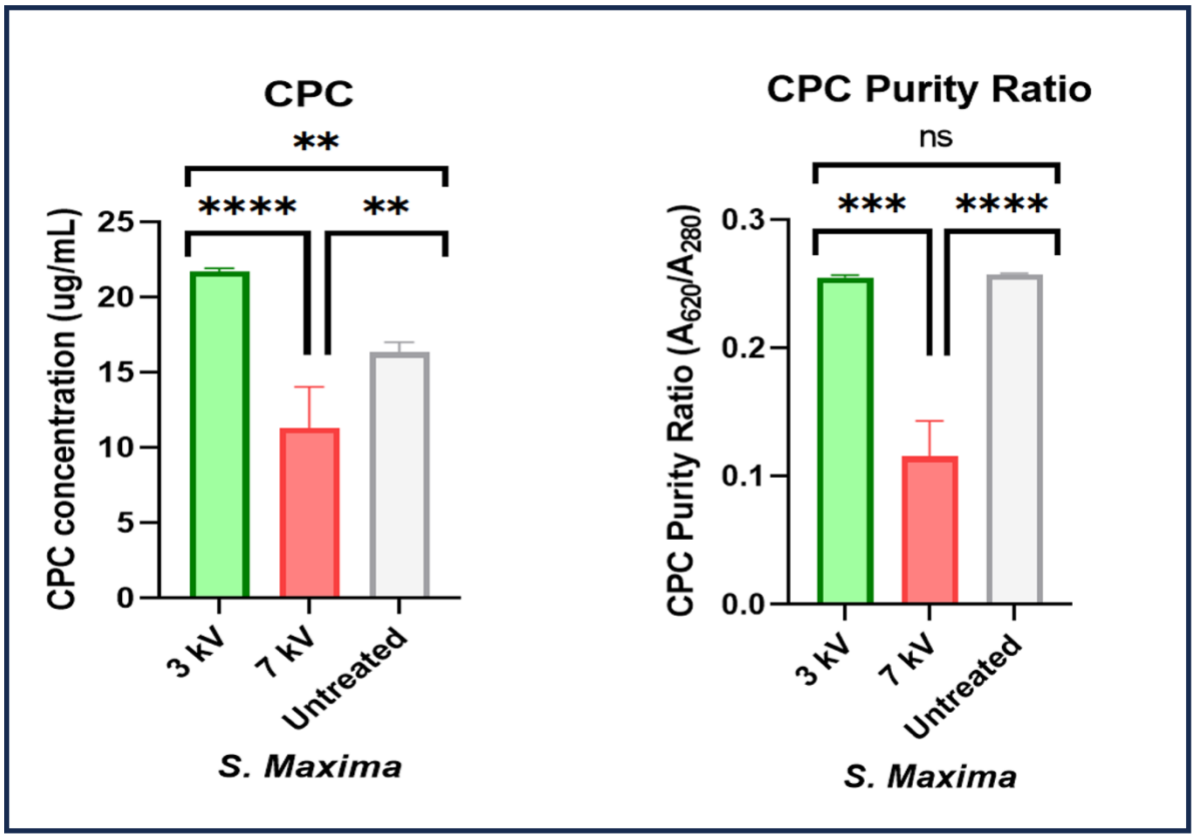

Figure 26. A.) C-phycocyanin (CPC) concentration (µg/ml) for plasma-treated and untreated *Spirulina maxima* **B.)** C-phycocyanin (CPC) concentration (µg/ml) purity for plasma-treated and untreated *Spirulina maxima*. The level of significance was set at $p<0.05$.

3.2.2 Total protein concentration of *S. maxima* extract

After incorporation of the plasma-treatment, the total protein content concentration in *S. maxima* did not show any significant differences among 3kV plasma having 47 µg/mg biomass , compared to 7kV plasma at 53 µg/mg biomass and 46 µg/mg biomass for the untreated group which does not significantly affect the amount of total protein biomass compared to the untreated group suggesting that plasma exposure does not have a major impact on the total protein (Figure 27). Just to supplement the result for the untreated group, this group does have some obvious bioactive properties, indicating that there is almost certainly bioactive compound specifically protein present in the extracellular environment when suspended the cell into the water. These proteins contributes to the overall wound healing potential of *S. maxima*.

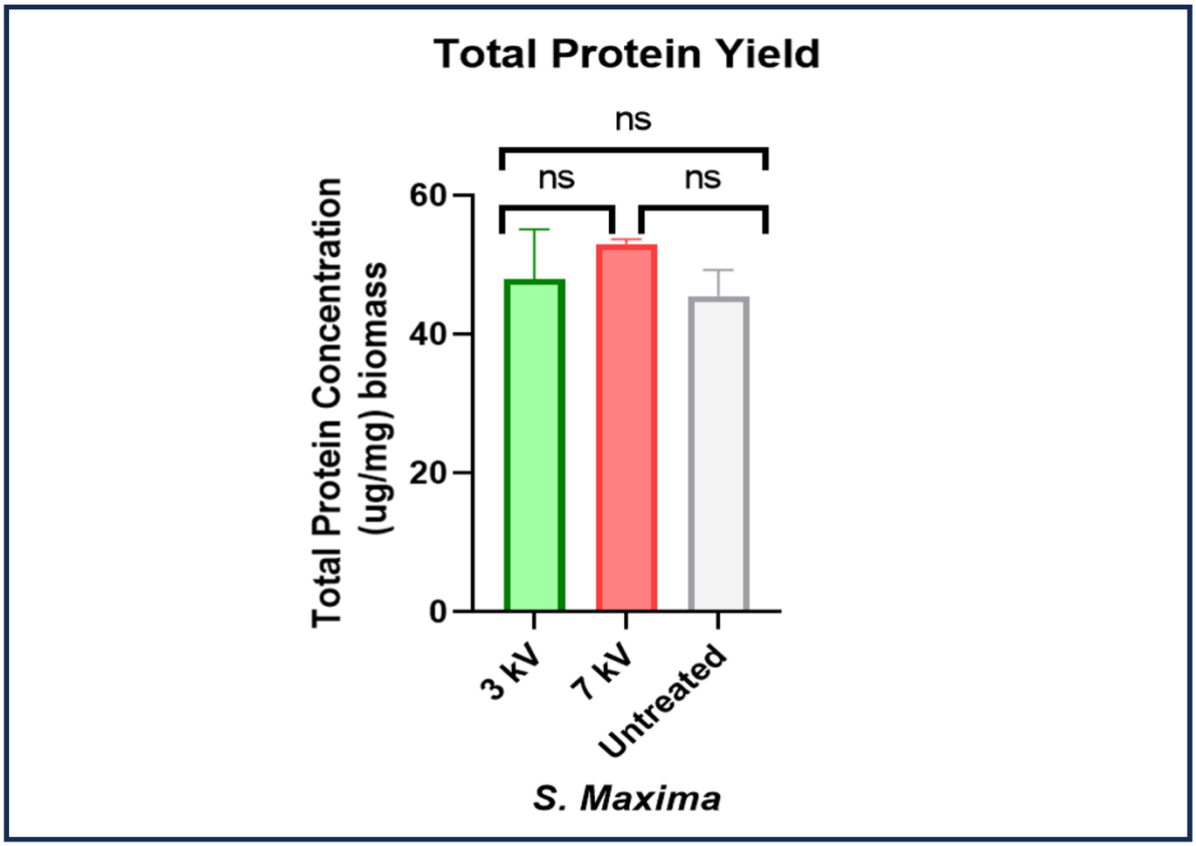

Figure 27. Total Protein Yield concentration (µg /mg) biomass of plasma-treated and untreated *Spirulina maxima.*

3.3 DPPH Radical Scavenging Assay for antioxidant activity

After incorporation of the plasma-treatment, the total antioxidant activity of the plasma- treated *S. maxima* was measured in µM Trolox equivalent per mg biomass. Both 3kV and 7kV plasma treatments demonstrates a higher antioxidant activity compared to the untreated group. The asterisk indicates a statistically significant difference wherein the antioxidant activity of 3kV indicates a statistically significant increase ($p \leq 0.001$) than the untreated group while the difference between a 0.058 µM Trolox TE/mg of 3kV treatment and 0.054 µM Trolox TE/mg of 7kV treatment is not statistically significant (Figure 28).

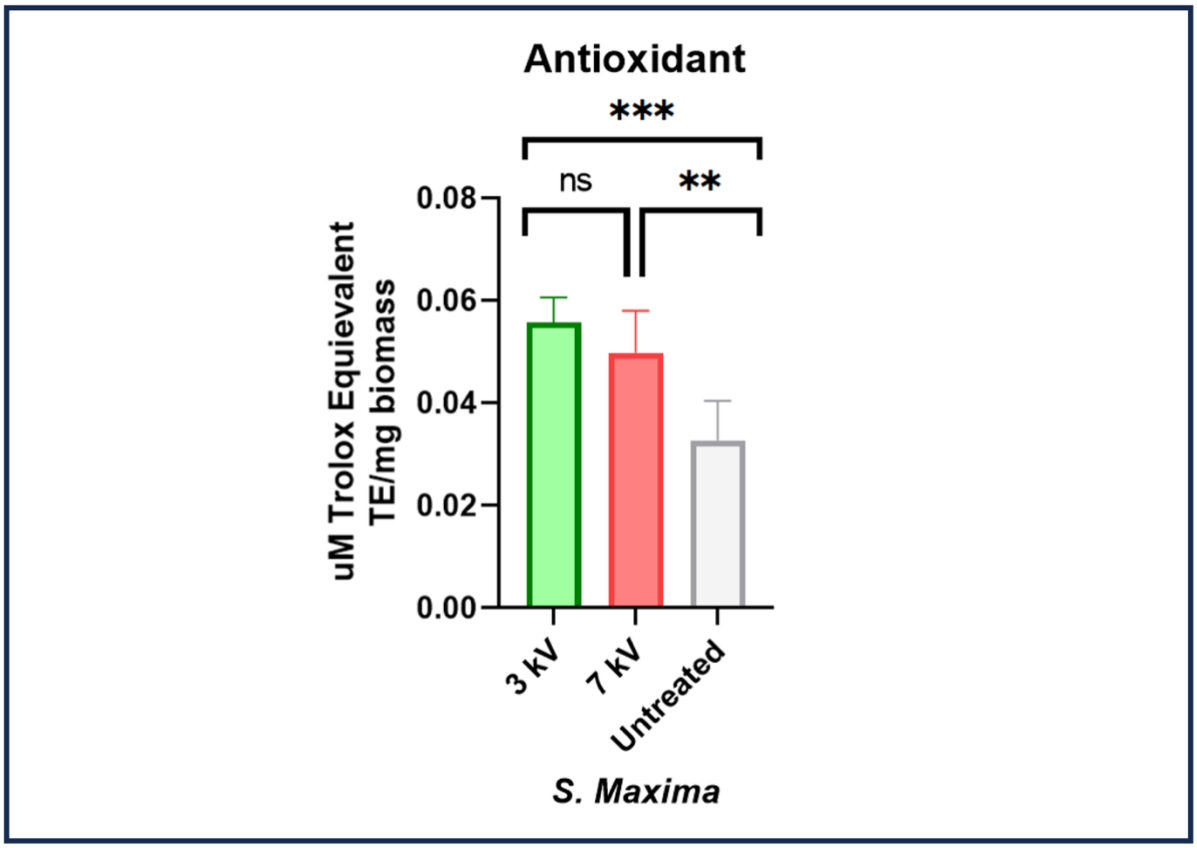

Figure 28. Highest Antioxidant capacity of plasma-treated and untreated *Spirulina maxima*.

3.4 Comparative analysis of the optimized plasma condition (3kV, 7.42 min, 0.75g/L), untreated and conventional freeze-thaw method

The process parameter of 3kV, 7.42 min, 0.75g/L process was deemed to be the optimal plasma-assisted extraction condition, and all subsequent experiments will be using the optimal plasma-assisted extract. To assess the optimized plasma-assisted condition, comparative analysis was conducted on the antibacterial efficacy of *S. maxima* in comparison to extract obtained via conventional freeze-thaw method, and untreated conditions. Freeze-thaw method is chosen for this comparative analysis for its well-established method and has been reported to be the best for phycobiliprotein extraction widely used for microalgal cell membrane (Tan et al., 2020). It works by forming ice crystals during freezing, which ruptures cell membrane upon thawing, allowing release of intracellular bioactive compound without using any harsh procedures that cause a possibility of extensive membrane disruption that may compromise the quality of *S. maxima* extracts leading to a reduced extraction yield which minimize risk of denaturing antioxidant and antibacterial properties (Jaeschke et al., 2021). This comparative analysis approach enables direct evaluation of a newly developed plasma-assisted treatment approach with conventional method aiming to increase extraction yield of valuable bio actives through for innovative treatment.

3.5 Influence of plasma exposure on *S. maxima* cell morphology

3.5.1 Surface Morphology of *S. maxima* under Scanning Electron Microscope (SEM)

The surface morphology of *S. maxima* has been examined and visualized using SEM at magnifications of 5,000x, 6,000x and 12,000x under imaging settings, including a working distance (WD) between 10.7 - 11.2 mm, an accelerating voltage (HV) of 10.0 kV, horizontal field width (HFW) ranging from 24.9 μm to 59.7 μm, and a spot size of 3.0 for ETD detector (Table 8) in comparison among plasma-treated conventional freeze-thaw disruption, and untreated sample. Untreated *S. Maxima* around 100 μm in length was used as reference for comparison.

S. maxima exposed to 3kV plasma treatment condition (Figure 29 C;D), displayed visible small fragmentation, small holes and surface irregularities, with each fraction approximately about 12 μm to 22 μm without totally damaging the cell membrane. These results indicate plasma exposure significantly compromised cell wall integrity. In contrast, *S. maxima* subjected to the conventional freeze-thaw method exhibited moderate evidence of cracks, and the majority of filaments maintained their overall structure with a surface irregularities ranging from 9 to 10 μm suggesting less extensive damage than the plasma-exposed *S. maxima.* These changes may be associated with mechanical stress and ice crystal formation during thawing process. While untreated *S. maxima* filaments showed fully intact structures with minimal evidence of cracks or disruptions.

Table 8. Properties of *Spirulina maxima* filaments with SEM imaging parameters under different treatment conditions.

Sample	Magnification	Detector	Accelerating Voltage (kV)	Working Distance (mm)	Horizontal Field Width (μm)
3kV Plasma Treated	6,000x/ 12,000x	ETD	10.0	11.2	24.9/ 49.7
Freeze Thaw	6,000x/ 12,000x	ETD	10.0	11.1	24.9/49.7
Untreated	5,000x/ 12,000x	ETD	10.0	10.7-10.8	24.9/59.7

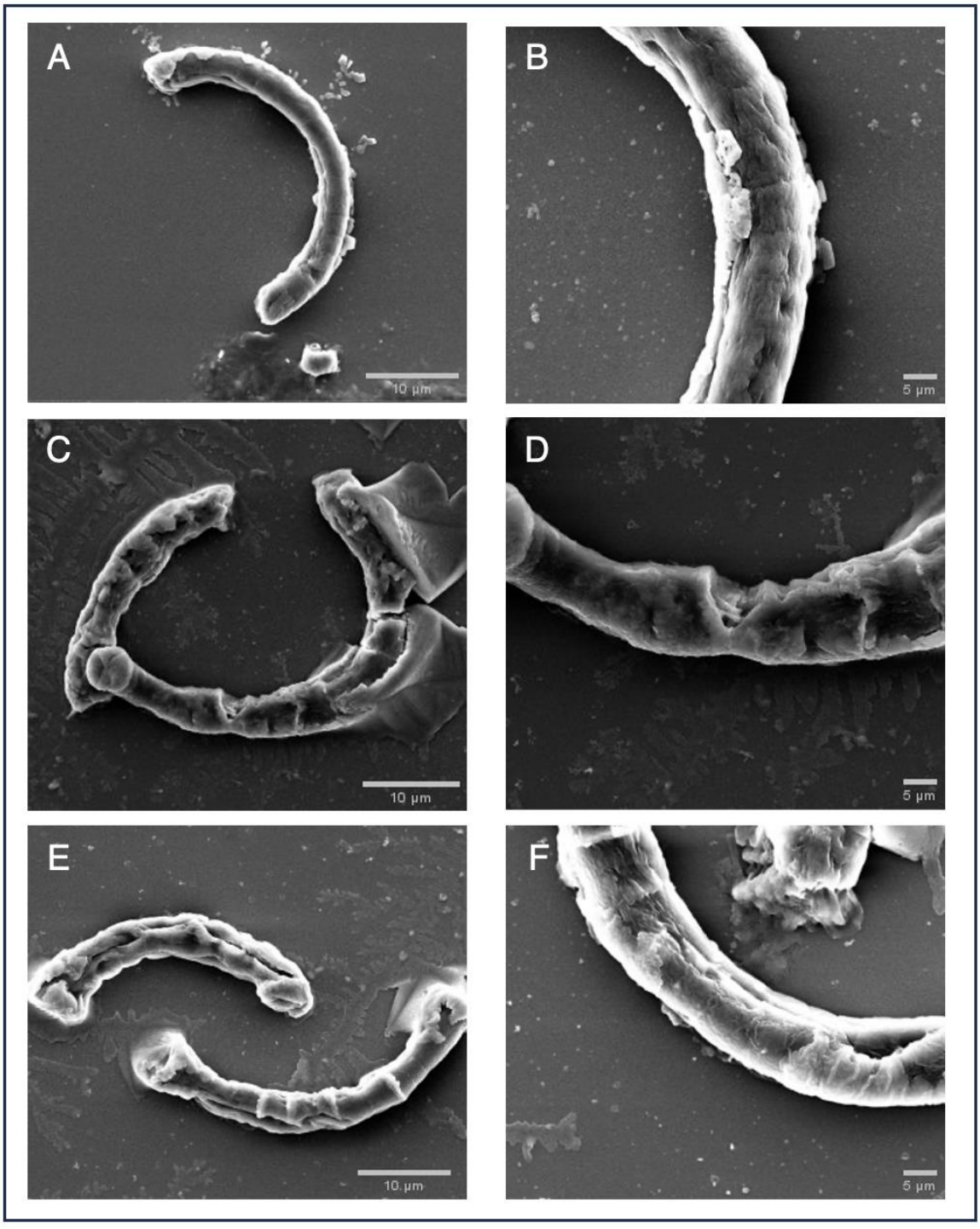

Figure 29. Surface Morphology of *S. maxima* of three different conditions under SEM microscopy (A;B) Untreated *S.maxima* supernatant **(C;D)** Plasma-treated sample **(E;F)** Conventional freeze-thaw sample.

3.5.2 Surface Morphology of *S. maxima* under Epifluorescence Microscopy

The surface morphology of *S. maxima* has been examined and visualized using epifluorescence microscopy at magnification of 60 x and 100x, with scale bar of 20 μm and 10 μm (Figure 30). To measure relevant differences of fluorescence intensity, Fiji Image J was used among treatment groups interpreted as mean integrated density. *S. maxima* exposed to 3kV plasma treatment exhibited extensive fragmentation, and surface irregularities and less defined filamentous structure due to significantly compromised cell wall integrity resulting in the lowest measured fluorescence intensity (Mean IntDen:317,981.5±342,268). In contrast, *S. maxima* subjected to the conventional freeze-thaw method showed a partial fragmentation to the structural integrity but less extensive compared to plasma-treated sample showing an intermediate fluorescence intensity (Mean IntDen: 476,355.0±471,106). While untreated *S. maxima* showed a highly bright filamentous structure with minimal fragmentation giving a high fluorescence intensity (Mean Int Den: 9,253,274.5±3,855,434) preserving cellular integrity (Table 9).

Table 9. Properties of *Spirulina maxima* filaments with epifluorescence imaging parameters under different treatment conditions.

Sample	Magnification	Mean Integrated Density	Fragmentation
3Kv Plasma Treated	60x/ 100x	317,981.5±342,268	High
Freeze Thaw	60x/ 100x	476,355.0±471,106	Moderate
Untreated	60x/ 100x	9,253,274.5±3,855,434	Low

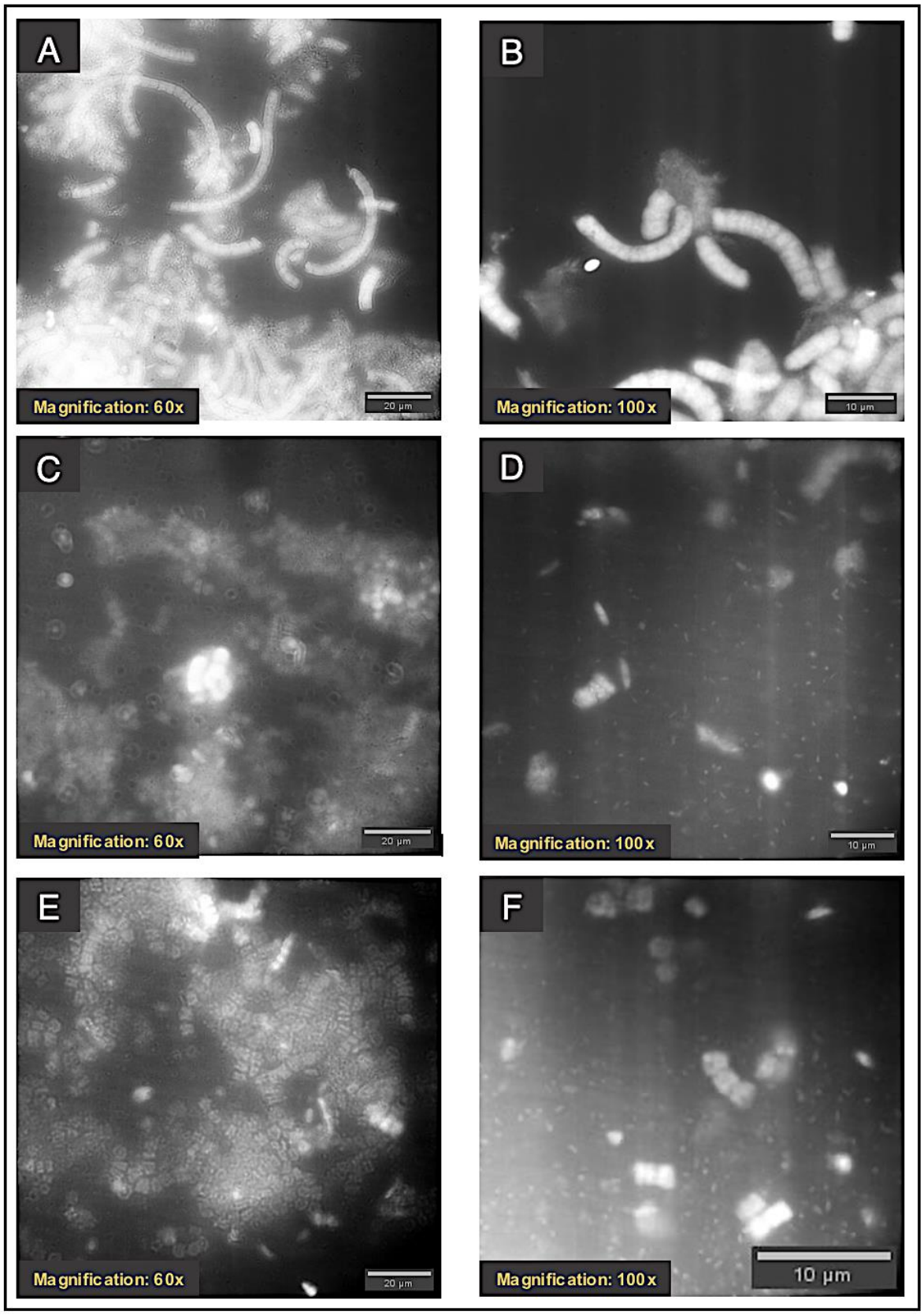

Figure 30. Surface Morphology of *S. maxima* of three different conditions under epifluorescence microscopy (A;B) Untreated *S.maxima* supernatant **(C;D)** Plasma-treated sample **(E;F)** Conventional freeze-thaw sample.

3.6 Colony Forming Unit (CFU) Assay for antibacterial properties

3.6.1 Evaluating the effect of *S. maxima* extract antibacterial potential on *S. aureus*, *S. epidermidis*, *E. coli* and *P. aeruginosa*

The antibacterial efficacy of the *S. maxima* extract subjected in different treatment conditions including optimal plasma-assisted extract, conventional freeze-thaw and untreated *S. maxima* supernatant without any cell-disrupting treatment was preliminarily evaluated against Gram-positive bacteria *S. aureus* (ATCC 25923) and *S.epidermidis* (ATCC 12228), using colony forming unit (CFU) assay. To evaluate potential antibacterial effect of each, sample were tested at the same concentration to ensure direct comparability. Across all tested bacteria, plasma-assisted extract demonstrated potent antibacterial efficacy exhibiting reductions in bacterial viability. For Gram-positive species, plasma-assisted extract resulted to 55.19 % reduction for *S. aureus* (***$p<0.001$), and a 56.64 % for *S. epidermidis* (****$p<0.0001$) compared to the untreated bacterial control. These reduction were significantly greater than those observed with the freeze-thaw (47.18% *S. aureus*, 38.98 % *S. epidermidis*) and a low reduction in bacterial viability is observed in untreated *S.maxima* supernatant (36.80% *S. aureus*, 12.93 % *S. epidermidis*). For Gram-negative species, plasma-assisted extract achieved 21.96% reduction for *E. coli* which is notably lower compared to other treatment conditions wherein, freeze-thaw resulted to 52.52% (***$p<0.001$), and 36.80% (****$p<0.0001$) for the untreated *S. maxima* supernatant. While in *P. aeruginosa* exhibited a higher reduction of 76.22% compared with freeze-thaw 38.70 % and 12.85% for untreated *S. maxima* supernatant (****$p<0.0001$) (Figure 31).

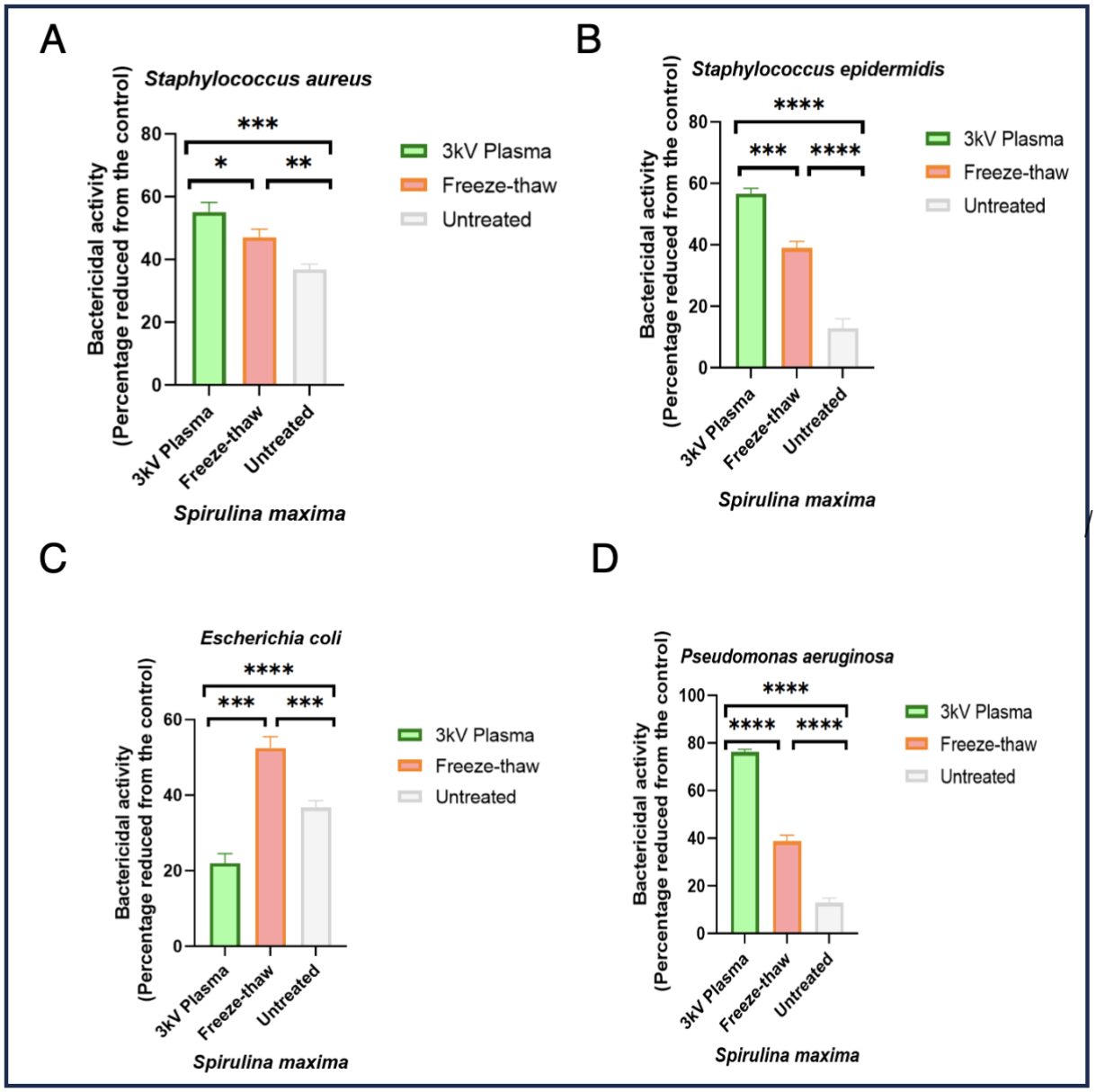

Figure 31. Colony enumeration A.) *S. aureus*, **B.)** *S. epidermidis* **C.),** *E. coli* and **D.)** *P. aeruginosa* expressed as percentage reduced from the untreated bacterial control (no *S. maxima* sample).

3.7 Flow cytometric analysis of *S. maxima* extract antibacterial activity on Gram- positive and Gram-negative pathogens

3.7.1 Evaluating the effect of *S. maxima* extract antibacterial activity on *S. aureus* and *S. epidermidis* via flow cytometry

S. maxima extract antibacterial efficacy was preliminarily evaluated against Gram–positive bacteria *S. aureus* (ATCC 25923); and *S.epidermidis* (ATCC 12228) using SYTO 9 and PI staining and measured via flow cytometry to assess bacterial viability and membrane integrity for all treatment conditions. For Gram-positive strains, *S. aureus* and *S. epidermidis*, plasma-assisted extract resulted in 53.67% (Figure 34 B) and 64.52% (Figure 33 B) dead cell fraction significantly exceed both

freeze-thaw, 18.13% for *S. aureus* (Figure 34 D) and 11.75% for *S. epidermidis* (Figure 33 D) and 14.88% (Figure 34 F) and 23.07%(Figure 33 F) untreated *S.maxima* supernatant.

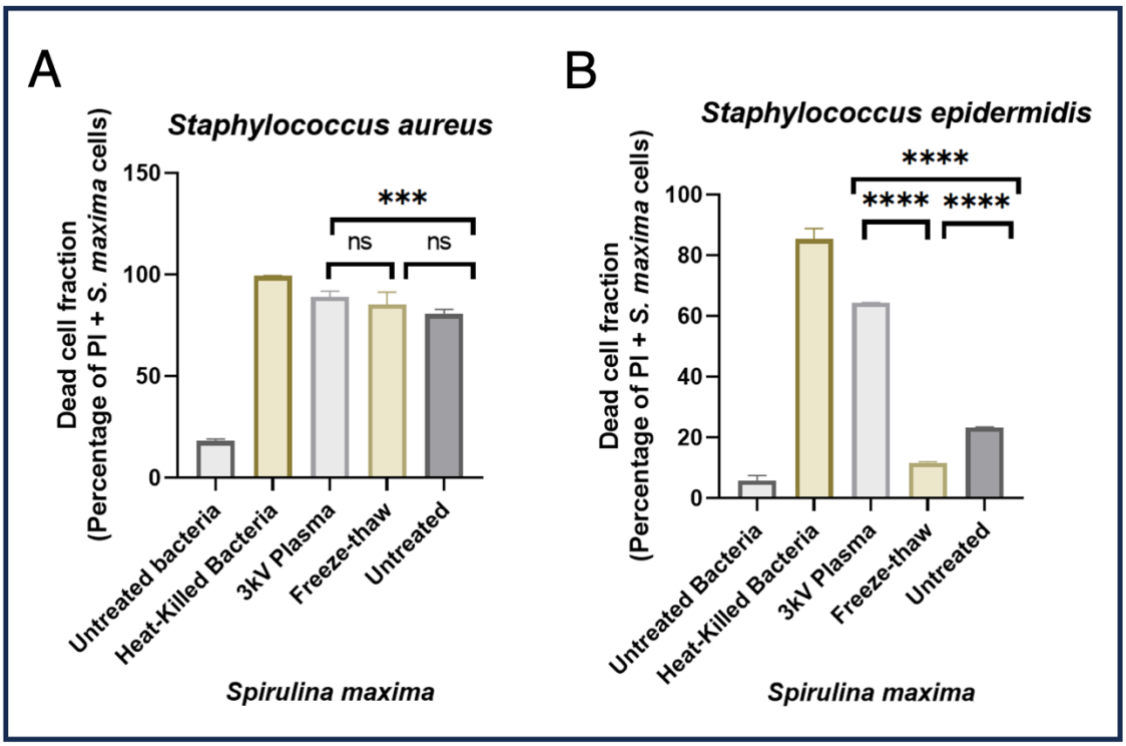

Figure 32. Percentage viability under different conditions under flow cytometry analysis. A.) *S. aureus*, **B.)** *S. epidermidis.*

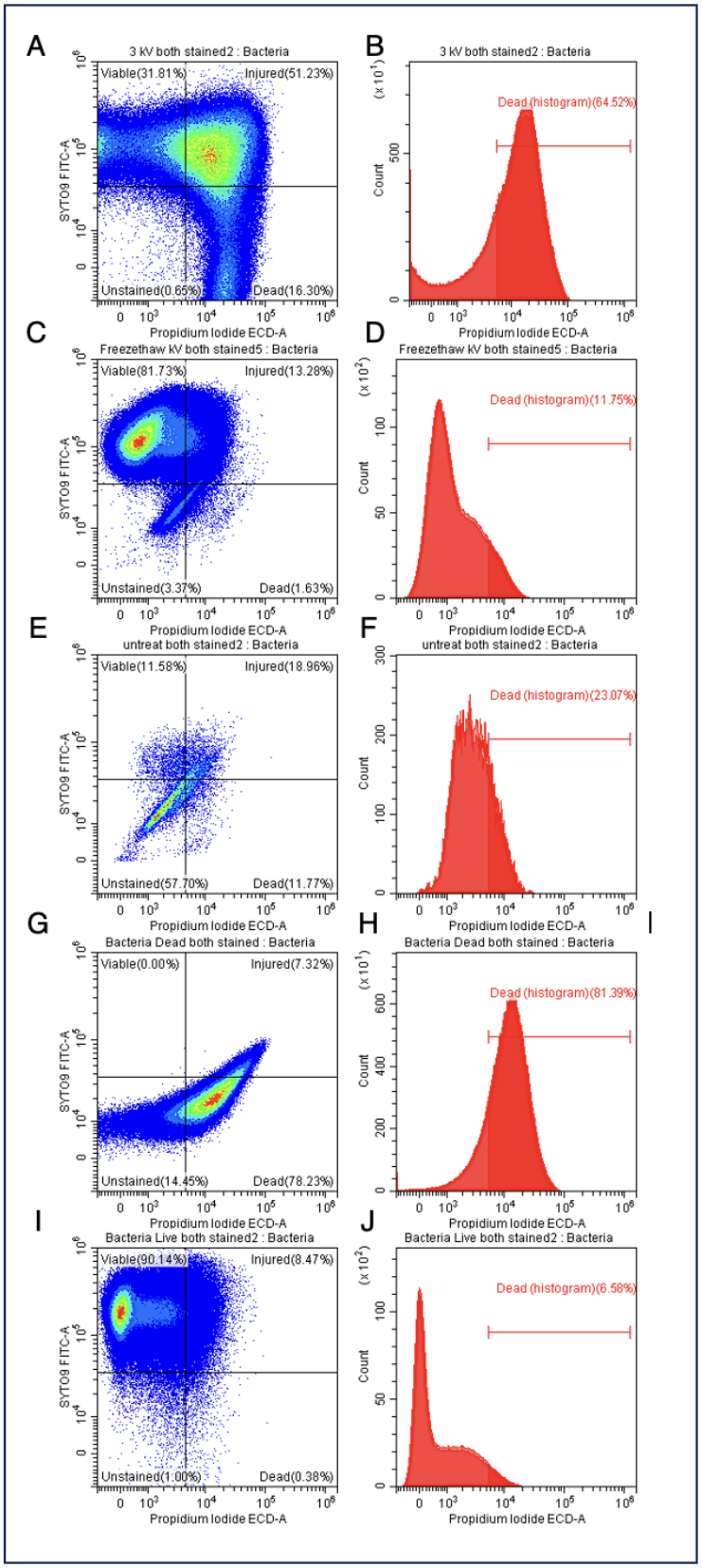

Figure 33. Flow cytometry analysis for live, injured, and dead cell population of *S. epidermidis* under different treatment conditions, using SYTO9 live cell stain and PI dead cell stain. A.) Cell viability for plasma-assisted extract **B.)** Histogram data for plasma-assisted extract, **C.)** Cell viability for freeze-thaw extract **D.)** Histogram data for freeze-thaw extract **E.)** Cell viability of untreated *S. maxima* supernatant **F.)** Histogram data for untreated *S. maxima* supernatant **G.)** Cell viability for dead bacterial control **H.)** Histogram data for dead bacteria control **I.)** Cell viability for live bacterial control **J.)** Histogram data for live bacterial control.

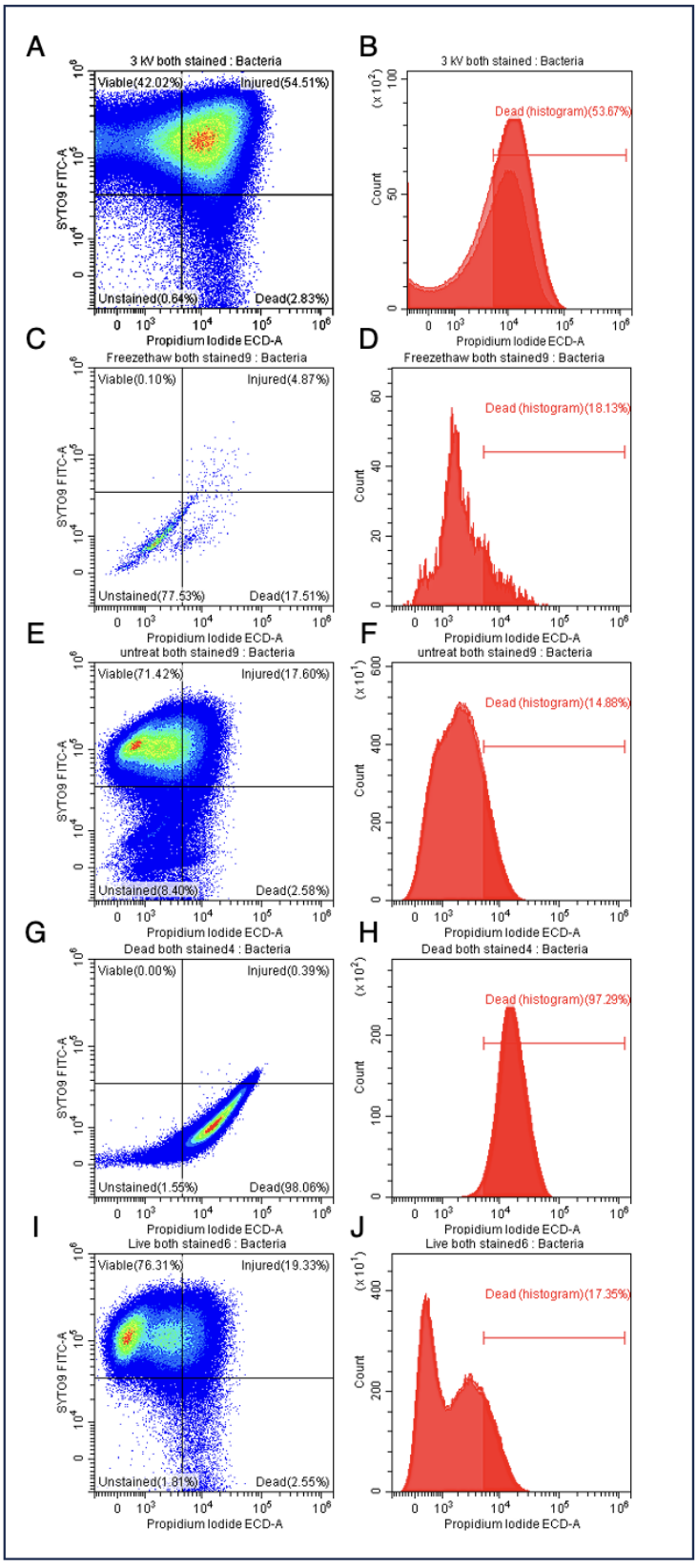

Figure 34. Flow cytometry analysis for live, injured, and dead cell population of *S. aureus* under different treatment conditions, using SYTO9 live cell stain and PI dead cell stain. A.) Cell viability for plasma-assisted extract **B.)** Histogram data for plasma-assisted extract, **C.)** Cell viability for freeze-thaw extract **D.)** Histogram data for freeze-thaw extract **E.)** Cell viability of untreated *S. maxima* supernatant **F.)** Histogram data for untreated *S. maxima* supernatant **G.)** Cell viability for dead bacterial control **H.)** Histogram data for dead bacteria control **I.)** Cell viability for live bacterial control **J.)** Histogram data for live bacterial control.

3.7.2 Evaluating the effect of *S. maxima* extract antibacterial activity on *E. coli* and *P. aeruginosa* via Flow cytometry

S. maxima extract antibacterial efficacy was preliminarily evaluated against Gram-negative bacteria, *E. coli* (ATCC 25922) and *P. aeruginosa* (ATCC 15692), using SYTO 9 and PI staining and quantified via flow cytometry to assess bacterial viability and membrane integrity for all treatment conditions. For Gram-negative strains, *E. coli* plasma-assisted extract did not produce a significant increase in dead cell fraction giving 12.66% as shown in the flow cytometry histogram (Figure 36 B) which is notably lower compared to other treatment condition, both freeze-thaw, 31.23% (Figure 36 D) and for untreated *S.maxima* supernatant, 19.81% (Figure 36 F) while *P. aeruginosa* gives a different response profile of 73.41% dead cell fraction not significantly exceed the conventional freeze thaw 87.87% (Figure 37 D) and significantly exceed untreated *S.maxima* supernatant at 80.38% (Figure 37 F).

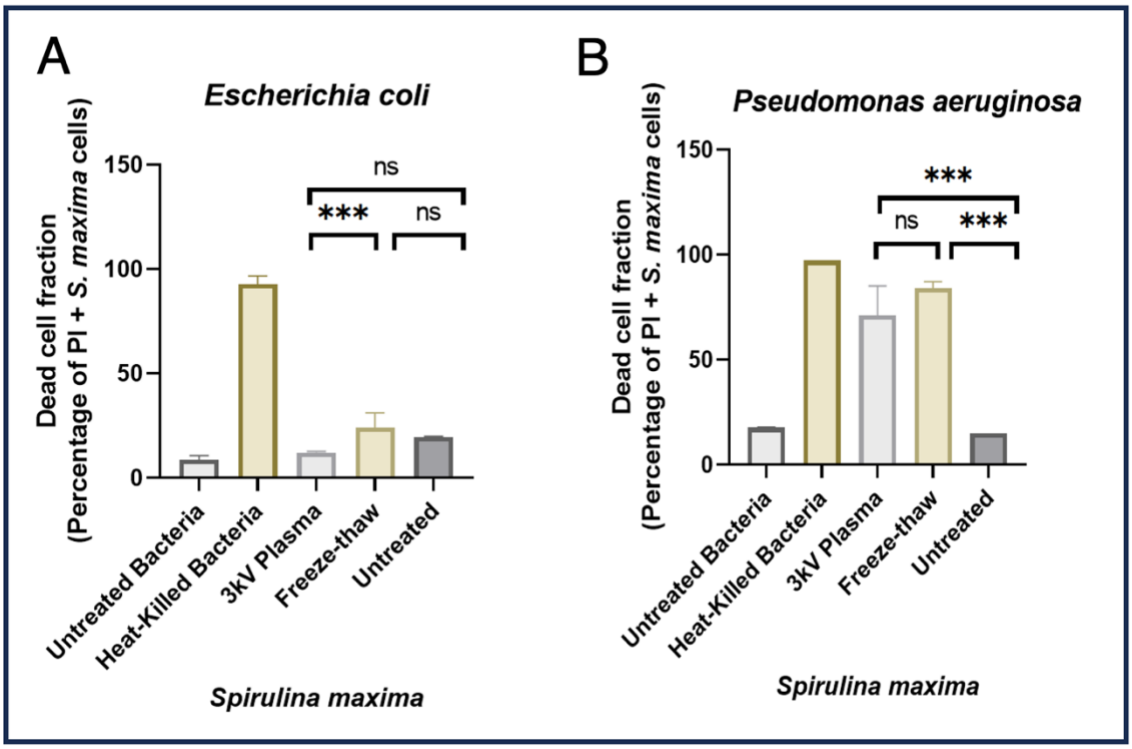

Figure 35. Percentage viability under different conditions under flow cytometry analysis (A) *E. coli* and **(B)** *P. aeruginosa.*

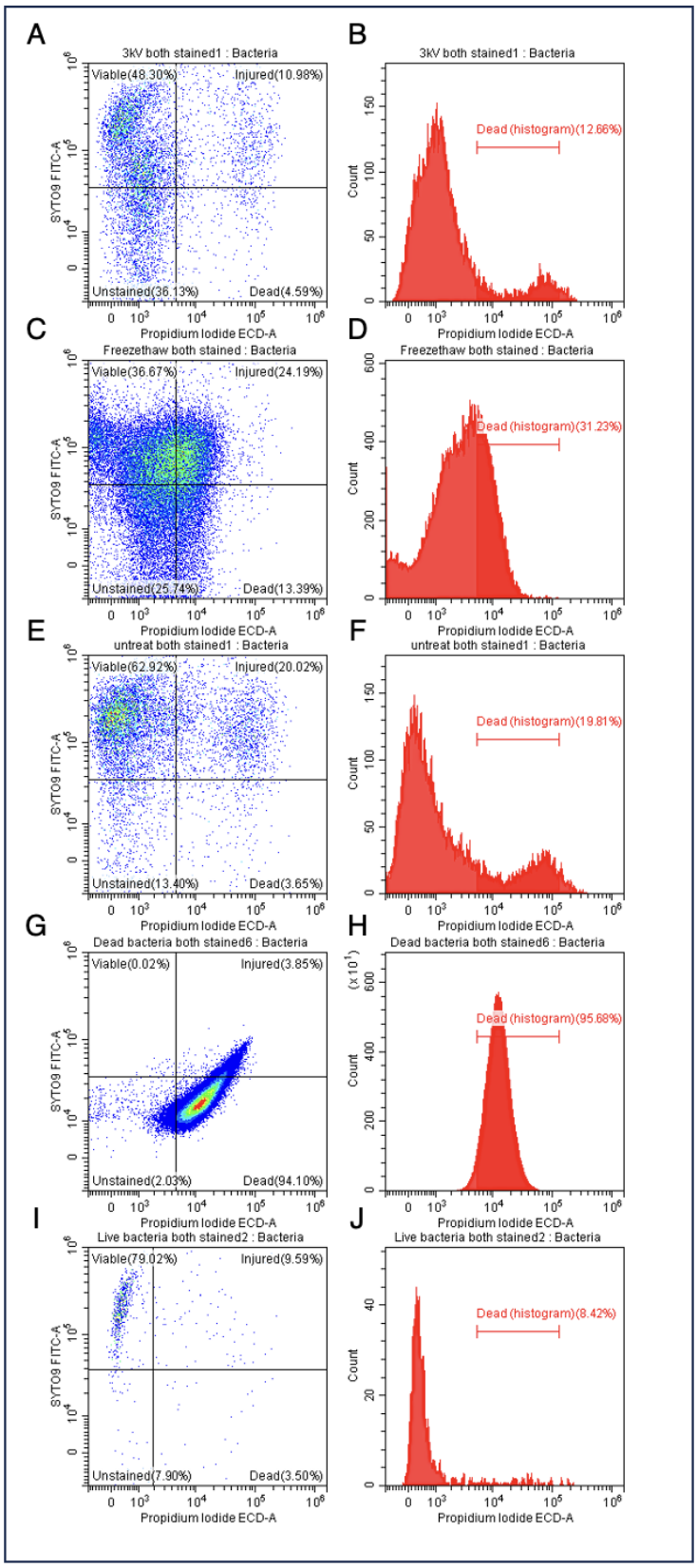

Figure 36. Flow cytometry analysis for live, injured, and dead cell population of *E. coli* under different treatment conditions, using SYTO9 live cell stain and PI dead cell stain. A.) Cell viability for plasma-assisted extract **B.)** Histogram data for plasma-assisted extract, **C.)** Cell viability for freeze-thaw extract **D.)** Histogram data for freeze-thaw extract **E.)** Cell viability of untreated *S. maxima* supernatant **F.)** Histogram data for untreated *S. maxima* supernatant **G.)** Cell viability for dead bacterial control **H.)** Histogram data for dead bacteria control **I.)** Cell viability for live bacterial control **(J)** Histogram data for live bacterial control.

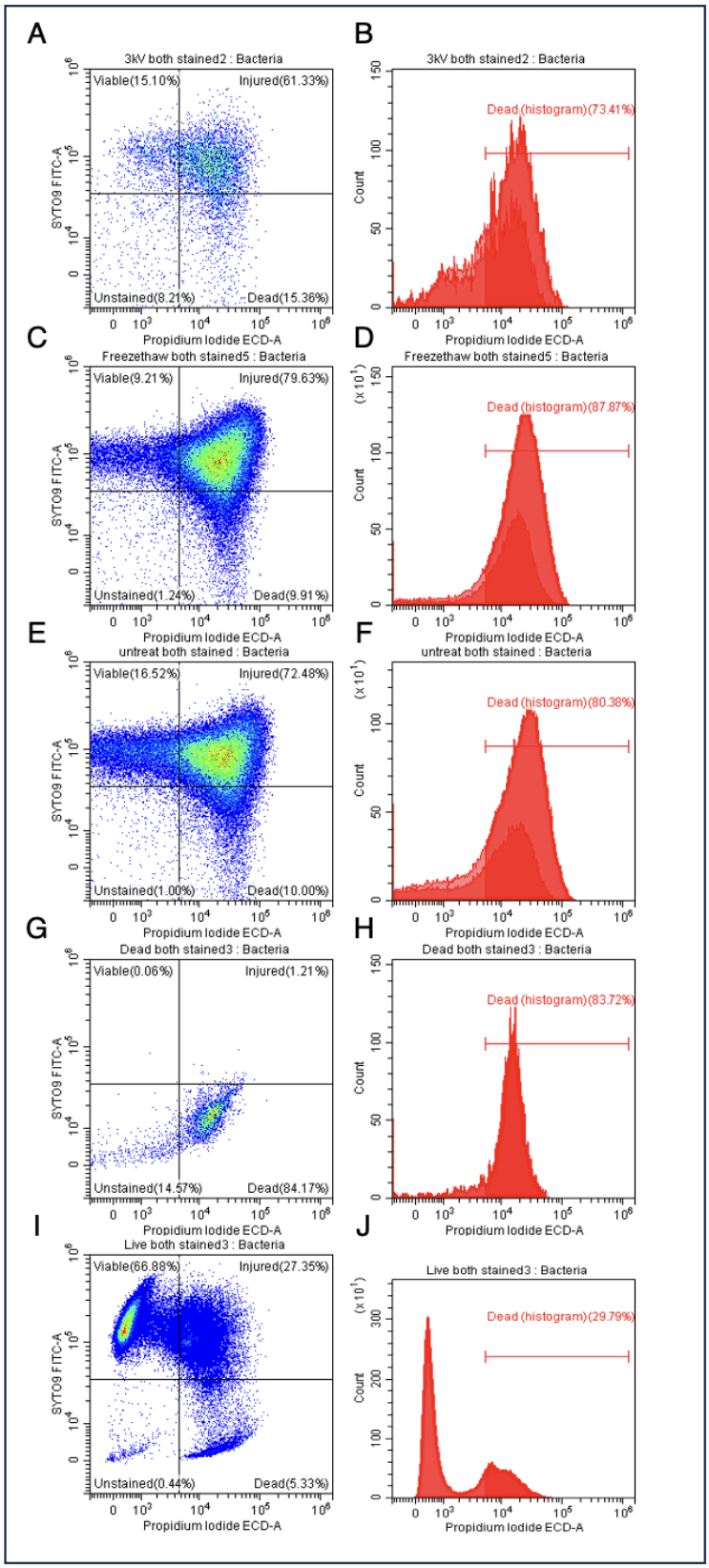

Figure 37. Flow cytometry analysis for live, injured, and dead cell population of *P. aeruginosa* under different treatment conditions, using SYTO9 live cell stain and PI dead cell stain. A.) Cell viability for plasma-assisted extract **B.)** Histogram data for plasma-assisted extract, **C.)** Cell viability for freeze-thaw extract **D.)** Histogram data for freeze-thaw extract **E.)** Cell viability of untreated *S. maxima* supernatant **F.)** Histogram data for untreated *S. maxima* supernatant **(G)** Cell viability for dead bacterial control **H.)** Histogram data for dead bacteria control **I.)** Cell viability for live bacterial control **J.)** Histogram data for live bacterial control.

CHAPTER FOUR: DISCUSSION

4.1 Parameters in atmospheric plasma technology

Atmospheric plasma technology has been utilized for this study to assess its suitability as an alternative extraction method for obtaining microalgae-derived bioactive compounds. This technology has broad application not only limited to microalgae but also to extends to plants and food matrices because of their excellent selectivity and ability to function at low temperatures, and making it ideal for delicate processes (Nehra et al., 2008). In this study, DBD was specifically chosen to avoid the issues of localized heating and non-uniform exposure which has been reported in other approaches. It functions by subjecting a nitrogen gas to a high-voltage of electric discharge, enabling nitrogen gas to ionize and generate plasma requiring more energy per unit volume of gas from plasma formation (Kogelschatz, 2003). Nitrogen has been one of the most popular gas choice due to its inert nature being not chemically reactive and most stable in any plasma conditions (Monfaredi et al., 2024). This makes it suitable for sensitive applications such as the extraction of *S. maxima* bioactive compounds. When combined with DBD, nitrogen enables the controlled generation of reactive ROS crucial for cell disruption.

In this research, the plasma process parameters including voltage level, treatment time and salt concentration has been fined-tuned to enable the efficient desired extraction efficacy and bioactive compound yield. An optimized plasma parameter setting of 3kV voltage, 7.42 minutes 0.75 g/L NaCl concentration was identified using the Design Expert Software to provide sufficient energy causing to generate reactive oxygen and nitrogen species for effective cell wall disruption without any further degradation. The 7.42 minutes ensure an ample compound release without causing oxidative damage from overexposure and 0.75 g/L NaCl concentration for enhanced compound release by imposing osmotic pressure stress on the cell membrane and enhanced ionic conductivity. CPC, known to be a strong antioxidant, is also indeed very susceptible to oxidation due to its tetrapyrrole chromophore phycocyanobilin (PCB) containing an alternating double bonds rich in electrons, allowing it to donate electron making it susceptible to attack by radicals by absorbing some of the oxidative stress losing its structural integrity (Minić, 2021). The results also shown that these optimized conditions resulted in the highest CPC concentration of 21 μg/mg outperforming a higher voltage level of 7kV, a longer treatment time of 9.96 minutes and a greater salt concentration 1.00 g/L NaCl in optimal antioxidant capacity. This suggest that increased intensity does not mean a better extraction or bioactivity, thus, can compromise compound integrity. The vulnerability of CPC under oxidative attacks during extensive extraction protocol can result to loss of structural integrity (Li, 2022). Increased power

duration of the 7kV extraction may compromise CPC integrity and the bioactive compounds through oxidation.

4.2 Influence of plasma exposure on *S. maxima* cell morphology

As plasma-assisted extraction has been reported to finely disrupt biological matrices and enhance extraction efficiency (Xi et al., 2024), the result in the study confirmed the efficacy of optimized plasma exposure on *S. maxima* under both scanning electron microscope (SEM) and epifluorescence imaging showing a moderate to low loss of integrity retaining intact morphology. The plasma-treated filament exhibited more evident fragmentation, loss of structural irregularities and compromised cell wall integrity which is greater compared to conventional freeze thaw and untreated filaments. This findings has been further supported by the epifluorescence result where optimized plasma exposure on *S. maxima* reduced fluorescence intensity which gives less defined structure wherein intense treatment lead to more depletion of fluorescence signal (Nishida et al., 2014). Evidently, it showed that optimized plasma-treated filaments had a displayed visible small fragmentation, and surface irregularities, suggesting morphological disruption which correlates with extraction efficiency. Furthermore, Plasma-assisted extraction mechanism introduces reactive ions, electrons, and radicals to drive cell wall disruption, by breaking important peptidoglycan bonds (Heydari et al., 2023). This targeted disruption of the cell wall polymer in *S. maxima* results in localized cellular fragmentation and surface irregularities can be related by induced RONS molecular disruption.

4.3 Biochemical compounds

4.3.1 C-phycocyanin concentration and purity

The result of the optimized plasma exposure on *S. maxima* showed a significant increase on the extraction yield of 21 μg/ml compared to 7kV result at 12 μg/ml, and 15 μg/ml for the untreated *S. maxima* supernatant. These results further emphasize that efficient plasma treatment facilitate an efficient cell wall disruption, leading to an improved extraction yield and greater purity of CPC. The optimal 3kV processing parameters provide an appropriate balance of power and sensitivity, enabling breakage of the cell wall while also not overexposing the contents to plasma which may disrupt its structural integrity. The use of DBD allows for controlled, and lower temperature processing which can improve CPC recovery without any excessive protein contamination under the optimized plasma condition. Therefore, we can say that this technique has high potential for extracting high-value

bioactive compounds from *S. maxima* outperforms other conventional methods in both yield and selectivity.

4.3.2 Total protein concentration of *S. maxima* extract

The key findings (Figure 27) demonstrates no significant change in total protein content across all treatment condition, with values having 47 μg/mg biomass for optimized plasma exposure, compared to 7kV plasma at 53 μg/mg biomass and 46 μg/mg biomass for the untreated *S. maxima* supernatant. This suggest that optimized plasma condition effectively disrupted *S. maxima* cell walls sufficiently to release compounds without any degradation or loss of protein. Similar outcome have been reported by (Xu et al., 2022) who reported that non-thermal plasma can increase extraction efficiency while preserving protein integrity. Therefore, the observed increase in CPC concentration can attribute to improved extraction rather than the total protein yield. One potential reason is due to its short exposure, low intensity of the non-targeted plasma that does not cause chemical modification of protein but targets polysaccharides and lipid layers, thereby preserving its structural integrity and functionality of proteins (Xu et al., 2022).

4.4 DPPH Radical scavenging assay for antioxidant activity

The antioxidant capacity of *S. maxima* following the optimized plasma exposure at 3kV achieved a high DPPH activity measured at 0.058 μM Trolox equivalent per mg of biomass, achieving a measurable radical scavenging performance. However, demonstrates not significant changes to those achieved with the 7kV plasma treatment condition and untreated *S. maxima* supernatant suggesting that plasma application under these conditions primarily facilitates efficient extraction rather than increasing the overall antioxidant capacity or possible degradation. Antioxidant are necessary in wound healing as they neutralizing excessive oxidative stress which can delayed tissue repair by acting as shield protecting healthy cells which can reduce chronic inflammation promoting wound closure (Pinto et al., 2021). In this study, antioxidant capacity and CPC release were not correlated. One possible explanation is that CPC is not the only important bioactive compound that is responsible for the antioxidant activity measured by DPPH assay in the 7kV treatment condition. Thus, other source of antioxidant including some phenolics and flavonoids may be present in higher quantities in 7kV *S. maxima* extract. This suggests that a comprehensive compositional analysis and chemical profiling like liquid chromatography mass spectrometry (LC/MS) is needed to fully determine non-CPC antioxidants which elevated at higher voltages.

4.5 Antibacterial property of plasma-treated *Spirulina maxima*

4.5.1 Antibacterial capacity against Gram-positive *Staphylococcus aureus* and *Staphylococcus epidermidis*

The antibacterial property of *S. maxima* extract was evaluated against both Gram-positive *S. aureus* and *S. epidermidis*. The reduction in viable cells, as determined via colony enumeration, and was supported by flow cytometry analysis. The result revealed that optimized plasma exposure at 3kV resulted in an 55.19 % reduction in viable *S. aureus* and a 56.6% reduction in *S. epidermidis* after plasma treatment, surpassing both the freeze thaw method and untreated *S. maxima* supernatant. While flow cytometry confirmed that these findings, showing a dead fraction of 53.67% *S. aureus* and 64.52% for *S. Epidermidis* surpassing both the freeze thaw method and untreated *S. maxima* supernatant. These findings, highlight the membrane integrity and a significant bacterial proliferation capacity on the inherently thick peptidoglycan layer provides barrier on Gram-positive bacteria.

CFU assay only count bacteria capable of dividing and form colonies, while flow cytometry detects compromised membrane (Massicotte et al., 2017). This difference in principle means flow cytometry can be more sensitive, often identifying a higher proportion of damage compared to CFU. However in some cases, CFU assay shows a higher percentage of reduction than flow cytometry, this can happen when severely stressed bacteria whose internal function are irreversibly damaged by plasma may still maintain their membrane integrity in which flow cytometry may not classify these as dead unless severely compromised (Massicotte et al., 2017). Therefore, these two different antibacterial performance needs to be understood with consideration to both measurements.

4.5.2 Antibacterial capacity against Gram-negative *Pseudomonas aeruginosa* and *Escherichia Coli*

The antibacterial property of *S. maxima* extract as also evaluated against both Gram-negative *E. coli* and *P. aeruginosa.* The reduction in viable cell, as determined via colony enumeration and was confirmed by flow cytometry analysis. The results on both assays revealed that optimized plasma exposure at 3kV in a notably lower reduction for *E. coli* compared to other treatment condition while *P. aeruginosa* gives a distinct response profile surpassing both the freeze thaw method and untreated *S. maxima* supernatant likely results from oxidative stress resistance and envelope structure (Maybin et al., 2023). According to Seaver and Imlay (2001), *E. coli* can highly manage oxidative stress produces by plasma generated oxygen species due to extremely low intracellular level of hydrogen peroxide (H_2O_2) mainly by compartmentalization keeping the concentration inside the cell at

extremely low concentration regardless of exposure to plasma. The rapid antioxidant defenses of catalase, alky hydroperoxide reductase (Ahp), and other peroxide-scavenging enzymes produced by *E. coli* breakdown H_2O_2 into water and oxygen reducing or neutralizing its toxic effect. These findings could therefore justify for a relatively low percentage reduction in CFU and flow cytometry assay after plasma treatment. In contrast, *P. aeruginosa* demonstrated a higher plasma sensitivity resulting to a less robust H_2O_2 compartmentalization that might explain the greater antibacterial activity in comparison to *E. coli*. Another plausible explanation is that the particular isolate of *E. coli* used in this study may express more efflux pumps compared to the strain of *P. aeruginosa* thereby reducing its antimicrobial sensitivity. These efflux pumps pushes out harmful compounds and substances that might do damage inside the cell (Anes et al., 2015).

CONCLUSION, LIMITATIONS AND FUTURE VISION

In the current study, we have successfully demonstrated that optimized plasma process parameter of 3kV, 7.42 min, 0.75 g/L NaCl plasma-assisted extraction evidently enhances extraction yield and purity efficacy of C-phycocyanin (CPC) and showed that *Spirulina maxima* extract obtained during optimal plasma-assisted extraction had a better antibacterial activity which outperforms the conventional freeze-thaw method and untreated *S. maxima* supernatant. Although CPC concentration was higher at 3kV, the antioxidant activity measured in DPPH radical scavenging assay was equivalent to that observed at 7kV treatment. This indicated that there might be other antioxidants such as phenol-based compounds present at differing concentrations, across the two different extracts across the two different extracts, indicating the need for full compositional analysis. While, total protein concentration was preserved across all plasma treatment conditions. These findings suggest potential for broad applications extending well beyond biomedical fields for wound healing applications.

Morphological analyses in SEM and Epifluorescence reveals that extensive cell wall disruption after plasma exposure can directly correlate with improved bioactive compound release ensuring a proper optimized plasma process parameters set-up. While, the antibacterial capacity was determined via colony enumeration and flow cytometry against Gram-positive bacteria *S. aureus* and *S. epidermidis* and Gram-negative bacteria *E. coli* and *P. aeruginosa* and exhibited a satisfactory antibacterial performance achieving up to 59.10% dead cell fraction for Gram-positive bacteria and 43.04% dead cell fraction for Gram-negative bacteria in flow cytometry assay and up to 55.92% and 49.09% bactericidal activity in CFU assay.

Despite these current results, some limitation must be recognized and be addressed for future visions. While the results we got are encouraging, the current data are based on limited bacterial strains and still needed a for a broader microbial testing for broad wound healing applications. Additionally, the detailed composition of the plasma-assisted extract remains unknown, and possible differences in composition could explain the observed difference in bioactivity. This suggests that a comprehensive compositional analysis like Liquid chromatography mass spectrometry (LC/MS) is needed to characterize extract composition. Also, a comprehensive safety evaluation including preservation of bioactive to ensure long-term preservation and doesn't degrade or lose their efficacy overtime. Consider to investigate combination therapies with antibiotics enabling synergistic interactions due to cell permeabilization like checkerboard assays and time-kill studies**.** This strategy can potentially

enhance antibacterial effects with reduced antibiotic doses treating persistent infection in chronic wound. This study may be further supplemented with further in-vitro cytotoxicity assay, in-vivo pharmacodynamic and pharmacokinetic studies like wound healing assay, and histopathological analysis for additional safety measures and formulation stability optimization integration of the optimized *S. maxima* extracts potentially combine with a hydrogel matrix, and bandages suited for moist wound conditions.

APPENDICES

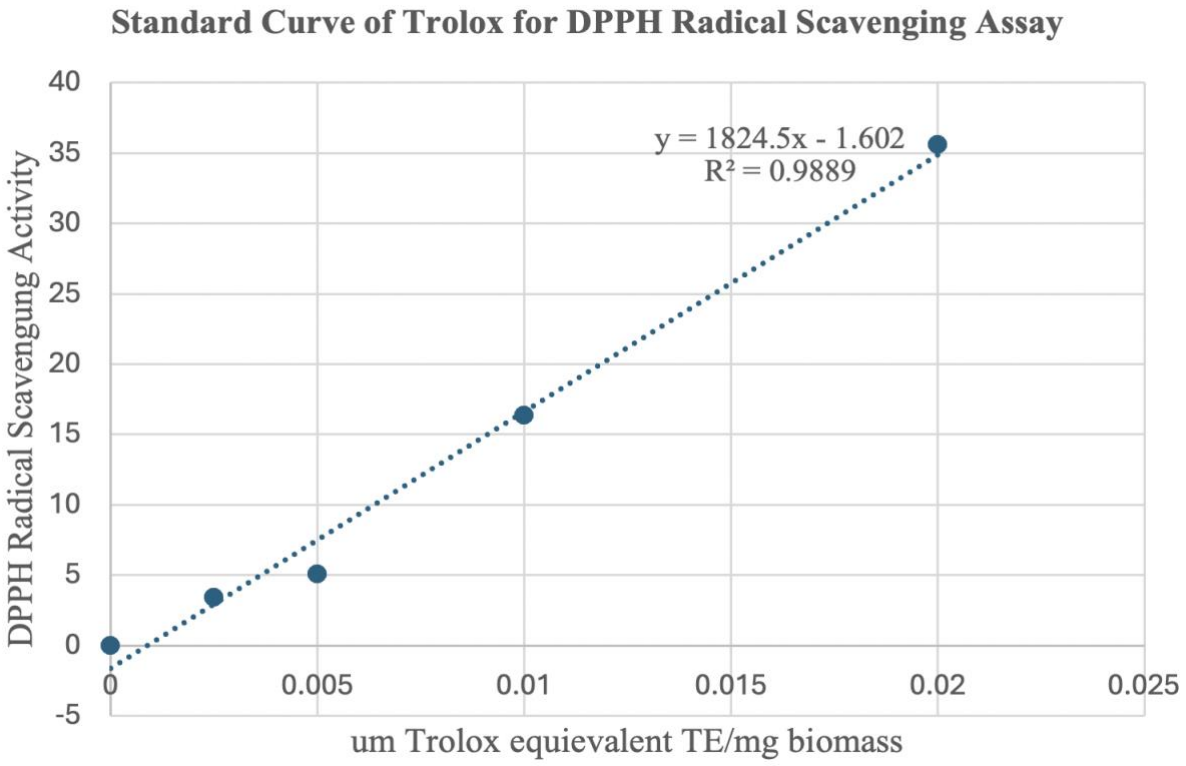

Figure 38. Standard Curve of Trolox for Antioxidant.

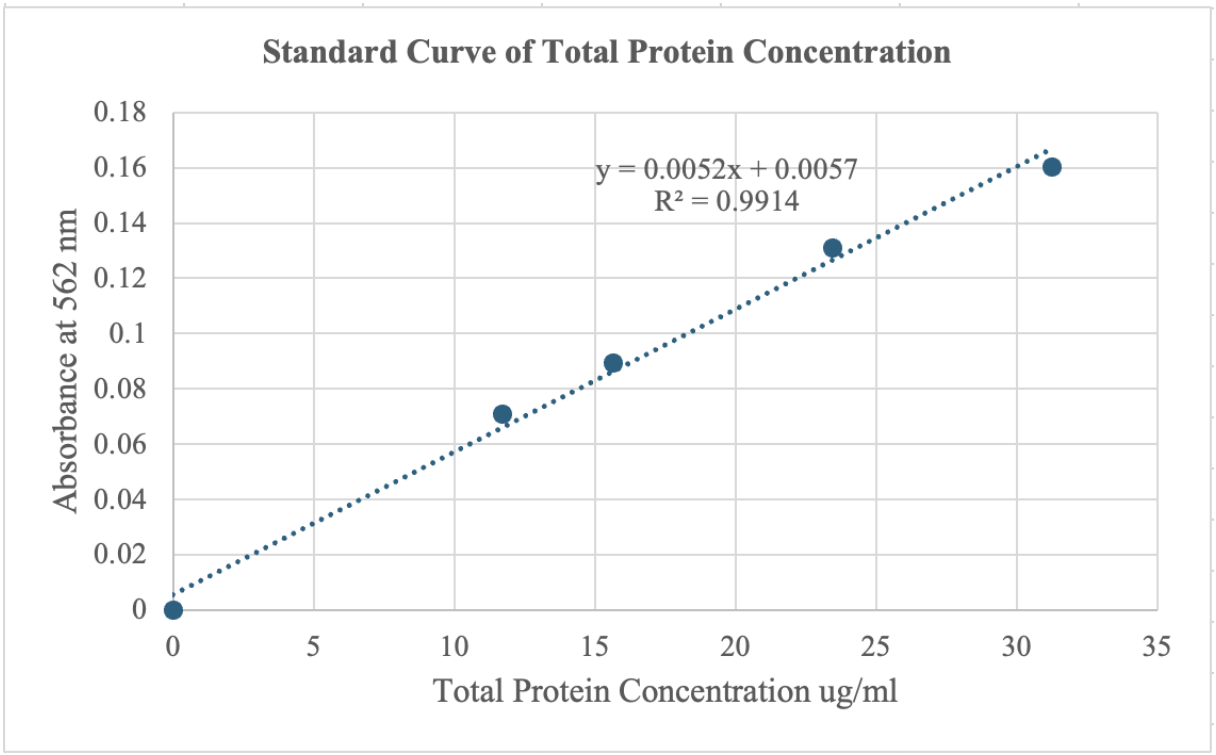

Figure 39. Standard Curve of BSA for Total Protein Concentration.

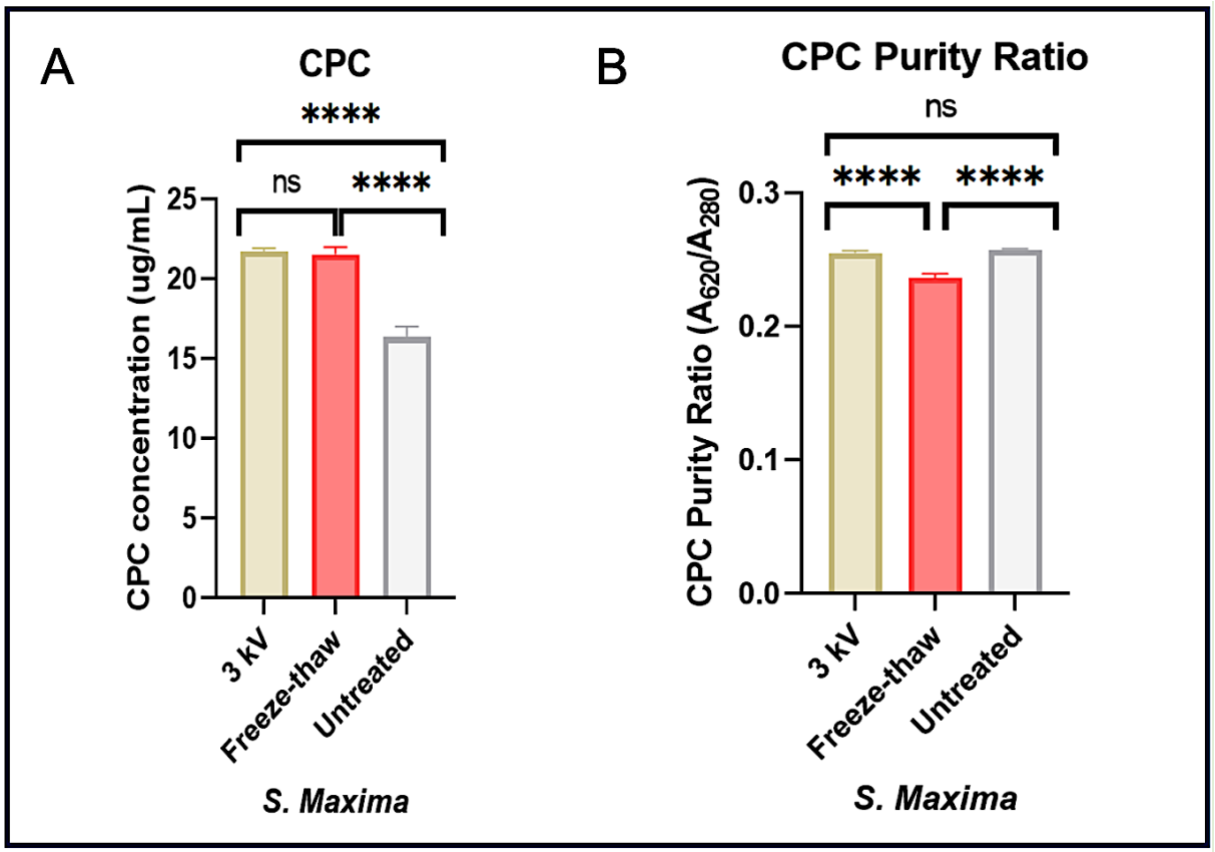

Figure 40. A.) C-phycocyanin (CPC) concentration (µg/ml) B.) C-phycocyanin (CPC) purity concentration relative to the optimal 3kV plasma treatment, conventional freeze-thaw method and untreated *S. maxima* supernatant.

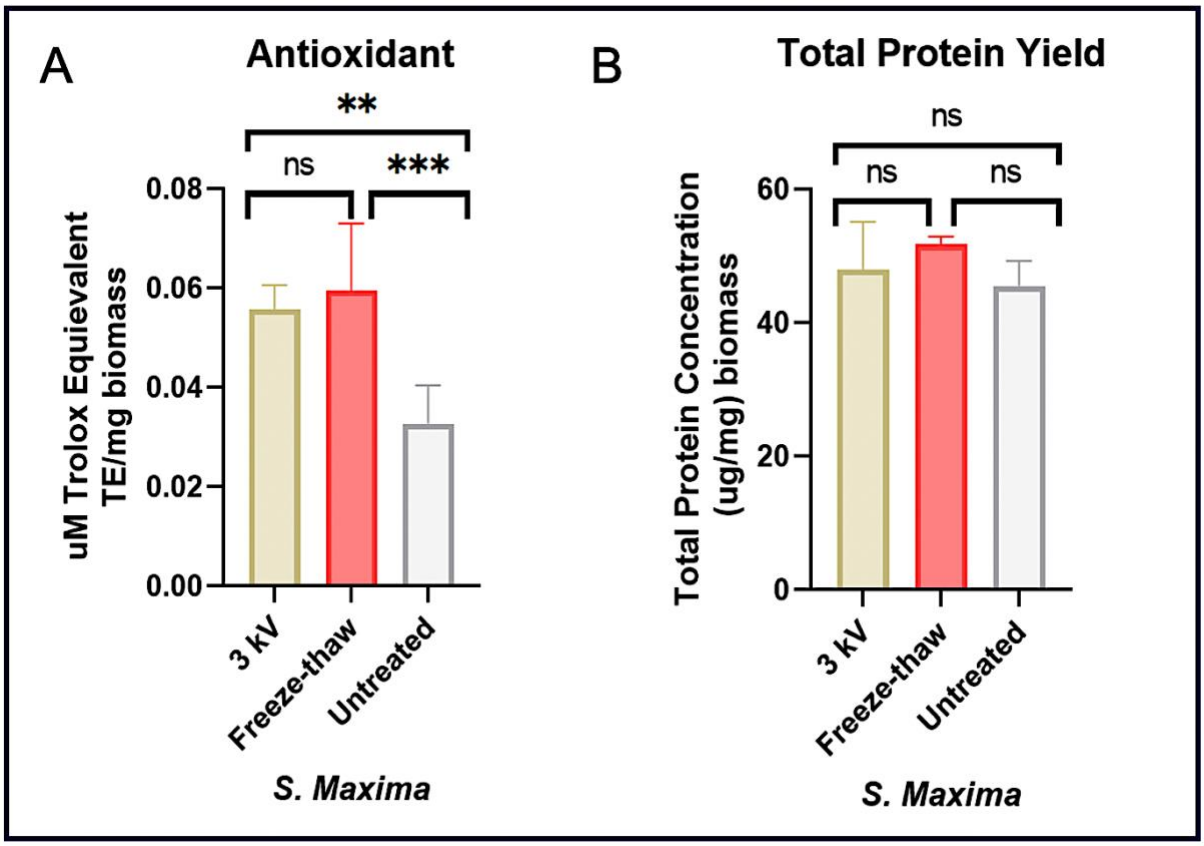

Figure 41. A.) Highest antioxidant capacity (TE/mg) B.) Total Protein Yield concentration (µg/mg) relative to the optimal 3kV plasma treatment, conventional freeze-thaw method and untreated *S. maxima* supernatant.

Table 10. Experimental reagents used for Laboratory Assay.

Experimental Reagent	Manufacturer	Application
***Spirulina maxima* biomass**	OXYMIN® SPIRULINA	C-phycocyanin extraction, Bioactivity assay
Trolox	Sigma -Aldrich	Standard reference for the antioxidant activity
DPPH-2,2 diphenyl-1-picrylhydrazyl	Sigma-Aldrich	Free radical scavenging reagent (DPPH Radical Scavenging Assay)
Sodium Chloride NaCl	Sigma-Aldrich	Increase osmotic pressure promoting CPC release (Optimization)
Methanol CH3OH	Sigma-Aldrich	Solvent for extraction (DPPH Radical Scavenging Assay)

Table 11. Bacterial Strains used in CFU enumeration and Flow Cytometry Analysis.

Bacterial Strain	ATCC Reference	Application
Staphylococcus aureus	ATCC 25923	Gram-positive pathogen (CFU Assay)
Staphylococcus epidermidis	ATCC 12228	Gram-positive pathogen (CFU Assay)
Escherichia coli	ATCC 25922	Gram-negative pathogen (CFU Assay)
Pseudomonas aeruginosa	ATCC 15692	Gram-positive pathogen (CFU Assay)

Table 12. Fluorescent Dyes and Staining Reagents used for Flow Cytometry Analysis.

Staining Reagent	Manufacturer	Application
Invitrogen SYTO 9	Thermo Fisher Scientific, Waltham, MA, USA	Live-cell staining for bacterial viability (Flowcytometry)
Invitrogen Propidium Iodide	Thermo Fisher Scientific, Waltham, MA, USA	Dead-cell staining (Flowcytometry)

Table 13. Culture media and Buffers.

Culture media/ Buffer	Manufacturer	Application
Phosphate-Buffered Saline-PBS	Sigma – Aldrich	Isotonic buffer (CFU Assay)
Tryptic Soy Broth-TSB	Sigma – Aldrich	Nutrient-rich medium (CFU Assay)
Agar powder	Merck KgaA, Darmstadt, Germany	Solid medium for plating and colony enumeration

Table 14. Laboratory Consumables, Equipment, and Software used for Optimization and Routine Laboratory Assay.

Consumable/ Equipment	Manufacturer	Application
96-well microtiter plates	Nunc, Thermo Scientific, MA, USA	High-throughput assay, sample + bacterial culturing
48-well microtiter plates	Corning Costar, Corning Inc., USA	High-throughput assay, sample + bacterial culturing
50 ml centrifuge tube	Corning Costar, Corning Inc., USA	Sample storage and handling
0.20 µm 3 mm filter	Agilent Technologies	Sterile filtration
0.45 µm 25 mm filter	Agilent Technologies	Sterile filtration
Micropipette/Multichannel pipette	Effendorf, Thermo Fisher	Precise liquid sample handling, reagent dispensing
GeneQuant Pro RNA/DNA Calculator Spectrophotometer	Pharmacia Biotech, Cambridge, UK	Optical Density OD absorbance reading (CFU Assay)
Synergy-HTX multi plate reader	Biotek	Optical Density OD absorbance reading (DPPH Radical Scavenging Assay)
UV/VIS Lambda 365	PerkinElmer	Optical Density OD absorbance reading (CPC concentration)
Biosafety cabinet	Thermoscientific	For a sterile work environment

Thermo Scientific Heratherm Microbiological Incubator	Thermoscientific	Controlled growth environment
FEI Quanta 450 Scanning Electron Microscope	Thermo Fisher Scientific, Waltham, MA, USA	Morphological analysis
Olympus IX83 Epifluorescence Microscope	Olympus Corporation, Tokyo, Japan	Morphological analysis
CytoFLEX S Flowcytometer	Beckman – Coulter, Brea, CA	Quantitative analysis of cell population
Thermo Scientific Heraeus Fresco 17 microcentrifuge	Thermo Fisher Scientific, Waltham, MA, USA	Separation of sample component for analysis
Central Composite Design-Design Expert Software	Stat-Ease Inc.	Statistical Optimization
CytExpert Version 2.6 Software	Beckman-Coulter, Brea, CA	Flowcytometry data analysis
GraphPad Prism version 8, GraphPad Software, LLC	San Diego, California, USA	Statistical analysis
Microsoft excel	Redmond, Washington, USA	Statistical analysis
FIJI Image J	National Institutes of Health (NIH)	Measuring and analyzing image features

BIBLIOGRAPHY

Adan, A., Alizada, G., Kiraz, Y., Baran, Y., & Nalbant, A. (2017). Flow cytometry: basic principles and applications. *Critical reviews in biotechnology*, *37*(2), 163-176. https://doi.org/https://doi.org/10.3109/07388551.2015.1128876

Adjali, A., Clarot, I., Chen, Z., Marchioni, E., & Boudier, A. (2022). Physicochemical degradation of phycocyanin and means to improve its stability: A short review. *Journal of Pharmaceutical Analysis*, *12*(3), 406-414. https://doi.org/https://doi.org/10.1016/j.jpha.2021.12.005

Advanced Wound Care Market. (2024).

AgriFarming. (2025). *Growing Spirulina from Scratch: Check How this Detailed Guide Helps Beginners*. Retrieved 7 October 2025 from https://www.agrifarming.in/growing-spirulina-from-scratch-check-how-this-detailed-guide-helps-beginners

Agustina, S., Aidha, N. N., Oktarina, E., & Kurniati, N. F. (2021). Evaluation of antioxidant and wound healing activities of Spirulina sp. extract. *Egyptian Journal of Chemistry*, *64*(8), 4601-4610. https://doi.org/10.21608/ejchem.2021.48597.3008

Akhtar, K., Khan, S. A., Khan, S. B., & Asiri, A. M. (2018). Scanning electron microscopy: Principle and applications in nanomaterials characterization. In *Handbook of materials characterization* (pp. 113-145). Springer. https://doi.org/https://doi.org/10.1007/978-3-319-92955-2_4

Ali, P., & Younas, A. (2021). Understanding and interpreting regression analysis. *Evidence-Based Nursing*, *24*(4), 116-118. https://doi.org/https://doi.org/10.1136/ebnurs-2021-103425

Anes, J., McCusker, M., Fanning, S., & Martins, M. (2015). The ins and outs of RND efflux pumps in Escherichia coli. Front Microbiol 6: 587. In.

Anvara, A. A., & Nowruzib, B. (2021). Bioactive properties of spirulina: A review. *Microbial bioactives*, *4*(1), 134-142. https://doi.org/https://doi.org/10.25163/microbbioacts.412117B0719110521

Azwanida, N. (2015). A review on the extraction methods use in medicinal plants, principle, strength and limitation. *Med aromat plants*, *4*(196), 2167-0412. https://doi.org/10.4172/2167-0412.1000196

Behbahaninia, M., Martirosyan, N. L., Georges, J., Udovich, J. A., Kalani, M. Y. S., Feuerstein, B. G., Nakaji, P., Spetzler, R. F., & Preul, M. C. (2013). Intraoperative fluorescent imaging of intracranial tumors: a review. *Clinical neurology and neurosurgery*, *115*(5), 517-528. https://doi.org/https://doi.org/10.1016/j.clineuro.2013.02.019

Bhuyan, S., Yadav, M., Giri, S. J., Begum, S., Das, S., Phukan, A., Priyadarshani, P., Sarkar, S., Jayswal, A., & Kabyashree, K. (2023). Microliter spotting and micro-colony observation: A rapid and simple approach for counting bacterial colony forming units. *Journal of Microbiological Methods*, *207*, 106707. https://doi.org/https://doi.org/10.1016/j.mimet.2023.106707

Breijyeh, Z., & Karaman, R. (2024). Antibacterial activity of medicinal plants and their role in wound healing. *Future Journal of Pharmaceutical Sciences*, *10*(1), 68. https://doi.org/https://doi.org/10.1186/s43094-024-00634-0

Carter, M., DaVanzo, J., Haught, R., Nusgart, M., Cartwright, D., & Fife, C. (2023). EE229 The Effect of COVID-19 on Care for Chronic Wounds Among Medicare Beneficiaries Using Medicare Claims–2019, 2020, and 2021. *Value in Health*, *26*(6), S101. https://doi.org/https://doi.org/10.1016/j.jval.2023.03.530

D'Angola, A., Colonna, G., & Kustova, E. (2022). Thermal and Non-thermal plasmas at atmospheric pressure. In (Vol. 10, pp. 852905): Frontiers Media SA.

Dinić, M., Verpile, R., Burgess, J. L., Ming, J., Marjanovic, J., Beliz, C. N., Plano, L., Hower, S., Thaller, S. R., & Banerjee, S. (2024). Multi-drug resistant Staphylococcus epidermidis from chronic wounds impair healing in human wound model. *Wound repair and regeneration*, *32*(6), 799-810. https://doi.org/https://doi.org/10.1111/wrr.13231

Frost, J. (2020). Statistics by Jim: Making statistics intuitive. In: Retrieved from How High Does R-squared Need to Be.

Ghelich, R., Jahannama, M. R., Abdizadeh, H., Torknik, F. S., & Vaezi, M. R. (2019). Central composite design (CCD)-Response surface methodology (RSM) of effective electrospinning parameters on PVP-B-Hf hybrid nanofibrous composites for synthesis of HfB2-based composite nanofibers. *Composites Part B: Engineering*, *166*, 527-541. https://doi.org/https://doi.org/10.1016/j.compositesb.2019.01.094

Grossart, H.-P., Kiørboe, T., Tang, K., & Ploug, H. (2003). Bacterial colonization of particles: growth and interactions. *Applied and environmental microbiology*, *69*(6), 3500-3509. https://doi.org/https://doi.org/10.1128/AEM.69.6.3500-3509.2003

Grosshagauer, S., Kraemer, K., & Somoza, V. (2020). The true value of Spirulina. *Journal of agricultural and food chemistry*, *68*(14), 4109-4115. https://doi.org/https://doi.org/10.1021/acs.jafc.9b08251

Hadiyanto, H., & Adetya, N. P. (2018). Response surface optimization of lipid and protein extractions from Spirulina platensis using ultrasound assisted osmotic shock method. *Food Science and Biotechnology*, *27*(5), 1361-1368. https://doi.org/https://doi.org/10.1007/s10068-018-0389-y

Haldane, D. J., & Robart, E. (1990). A comparison of calcofluor white, potassium hydroxide, and culture for the laboratory diagnosis of superficial fungal infection. *Diagnostic microbiology and infectious disease*, *13*(4), 337-339. https://doi.org/https://doi.org/10.1016/0732-8893(90)90027-S

He, F. (2011). BCA (bicinchoninic acid) protein assay. *Bio-protocol*, e44-e44. https://bio-protocol.org/epdf/44

Heydari, M., Carbone, K., Gervasi, F., Parandi, E., Rouhi, M., Rostami, O., Abedi-Firoozjah, R., Kolahdouz-Nasiri, A., Garavand, F., & Mohammadi, R. (2023). Cold plasma-assisted extraction of phytochemicals: A review. *Foods*, *12*(17), 3181. https://doi.org/https://doi.org/10.3390/foods12173181

Hoang, T., Ghori, M. U., Ousey, K. J., & Conway, B. (2022). Current and advanced therapies for chronic wound infection. *Pharm J*, *309*. https://doi.org/https://www.researchgate.net/profile/Phuong_Nga_Hoang/publication/362252205_Current_and_advanced_therapies_for_chronic_wound_infection/links/6303b7c2e3c7de4c347670f8/Current-and-advanced-therapies-for-chronic-wound-infection.pdf

Hudzicki, J. (2009). *Kirby-Bauer disk diffusion susceptibility test protocol* (American society for microbiology, Issue. https://asm.org/getattachment/2594ce26-bd44-47f6-8287-0657aa9185ad/kirby-bauer-disk-diffusion-

Hurlow, J., & Bowler, P. G. (2022). Acute and chronic wound infections: microbiological, immunological, clinical and therapeutic distinctions. *Journal of wound care*, *31*(5), 436-445. https://doi.org/https://doi.org/10.12968/jowc.2022.31.5.436

Jaeschke, D. P., Teixeira, I. R., Marczak, L. D. F., & Mercali, G. D. (2021). Phycocyanin from Spirulina: A review of extraction methods and stability. *Food Research International*, *143*, 110314. https://doi.org/https://doi.org/10.1016/j.foodres.2021.110314

Kalantari, K., Mostafavi, E., Afifi, A. M., Izadiyan, Z., Jahangirian, H., Rafiee-Moghaddam, R., & Webster, T. J. (2020). Wound dressings functionalized with silver nanoparticles: promises and pitfalls. *Nanoscale*, *12*(4), 2268-2291. https://doi.org/https://doi.org/10.1039/C9NR08234D

Kaushik, P., & Chauhan, A. (2008). In vitro antibacterial activity of laboratory grown culture of Spirulina platensis. *Indian Journal of Microbiology*, *48*, 348-352. https://doi.org/https://doi.org/10.1007/s12088-008-0043-0

Kowalska-Krochmal, B., & Dudek-Wicher, R. (2021). The minimum inhibitory concentration of antibiotics: methods, interpretation, clinical relevance. *Pathogens*, *10*(2), 165. https://doi.org/https://doi.org/10.3390/pathogens10020165

Kumar, L., Bisen, M., Harjai, K., Chhibber, S., Azizov, S., Lalhlenmawia, H., & Kumar, D. (2023). Advances in Nanotechnology for Biofilm Inhibition. *ACS Omega*, *8*(24), 21391-21409. https://doi.org/10.1021/acsomega.3c02239

Landén, N. X., Li, D., & Ståhle, M. (2016). Transition from inflammation to proliferation: a critical step during wound healing. *Cellular and Molecular Life Sciences*, *73*, 3861-3885. https://doi.org/https://doi.org/10.1007/s00018-016-2268-0

Leaper, D., Assadian, O., & Edmiston, C. E. (2015). Approach to chronic wound infections. *British Journal of Dermatology*, *173*(2), 351-358. https://doi.org/https://doi.org/10.1111/bjd.13677

Li, J., Ma, C., Zhu, S., Yu, F., Dai, B., & Yang, D. (2019). A review of recent advances of dielectric barrier discharge plasma in catalysis. *Nanomaterials*, *9*(10), 1428. https://doi.org/https://doi.org/10.3390/nano9101428

Liang, Y., He, J., & Guo, B. (2021). Functional hydrogels as wound dressing to enhance wound healing. *ACS nano*, *15*(8), 12687-12722. https://doi.org/https://doi.org/10.1021/acsnano.1c04206

Manohar, S. M., Shah, P., & Nair, A. (2021). Flow cytometry: principles, applications and recent advances. *Bioanalysis*, *13*(3), 181-198. https://doi.org/https://doi.org/10.4155/bio-2020-0267

Marjanović, B., Benković, M., Jurina, T., Sokač Cvetnić, T., Valinger, D., Gajdoš Kljusurić, J., & Jurinjak Tušek, A. (2024). Bioactive Compounds from Spirulina spp.—Nutritional Value, Extraction, and Application in Food Industry. *Separations*, *11*(9), 257. https://doi.org/https://doi.org/10.3390/separations11090257

Massicotte, R., Mafu, A. A., Ahmad, D., Deshaies, F., Pichette, G., & Belhumeur, P. (2017). Comparison between flow cytometry and traditional culture methods for efficacy assessment of six disinfectant agents against nosocomial bacterial species. *Frontiers in microbiology*, *8*, 112. https://doi.org/https://doi.org/10.3389/fmicb.2017.00112

Maybin, J.-A., Thompson, T. P., Flynn, P. B., Skvortsov, T., Hickok, N. J., Freeman, T. A., & Gilmore, B. F. (2023). Cold atmospheric pressure plasma-antibiotic synergy in Pseudomonas aeruginosa biofilms is mediated via oxidative stress response. *Biofilm*, *5*, 100122. https://doi.org/https://doi.org/10.1016/j.bioflm.2023.100122

Minić, S. (2021). Bioactive properties of Spirulina-derived phycobiliproteins and phycobilins. *Biologia Serbica*, *43*(1). https://doi.org/10.5281/zenodo.5512528

Miranda, M., Cintra, R., Barros, S. B. d. M., & Mancini-Filho, J. (1998). Antioxidant activity of the microalga Spirulina maxima. *Brazilian Journal of Medical and biological research*, *31*, 1075-1079. https://doi.org/https://doi.org/10.1590/S0100-879X1998000800007

Monfaredi, M., Mohajer, M., Khademi, A., Salavati, M., Ramezan, Y., & Ghomi, H. (2024). Effects of Dielectric Barrier Discharge Cold Plasma on the Extraction of Bioactive Compounds from Colombian Arabica Coffee Powder. *Food and Bioprocess Technology*, 1-11. https://doi.org/https://doi.org/10.1007/s11947-024-03605-8

Montgomery, D. C., Peck, E. A., & Vining, G. G. (2021). *Introduction to linear regression analysis*. John Wiley & Sons.

Na, J., Jang, S., Song, M., Nam, S., Choi, W.-Y., Shin, H., Kwon, S., & Baek, Y. (2025). Unraveling the unique bioactivities of highly purified C-phycocyanin and allophycocyanin. *Journal of Biological Engineering*, *19*(1), 34. https://doi.org/10.1186/s13036-025-00496-x

Nanoscience Instruments, I. (2025). *Scanning Electron Microscopy*. Retrieved October 6, 2025 from https://www.nanoscience.com/techniques/scanning-electron-microscopy/

Nehra, V., Kumar, A., & Dwivedi, H. (2008). Atmospheric non-thermal plasma sources. *International Journal of Engineering*, *2*(1), 53-68. https://doi.org/https://citeseerx.ist.psu.edu/document?repid=rep1&type=pdf&doi=2c847268223afb641f274bfcad1b65e4fc336d98

Nishida, K., Ono, K., Kanaya, S., & Takahashi, K. (2014). KEGGscape: a Cytoscape app for pathway data integration. *F1000Research*, *3*, 144. https://doi.org/10.12688/f1000research.4524.1

Njoku, C. N., & Otisi, S. K. (2023). Application of central composite design with design expert v13 in process optimization. In *Response Surface Methodology-Research Advances and Applications*. IntechOpen. https://doi.org/DOI: 10.5772/intechopen.109704

Oliveira, M. d., Monteiro, M., Robbs, P., & Leite, S. (1999). Growth and chemical composition of Spirulina maxima and Spirulina platensis biomass at different temperatures. *Aquaculture international*, *7*, 261-275. https://doi.org/https://doi.org/10.1023/A:1009233230706

Pan-utai, W., & Iamtham, S. (2019). Physical extraction and extrusion entrapment of C-phycocyanin from Arthrospira platensis. *Journal of king saud university-Science*, *31*(4), 1535-1542. https://doi.org/https://doi.org/10.1016/j.jksus.2018.05.026

Percival, S. L., Bowler, P., & Russell, D. (2005). Bacterial resistance to silver in wound care. *Journal of hospital infection*, *60*(1), 1-7. https://doi.org/https://doi.org/10.1016/j.jhin.2004.11.014

Pham, T., Nguyen, T. T., Nguyen, N. H., Hayles, A., Li, W., Pham, D. Q., Nguyen, C. K., Nguyen, T., Vongsvivut, J., & Ninan, N. (2024). Transforming spirulina maxima biomass into ultrathin bioactive coatings using an atmospheric plasma jet: A new approach to healing of infected wounds. *Small*, *20*(39), 2305469. https://doi.org/https://doi.org/10.1002/smll.202305469

Pham, T. G. T. (2023). *Plasma-treated coatings of Spirulina maxima promotes wound healing and antibacterial capacity*

Pinto, D., Vieira, E. F., Peixoto, A. F., Freire, C., Freitas, V., Costa, P., Delerue-Matos, C., & Rodrigues, F. (2021). Optimizing the extraction of phenolic antioxidants from chestnut shells by subcritical water extraction using response surface methodology. *Food Chemistry*, *334*, 127521. https://doi.org/https://doi.org/10.1016/j.foodchem.2020.127521

Pochampally, R. (2008). Colony forming unit assays for MSCs. In *Mesenchymal Stem Cells: Methods and Protocols* (pp. 83-91). Springer. https://doi.org/https://doi.org/10.1007/978-1-60327-169-1_6

Protein, V. (2025). *BCA Protein Assay Kit - Visual Protein*. https://www.visualprotein.com/en/product/8/37/48

Ragusa, I., Nardone, G. N., Zanatta, S., Bertin, W., & Amadio, E. (2021). Spirulina for skin care: A bright blue future. *Cosmetics*, *8*(1), 7. https://doi.org/https://doi.org/10.3390/cosmetics8010007

Rosiak, J. M., & Yoshii, F. (1999). Hydrogels and their medical applications. *Nuclear Instruments and Methods in Physics Research Section B: Beam Interactions with Materials and Atoms*, *151*(1-4), 56-64. https://doi.org/https://doi.org/10.1016/S0168-583X(99)00118-4

Scientific, T. F. (2025). Micro BCA Protein Assay Kit User Guide. In.

Seaver, L. C., & Imlay, J. A. (2001). Hydrogen peroxide fluxes and compartmentalization inside growing Escherichia coli. *Journal of bacteriology*, *183*(24), 7182-7189. https://doi.org/https://doi.org/10.1128/jb.183.24.7182-7189.2001

Selim, M. I., El-Banna, T., Sonbol, F., Negm, W. A., & Elekhnawy, E. (2025). Unveiling the potential of spirulina algal extract as promising antibacterial and antibiofilm agent against carbapenem-resistant Klebsiella pneumoniae: in vitro and in vivo study. *Microbial Cell Factories*, *24*(1), 7. https://doi.org/https://doi.org/10.1186/s12934-024-02619-3

Sen, C. K. (2021). Human wound and its burden: updated 2020 compendium of estimates. *Advances in wound care*, *10*(5), 281-292. https://doi.org/https://doi.org/10.1089/wound.2021.002

Siddiqui, A. R., & Bernstein, J. M. (2010). Chronic wound infection: facts and controversies. *Clinics in dermatology*, *28*(5), 519-526. https://doi.org/https://doi.org/10.1016/j.clindermatol.2010.03.009

Singh, S., Young, A., & McNaught, C.-E. (2017). The physiology of wound healing. *Surgery (Oxford)*, *35*(9), 473-477. https://doi.org/https://doi.org/10.1016/j.mpsur.2017.06.004

Stat-Ease, I. (2025). *Design-Expert software, version 13*. In https://www.statease.com/docs/v22.0/contents/analysis/interpretation-of-r-squared/

Stiefel, P., Schmidt-Emrich, S., Maniura-Weber, K., & Ren, Q. (2015). Critical aspects of using bacterial cell viability assays with the fluorophores SYTO9 and propidium iodide. *BMC microbiology*, *15*(1), 36. https://doi.org/https://doi.org/10.1186/s12866-015-0376-x

Syarina, P. N. A., Karthivashan, G., Abas, F., Arulselvan, P., & Fakurazi, S. (2015). Wound healing potential of Spirulina platensis extracts on human dermal fibroblast cells. *EXCLI journal*, *14*, 385. https://doi.org/ 10.17179/excli2014-697

Tan, H. T., Khong, N. M., Khaw, Y. S., Ahmad, S. A., & Yusoff, F. M. (2020). Optimization of the freezing-thawing method for extracting phycobiliproteins from Arthrospira sp. *Molecules*, *25*(17), 3894. https://doi.org/10.3390/molecules25173894

Thaipong, K., Boonprakob, U., Crosby, K., Cisneros-Zevallos, L., & Byrne, D. H. (2006). Comparison of ABTS, DPPH, FRAP, and ORAC assays for estimating antioxidant activity from guava fruit extracts. *Journal of food composition and analysis*, *19*(6-7), 669-675. https://doi.org/https://doi.org/10.1016/j.jfca.2006.01.003

Thomson, C. H. (2011). Biofilms: do they affect wound healing? *International wound journal*, *8*(1), 63-67. https://doi.org/https://doi.org/10.1111/j.1742-481X.2010.00749.x

Veza, I., Spraggon, M., Fattah, I. R., & Idris, M. (2023). Response surface methodology (RSM) for optimizing engine performance and emissions fueled with biofuel: Review of RSM for sustainability energy transition. *Results in Engineering*, *18*, 101213. https://doi.org/https://doi.org/10.1016/j.rineng.2023.101213

Vogt, C., Wondergem, C. S., & Weckhuysen, B. M. (2023). Ultraviolet-visible (UV-Vis) spectroscopy. In *Springer handbook of advanced catalyst characterization* (pp. 237-264). Springer. https://doi.org/https://doi.org/10.1007/978-3-031-07125-6_11

Weremfo, A., Abassah-Oppong, S., Adulley, F., Dabie, K., & Seidu-Larry, S. (2023). Response surface methodology as a tool to optimize the extraction of bioactive compounds from plant sources. *Journal of the Science of Food and Agriculture*, *103*(1), 26-36. https://doi.org/https://doi.org/10.1002/jsfa.12121

Wound Australia (2022). https://doi.org/https://treasury.gov.au/sites/default/files/2022-03/258735_wounds_australia.pdf

Xi, J., Wang, Y., Zhou, X., Wei, S., & Zhang, D. (2024). Cold plasma pretreatment technology for enhancing the extraction of bioactive ingredients from plant materials: A review. *Industrial Crops and Products*, *209*, 117963. https://doi.org/https://doi.org/10.1016/j.indcrop.2023.117963

Xu, Y., Bai, Y., Dai, C., Lv, H., Zhou, X., & Xu, Q. (2022). Effects of non-thermal atmospheric plasma on protein. *Journal of Clinical Biochemistry and Nutrition*, *71*(3), 173. https://doi.org/10.3164/jcbn.22-17

Yang, K., Han, Q., Chen, B., Zheng, Y., Zhang, K., Li, Q., & Wang, J. (2018). Antimicrobial hydrogels: promising materials for medical application. *International journal of nanomedicine*, 2217-2263. https://doi.org/https://doi.org/10.2147/IJN.S154748

Zhang, Y., Kang, X., Zhen, F., Wang, Z., Kong, X., & Sun, Y. (2022). Assessment of enzyme addition strategies on the enhancement of lipid yield from microalgae. *Biochemical Engineering Journal*, *177*, 108198. https://doi.org/https://doi.org/10.1016/j.bej.2021.108198

Zhou, W., Apkarian, R., Wang, Z. L., & Joy, D. (2006). Fundamentals of scanning electron microscopy (SEM). In *Scanning microscopy for nanotechnology: techniques and applications* (pp. 1-40). Springer. https://link.springer.com/content/pdf/10.1007/978-0-387-39620-0_1.pdf